ON THE EXISTENCE AND STABILITY OF CARBON -BASED SILICON FULLERENES -A DENSITY FUNCTIONAL THEORETIC STUDY

By

ARAVIND SRINIVASAN

Presented to the Faculty of the Graduate School of

The University of Texas at Arlington in Partial Fulfillment

of the Requirements

for the Degree of

MASTER OF SCIENCE IN PHYSICS

THE UNIVERSITY OF TEXAS AT ARLINGTON

DECEMBER 2005

ACKNOWLEDGEMENTS

I would like to thank Dr. Ray for his mentorship throughout my academics and research work. I would like to express my gratitude to the members of my thesis committee Dr. Horwitz, Dr. Zhang and other faculty members of the Physics department for helping me to gain knowledge in the area of Physics. I gratefully acknowledge the financial support from the Welch Foundation, Houston, Texas and the Department of Physics at the University of Texas at Arlington.

I would like to thank my research group members for their valuable suggestions and interesting discussions. I would like to express my thanks to Dr. M. N. Huda for helping with valuable suggestions. I would like to thank members of physics office: Margie, Amy, Jean and Doug for all the help they have given me during my stay here at UTA. Finally I would like to dedicate this work to my parents and brother, without their understanding, patience and encouragement it would have been difficult to complete this work.

November 4th, 2005

ABSTRACT

ON THE EXISTENCE AND STABILITY OF CARBON
-BASED SILICON FULLERENES
- A DENSITY FUNCTIONAL
THEORETIC STUDY

Publication No. _____

Aravind Srinivasan, M. S.

The University of Texas at Arlington, 2005

Supervising Professor: Dr. A. K. Ray

The electronic and geometric properties of silicon-carbon fullerene-like nanostructures with two, four, six, twenty and twenty four carbon atoms on the surface of the Si_{60} cages by substitution, as well as inside the cage at various symmetry orientations have been studied within the generalized gradient approximation to density functional theory (GGA-DFT). The Perdew-Wang 91 (PW91) functional has been used to treat exchange and correlation energies. Full geometry and spin optimizations have been performed using Gaussian 03 suite of programs and the LANL2DZ basis set. Thus for the silicon

atom, the Hay-Wadt pseudopotential with the associated basis set are used for the core and valence electrons respectively. For the carbon atom, the Dunning/Huzinaga double zeta basis set is employed. Results on electronic state, binding energy per atom, HOMO-LUMO gap (Band gap), vertical ionization potential (energy required to ionize the system), vertical electron affinity (energy required to add an electron to the system) and dipole moment for all the stable silicon –carbon fullerene like nanostructures are presented and discussed in detail. The average Si-C bond length and average C-C bond length are also presented. The natures of the bondings between the Si-C and C-C are studied in detail using the NBO (Natural Bond Orbital) program. It was found that the optimized silicon-carbon fullerene like nanostructures have increased stability compared to the bare Si_{60} cage. The binding energy per atom for the stable silicon-carbon fullerene like nanostructures increase with the number of carbon atoms, with the structures having carbon atoms on the surface having higher binding energies (3% for $Si_{58}C_2$ to 38% for $Si_{36}C_{24}$) than the structures with carbon atoms inside the Si_{60} cage (2.5 % for $Si_{60}C_2$ to 27% for $Si_{60}C_{24}$). The stability of these nanostructures depends on the orientation of carbon atoms, as well as on the nature of bonding between silicon and carbon atoms (for two and four carbon atoms) and nature of onding between Si-C and C-C bonding (for six, twenty and twenty four carbon atoms).

TABLE OF CONTENTS

LIST OF ILLUSTRATIONS

LIST OF TABLES

CHAPTER 1

INTRODUCTION

1.1 Cluster Physics

Atomic and molecular clusters continue to be a very active field of research and extend through physics, chemistry and engineering [1-5]. Their investigation helps to understand the first stages in the formation of condensed matter [6]. Clusters are entities intermediate between single atoms and molecules and bulk matter. Clusters exhibit many properties different from their constituent atoms and from their bulk states, which distinguishes their branch of science called "cluster science" [7-8]. A large surface/volume ratio and quantum effects resulting from small dimensions are usually prominent in clusters and ideas like "super-atoms", "magic numbers" or "fission" in clusters have prompted a wide class of scientists to study this "relatively" new area of the physical sciences [9]. Clusters present properties that vary dramatically with size, and this attribute opens the possibility of controlling these properties by precisely controlling their formation process [10]. Nanoclusters, aggregates of atoms and molecules of nanometric size, are very important as the potential building blocks of nanoscience and nanotechnology and also for their potential industrial applications such as for electronic devices, memory devices and catalysis [10]. Compared with molecules,

nanoclusters do not have a fixed size or composition. Important examples of nanoclusters are the so called "fullerenes", clusters composed of sixty carbon atoms in a spherical cage (also known as buckyballs). They are magically stable (high ionization potential, low electron affinicty and high binding energy) and can be easily produced in macroscopic amounts [10]. Cage like compact clusters/ nanostructures are particularly important as they may be used as building blocks of more stable materials and the hollow space inside the cage can be doped with different suitable atoms leading to atomically engineered nanostructures with specific scientific and technological applications. For example, well controlled nanostructures with varying HOMO-LUMO gaps (Highest Occupied Molecular Orbital – Lowest Unoccupied Molecular Orbital) and desired conduction properties can be achieved by controlling doping of atoms in C_{60} [11, 12]. Also, the spectral properties of C_{60} fullerenes can be tuned by substitutional doping of 12 boron and 12 nitrogen atoms ($C_{48}B_{12}$, $C_{48}N_{12}$) [13, 14].

1.2 Silicon Clusters

Metal and semiconductor clusters are the most extensively studied clusters both by theoretical and experimental methods [5-6, 10]. Semiconductor clusters are very important as they are the building blocks for the miniature devices. Silicon is one of the most important and extensively used semiconductors in the industry. Silicon nanoclusters are very important for their potential applications in microelectronics industry [10]. The continued miniaturization of the electronic devices has led to the studies on silicon nanostructures. *Ab initio* Hartree-Fock and density functional theories [15-21] have been used to predict the ground state structures of the bare silicon

clusters. Some of these structures are controversial and there are not enough experimental studies for confirmation of the ground state structures [22]. The discovery of magically stable C_{60} fullerene cage and subsequently carbon nanotubes have prompted scientists to study silicon fullerene like cage structures, as they can be used as building blocks for fabricating various nanostructures in electronic devices. Silicon nanoclusters are also important for their potential applications in optoelectronic devices, tunable lasers, tagging and display materials etc. However, though silicon and carbon occupy the same column of the periodic table, they exhibit different properties due to differences in their nature of bonding. Carbon clusters (C_n) preferring sp^2 hybridization have been found to exist in fullerene like structures for n as small as 20 [23-25], where as for silicon clusters (Si_n) these structures are unstable and starting from n=19, ground state structures drastically change from prolate assemblies of Si_9 subunits to more compact cage like geometries. Theoretical studies on the Si_{60} fullerene cage have indicated a distorted cage structure and that the Si_{60} fullerene cage is not as stable as the C_{60} fullerene cage [26-33]. Menon *et al* showed that replacement of carbon atoms in the C_{60} fullerene cage by silicon atoms yielded a puckered cage structure indicative of silicon's preference for sp^3 type bonding [34]. In a series of articles [35-38], Zheng and Zhao *et al* have recently studied stuffed fullerene structures for medium size silicon structures. For example, taking Si_{40} as prototype, they have investigated stuffed fullerene cages with different "stuffing/cage" ratios, a typical example being $Si_4@Si_{36}$. They suggest that stuffed fullerene cages are the preferred (comparing with the experimental results) structural growth pattern of medium-sized silicon clusters. Hiura

et al [39, 40] showed that the spin state of a tungsten atom inserted in to the Si_{12} hexagonal cage is preserved as it is quantum mechanically isolated from the cage and this preserved spin property of tungsten atom can be used as the smallest memory devices for quantum computers.

1.3 Stabilization of silicon fullerene like structures

Stabilization of silicon fullerene-like cage structures containing dopant atoms has actually been a major field of study in the last few years [41-51]. The major goal in this work is two-fold: (1) to design silicon based nanostructures with potential applications like carbon fullerenes (nanotubes, superconducting and field effect devices); and (2) is to study possible magnetic properties of these structures. The second property might be particularly important in memory devices though it has been noted that silicon cages can almost quench the magnetic moments of transition metal atoms (such as Cr, Mo, and W) encapsulated in the cage [41, 42]. Studies have showed that highly stable small silicon cage clusters can result if transition metal atoms are encapsulated inside the silicon cages [43-45] and in particular, the Si_{20} fullerene stabilization by thorium encapsulation [46]. Kumar *et al* [46] found the thorium to be the only element among those considered that stabilizes this fullerene with icosahedral symmetry in the neutral state (net charge zero). Jackson *et al* [47] showed that a strongly bound silicon endohedral system is possible with Zirconium inside the cage. Xiao *et al* [48] showed that stable small silicon cage-like structures can be created by doping copper atoms inside the silicon cages. Larger silicon clusters such as stable Si_{60} fullerene-like cages

are possible by doping magic clusters such as $Al_{12}X$(X=Si, Ge, Sn, Pb), $Ba@Si_{20}$ and $Au_{12}W$ inside the Si_{60} cage [49-51].

1.4 Silicon carbide clusters

Several theoretical and experimental studies have been performed to determine ground state structures for carbon and silicon clusters individually, but the combinations of silicon and carbon atoms in a cluster have generated numerous theoretical and experimental studies on silicon carbide clusters. First, investigation of these clusters allows further understanding of the differences between the properties of silicon and carbon, and the bonds they form. Second, SiC, SiC_2 and SiC_4 have been observed in interstellar space and they are thought to play important roles in chemical reactions [52, 53]. Third, SiC clusters are involved in technological processes such as chemical vapor deposition used for the manufacture of SiC thin films and this property is potentially important for electronics industry (superior electronic devices withstanding high temperature, pressure and corrosion)[54]. Theoretical studies have been reported for C_{60} inside Si_{60} fullerene-like cages which yielded a highly distorted structure [50, 51]. As said before, carbon-rich silicon carbide clusters have been investigated in detail in the fields ranging from cluster science to astrophysics [52-62]. Silicon carbide cluster studies have been mostly focused on carbon rich cage type clusters and, to the best of our knowledge, silicon-rich cage type silicon carbide clusters have not been investigated in detail so far. Huda *et al* have shown previously using Hartree-Fock based Moller-Plesset perturbation theory calculations, that carbon dimers trapped in medium size silicon clusters(Si_n , n=8-14) produced structures comparable in stability to the

transition metal encapsulated silicon cage clusters. In particular closed fullerene like $Si_{14}C_2$ structures could be candidates for highly stable clusters [63]. Stable Si_nC_2 (n=8-14) clusters are shown in figure 1.1. Huda *et al* also reported using gradient corrected density functional theory (DFT), a class of highly symmetric and stable novel silicon-carbide fullerene-like cage nanostructures with carbon atoms inside the Si_{20} cage ($Si_{20}C_n$, $3 \leq n \leq 6$) [64]. The stability of the clusters are found to be dependent on the orientation of carbon atoms inside the Si_{20} cage. Stable structures of $Si_{20}C_n$ are shown in Figure 1.2.

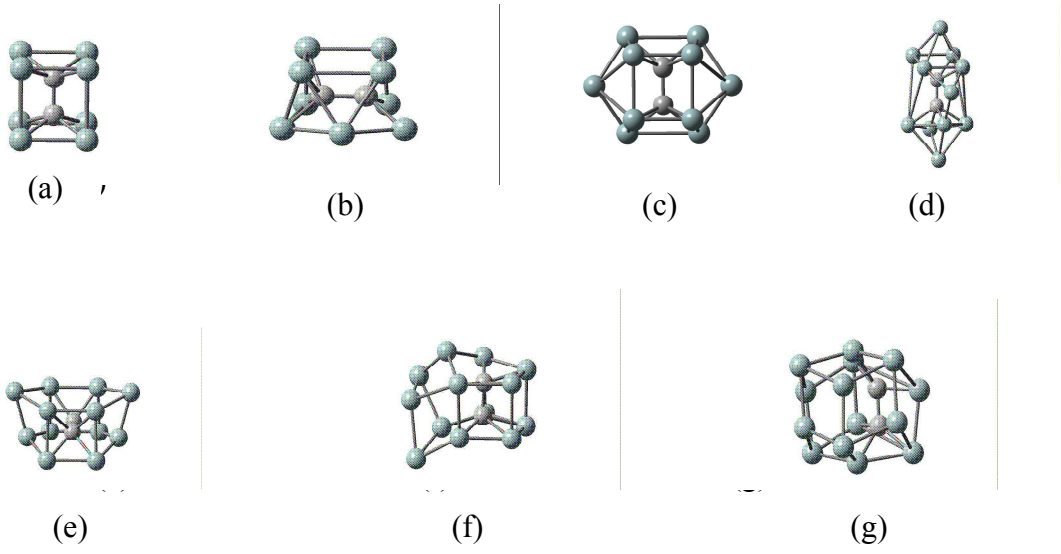

Figure 1.1: Stable Si_nC_2 structures [63] (a) Si_8C_2 (b) Si_9C_2 (c) $Si_{10}C_2$ (d)$Si_{11}C_2$ (e) $Si_{12}C_2$ (f) $Si_{13}C_2$ (g) $Si_{14}C_2$

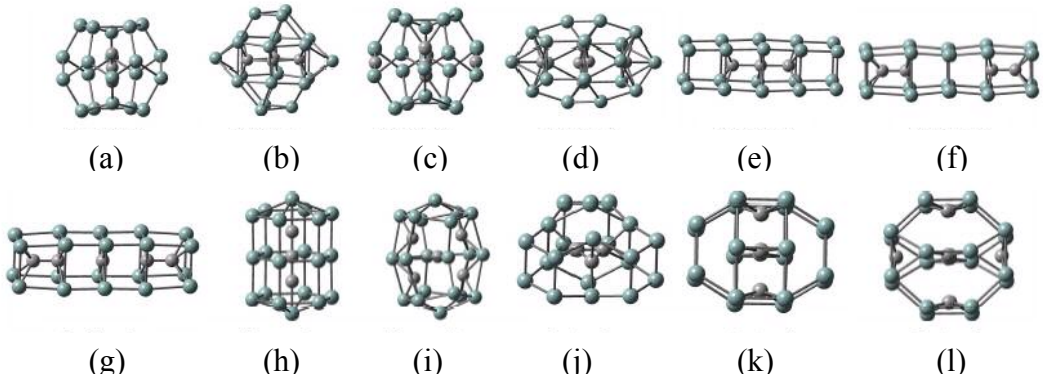

Figure 1.2: Stable $Si_{20}C_n$ structures ($3 \leq n \leq 6$) [64] (a) Penta-3 (b) Penta-4 (c) Penta-5 (d) Penta-6 (e) Cubic-3 (f) Cubic-4 (g) Cubic-5 (h) Hexa-3 (i) Hexa-5 (j) Octa-3 (k) Octa-4 (l) Octa-6.

1.5 Silicon –Carbon fullerene like nanostructures

To the best of our knowledge, there have been no attempts to synthesize silicon-carbon fullerene like nanostructures. By intuition, it is expected that silicon also forms stable fullerenes, since it is in the same column of periodic table as carbon, but due to their differences in the nature of bonding, silicon fullerene like nanostructures have been found to be unstable. Similar to carbon nanotubes, recent theoretical and experimental studies have shown that creation of silicon nanotubes is feasible, but they are not as smooth and stable as carbon nanotubes [65, 66]. We have shown before that stable silicon nanotubes and germanium nanotubes are theoretically plausible. Some structures of silicon and germanium nanotubes are shown in Figure 1.3.

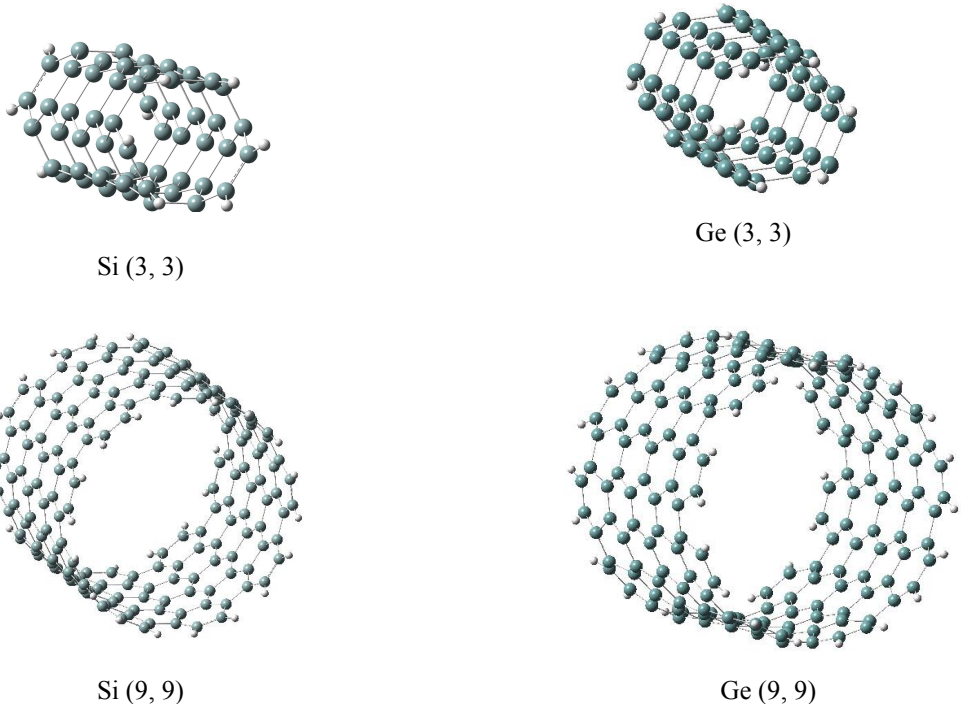

Figure1.3: Armchair (3, 3) and (9, 9) silicon and germanium nanotubes [67]

The purpose of this thesis is to explore the plausibility of stable silicon-carbon fullerene like nanostructures as a continuation of Huda *et al* [63-64] previous studies on stabilizing medium size silicon structures by the carbon atoms and also on the high stabilities of mixed silicon-carbon clusters. Here, we report our attempts to stabilize the Si_{60} fullerene cage by adding carbon atoms (2, 4, 6, 20 and 24) on the surface of the cage by substitution as well as inside the fullerene cage at different possible orientations. For the carbon atoms inside the fullerene cages, we have inserted the ground state structures of carbon atoms as well as repeated the surface orientations inside the cage as a test of Si-C bond strength. Our first objective in this work is to study how the number and orientations of carbon atoms on the surface as well as inside the Si_{60} fullerene like cage affect the stability of the cage. The second objective is to

study the nature of Si-C and C-C bonding with in novel carbon based silicon fullerene like nanostructures.

The thesis is organized as follows: Chapter 3 contains the discussions on $Si_{58}C_2$, $Si_{60}C_2$, $Si_{56}C_4$ and $Si_{60}C_4$ fullerene like nanostructures, followed by the discussions on $Si_{54}C_6$ and $Si_{60}C_6$ fullerene like nanostructures in Chapter 4, followed by the discussions on $Si_{40}C_{20}$, $Si_{60}C_{20}$, $Si_{36}C_{24}$ and $Si_{60}C_{24}$ fullerene like nanostructures in Chapter 5. Chapter 6 contains conclusions and suggestions for future work.

CHAPTER 2

THEORY

2.1 Density Functional Theory

2.1.1 Introduction

Density functional theory (DFT) is currently the most popular method in condensed matter physics and quantum chemistry for solving the many body quantum mechanical problems. Conceptually simpler and formally rigorous density functional theory provides an elegant way of mapping an N variable system to a single variable, the system's density [17]. This reduces the computational cost significantly over the traditional *ab initio* theories such as Hartree-Fock theory [15, 16], while retaining the much of the computational accuracy. In principal, density functional theory is an 'exact' theory and is applicable to any interacting system with an external potential. Approximations enter while treating the exchange-correlation effect by the functionals and the accuracy of the calculations depends on the representibility of the functionals, though the conditions for the representability of the functionals are still not well defined. However, continual developments of the functionals by including the local, semi-local and, recently, the dynamic effects (in DFT nomenclature these are called LDA, GGA and meta-GGA, respectively) increase the predictability and accuracy of

computations [70, 75-82]. In the following we will present a short description of density functional theory following mostly the reviews of Yang and Parr [17], Capelle [68] and Nagy [69].

2.1.2 Hohenberg-Kohn Theorem

Let us consider a system of N electrons under the influence of some time-independent external potential. Hohenberg-Kohn theorem [70] states that, the external potential $v(\vec{r})$ is determined solely by the electron density $\rho(\vec{r})$, within a trivial additive constant. The basic difference from the traditional quantum mechanics is that in density functional theory we solve for the density rather than the wave functions. Of course densities are defined from the wave function in a very trivial manner:

$$\rho(\vec{r}_1) = N\int \Psi^*(\vec{x}_1,\vec{x}_2,\ldots,\vec{x}_N)\Psi(\vec{x}_1,\vec{x}_2,\ldots,\vec{x}_N)ds_1 d\vec{x}_2 d\vec{x}_3 \ldots d\vec{x}_N \tag{2.1}$$

where Ψ is assumed to be normalized to unity; and $\vec{x}_i$'s include both spin and spatial variables which, in equation (1) are integrated out for i = 2 to N, including the spin part of the first particle. So once the density of electrons is known the other electronic properties can also be computed. For example, the total number of electrons is given by:

$$N = \int \rho(\vec{r})d\vec{r} \tag{2.2}$$

Also from Kato's theorem [71], which is applicable only to the Coulomb potential, we get:

$$Z_\beta = -\frac{1}{2\rho(\vec{r})}\frac{\partial\rho(\vec{r})}{\partial r}\bigg|_{r=R_\beta} \tag{2.3}$$

where the partial derivatives are taken at the nuclei β. So from the equation (3) we see that from the cusps of the density define the position of the nuclei, R_β, and the atomic number Z_β. In general $v(\vec{r})$ in the Hohenberg-Kohn theorem is not restricted to the Coulomb potentials.

Let us now proceed to prove the Hohenberg-Kohn theorem following the original approach of their papers. The original proof was both simple and elegant, and was done by reduction ad absurdum, basically for the non-degenerate systems. However the general conclusion is applicable to degenerate system as well. The proof follows like this:

Let us suppose that, in addition to $v(\vec{r})$ there exists another potential $v'(\vec{r})$ due to the same density $\rho(\vec{r})$, and that $v(\vec{r}) \neq v'(\vec{r}) + c$, where c is just an additive constant. Now due to this two potentials we will have two ground state wave functions Ψ and Ψ' corresponding to two Hamiltonian H and H' with the ground state energies of E and E', respectively. The Hamiltonians are defined as:

$$H = T + V_{ee} + \sum_i^N v(\vec{r}_i), \tag{2.4}$$

where T and V_{ee} are the kinetic energy and electron-electron repulsion operators defined as below:

$$T = -\frac{1}{2}\sum_i^N \nabla_i^2 , \tag{2.5}$$

$$V_{ee} = \sum_{i<j}^N \frac{1}{r_{ij}}, \tag{2.6}$$

Here we use the atomic units where

$$e^2 = \hbar = m_e = 1 .$$

where e is the electronic charge, $\hbar$ is the Plank's constant and m_e is the electron mass. In this unit energies are given in Hertrees, $1H$ = 27.2116 eV = 627.4 kcal/mol and the distances are in Bohr, a_o = 0.529 Å.

From Rayleigh_Ritz variational principal it follows that

$$E_0 = \langle \Psi | H | \Psi \rangle < \langle \Psi' | H | \Psi' \rangle = \langle \Psi' | H | \Psi' \rangle + \langle \Psi' | H - H' | \Psi' \rangle$$

$$= E_0' + \int \rho(\vec{r}) [v(\vec{r}) - v'(\vec{r})] dr \qquad (2.7)$$

Similarly, using the variational principle for the Hamiltonian H' with the trial wave function Ψ, we have

$$E_0' = \langle \Psi' | H' | \Psi' \rangle < \langle \Psi | H' | \Psi \rangle = \langle \Psi | H | \Psi \rangle + \langle \Psi | H' - H | \Psi \rangle$$

$$= E_0' + \int \rho(\vec{r}) [v(\vec{r}) - v'(\vec{r})] dr \qquad (2.8)$$

Addition of equation (2.7) and (2.8) leads to

$$E_0 + E_0' < E_0' + E_0 \qquad (2.9)$$

which clearly is a contradiction, so we can conclude that given the electronic density, the external potential is determined, so as all the other electronic properties, for example total energy.

Let us write the total energy as,

$$E_v(\rho) = T(\rho) + V_{ne}(\rho) + V_{ee}(\rho)$$

$$= \int \rho(\vec{r}) v(\vec{r}) d\vec{r} + F_{HK}[\rho] \qquad (2.10)$$

where,

$$F_{HK}[\rho] = T(\rho) + V_{ee}[\rho] \tag{2.11}$$

Here, V_{ee} includes both the classical and non-classical (for example, Coulomb and exchange interactions) contributions and F_{HK} is the Hohenberg-Kohn functional, which does not depend on the external potential as can be seen from equation (2.11) and so is a universal functional of $\rho(\vec{r})$.

The second Hohenberg-Kohn theorem states that for a trial density $\tilde{\rho}(\vec{r})$, such that $\tilde{\rho}(\vec{r}) \geq 0$, and $\int \tilde{\rho}(\vec{r})d\vec{r} = N$,

$$E_0 \leq E_v[\tilde{\rho}] \tag{2.12}$$

where, $E_v[\tilde{\rho}]$ is the energy functional of equation (2.10). The proof will be done by the use of variational principle. For any trial density $\tilde{\rho}(\vec{r})$, according to the Hohenberg-Kohn first theorem, it has its won potential $v(\vec{r})$, Hamiltonian *H* and wave function $\tilde{\Psi}$. So we get following equation (2.10),

$$\left\langle \tilde{\Psi} \middle| H \middle| \tilde{\Psi} \right\rangle = \int \tilde{\rho}(\vec{r})v(\vec{r})d\vec{r} + F_{HK} = E_v[\tilde{\rho}] \geq E_v[\rho] \tag{2.11}$$

Now the variation of total energy with the constraint that the total electrons are fixed, we get,

$$\delta\left\{E_v[\rho] - \mu\left[\int \rho(\vec{r})d\vec{r} - N\right]\right\} = 0 \tag{2.12}$$

which leads to the Euler-Lagrange equation

$$\mu = \frac{\delta E_v[\rho]}{\delta\rho(\vec{r})} = v(\vec{r}) + \frac{\delta F_{HK}}{\delta\rho(\vec{r})} \tag{2.13}$$

where the Lagrange multiplier μ is the chemical potential. Now if the exact form of the functional F_{HK} is known, the equation (2.12) then would be an exact equation for the ground state electron density. The functional F_{HK} is defined only for those trials $\rho(\vec{r})$ which are *v*-representable, meaning that the $\rho(\vec{r})$ corresponds to a anti-symmetric ground state wave function of some Hamiltonian with external potentials $v(\vec{r})$. The conditions for the density to be *v*-representable is yet unknown. However it turned out that the density functional theory can be formulated on a density which satisfies a weaker constraint than that of *v*-representability, namely *N*-representability. A density is *N*-representable if it can be derived from some anti-symmetric wave functions. Based on the *N*-representable density, Levy's constrained search method is described below which eliminates the degeneracy limitations in the proof of original Hohenberg-Kohn theorem.

2.1.2.1. The Method of Constrained Search

This method was first developed by Levy and Lieb [72-74]. A Universal function $F[\rho]$ defined as a sum of kinetic and Coulomb repulsion energies:

$$F[\rho] = \underset{\Psi \to \rho}{Min} \langle \Psi | T + V_{ee} | \Psi \rangle \tag{2.14}$$

$F[\rho]$ searches all wave functions Ψ which yield the fixed trial density ρ, and ρ need not to be *v*-representable.

Now the ground state energy can be written as:

$$E_0 = \underset{\Psi\to\rho}{Min}\left\langle \Psi \left| T + V_{ee} + \sum_i^N v(r_i) \right| \Psi \right\rangle \tag{2.15}$$

$$= \underset{\rho}{Min}\left\{ \underset{\Psi\to\rho}{Min}\left\langle \Psi \left| T + V_{ee} + \sum_i^N v(r_i) \right| \Psi \right\rangle \right\}$$

$$= \underset{\rho}{Min}\left\{ \left[\underset{\Psi\to\rho}{Min}\left\langle \Psi \left| T + V_{ee} \right| \Psi \right\rangle + \int v(\vec{r})\rho(\vec{r})d\vec{r} \right] \right\} \tag{2.16}$$

Now using the definition of $F[\rho]$ from equation (2.14) we can write equation (2.16) as:

$$E_0 = \underset{\rho}{Min}\left\{ F[\rho] + \int v(\vec{r})\rho(\vec{r})d\vec{r} \right\}$$

$$= \underset{\rho}{Min}\, E[\rho] \tag{2.17}$$

where

$$E[\rho] = F[\rho] + \int v(\vec{r})\rho(\vec{r})d\vec{r}. \tag{2.18}$$

In the constrained search formula for the functional $F[\rho]$ there is no reference that ρ needs to be *v*-representable ground state density, as long as it is constructed from an anti-symmetric wave function. However, when ρ is *v*-representable we get:

$$F[\rho] = F_{HK}[\rho] \tag{2.19}$$

The functional $F[\rho]$ is universal because it does not depend on the external potential $v(\vec{r})$. This constrained search method remove the degeneracy problem from the original Hohenberg-Kohn theorem, for in the approach only one of a set of degenerate wave functions is selected which is corresponding to the given ρ.

2.1.3 The Kohn-Sham Method

The ground state electron density can be in principle determined by solving the Eular-Lagrange equation (13)

$$\frac{\delta F(\rho)}{\delta \rho} + v(\vec{r}) = \mu. \tag{2.20}$$

where μ is the Lagrange multiplier associated with the constraint:

$$\int \rho(\vec{r}) d\vec{r} = N$$

Here the exact form of the functional $F[\rho]$ in equation (2.20) is not known:

$$F(\rho) = T[\rho] + V_{ee}[\rho]. \tag{2.21}$$

As can be seen from the above equation the basic problem is to evaluate the kinetic energy term. Kohn-Sham proposed [75] an indirect approach to this problem, which is described in the following.

Let us consider a non-interacting system where electrons move independently in a common local potential v_s, where the electronic density $\rho(\vec{r})$ is the same as the interacting electronic system. This can be done as long as we ensure that the wave functions, from which $\rho(\vec{r})$ is constructed, are *N*-representable Hamiltonian is:

$$H_s = \sum_i^N \left(-\frac{1}{2}\nabla_i^2 \right) + \sum_i^N v_s(\vec{r}_i). \tag{2.22}$$

In the above Hamiltonian there is non electron-electron repulsion term. For this system we can write the non-interacting wave-function as the Slater determinant:

$$\Psi_s = \frac{1}{\sqrt{N!}} \det[\psi_1 \psi_2 \cdots \psi_N] \tag{2.23}$$

where ψ_i are the N lowest eigenstates of the one-electron Hamiltonian h_s:

$$h_s\psi_i = \left[-\frac{1}{2}\nabla_i^2 + v_s(\vec{r}_i)\right]\psi_i = \varepsilon_i\psi_i \tag{2.24}$$

The kinetic energy of this non-interacting system is,

$$T_s[\rho] = \langle \Psi_s | \sum_{i=1}^{N}\left(-\frac{1}{2}\nabla_i^2\right) | \Psi_s \rangle = \sum_i^N \langle \psi_i | -\frac{1}{2}\nabla_i^2 | \psi_i \rangle \tag{2.25}$$

while the density of the non-interacting system

$$\rho(\vec{r}) = \sum_i^N |\psi_i(\vec{x}_i)|^2 \tag{2.26}$$

is equal to that of the interacting one.

The kinetic energy functional $T[\rho]$ in equation (2.21), as mentioned before, is unknown, so we simply take the kinetic energy functional $T_s[\rho]$ of non-interacting system instead of $T[\rho]$. Let the difference between this two functional is $T_c = T - T_s$, and substituting this in equation (21) we get:

$$F[\rho] = T_s[\rho] + V_{ee}[\rho] + T_c[\rho] \tag{2.27}$$

The last two terms in the right hand side of equation (2.27) representing the electron-electron interaction and we can rewrite them as the Coulomb and exchange-correlation terms, respectively:

$$V_{ee}[\rho] + T_c[\rho] = J[\rho] + E_{xc}[\rho] \tag{2.28}$$

So equation (2.27) can be written as:

$$F[\rho] = T_s[\rho] + J[\rho] + E_{xc}[\rho] \tag{2.29}$$

So with the above functional the total energy of equation (2.18) can be written as:

$$E[\rho] = T_s[\rho] + J[\rho] + E_{xc}[\rho] + \int \rho(\vec{r}) v(\vec{r}) d\vec{r} \ . \tag{2.30}$$

Now the variation of equation (2.30) gives the Euler-Lagrange equation:

$$\mu = \frac{\delta E[\rho]}{\delta \rho} = \frac{\delta}{\delta \rho} \int \rho(\vec{r}) v(\vec{r}) d\vec{r} + \frac{\delta T_s[\rho]}{\delta \rho} + \frac{\delta J[\rho]}{\delta \rho} + \frac{\delta E_{xc}[\rho]}{\delta \rho}$$

$$= v(\vec{r}) + \frac{\delta T_s[\rho]}{\delta \rho} + \frac{\delta J[\rho]}{\delta \rho} + \frac{\delta E_{xc}[\rho]}{\delta \rho} \tag{2.31}$$

$$= v_{eff}(\vec{r}) + \frac{\delta T_s[\rho]}{\delta \rho} \tag{2.32}$$

where the Kohn-Sham effective potential is defined by:

$$v_{eff} = v(\vec{r}) + \frac{\delta J[\rho]}{\delta \rho} + \frac{\delta E_{xc}[\rho]}{\delta \rho}$$

$$= v(\vec{r}) + \int \frac{\rho(\vec{r}')}{|\vec{r} - \vec{r}'|} d\vec{r}' + v_{xc}(\vec{r}) \tag{2.33}$$

here we also defined the exchange-correlation potential as:

$$v_{xc}(\vec{r}) = \frac{\delta E_{xc}(\rho)}{\delta \rho} \tag{2.34}$$

Now let us rewrite equation (2.30) in terms of one electron orbitals:

$$E(\rho) = \sum_i^N \int \psi_i^* \left(-\frac{1}{2} \nabla^2 \right) \psi_i d\vec{r} + J(\rho) + E_{xc}[\rho] + \int v(\vec{r}) \rho(\vec{r}) d\vec{r} \tag{2.35}$$

and the electron density is, as in equation (2.26):

$$\rho(\vec{r}) = \sum_i^N |\psi_i|^2$$

So in equation (2.35) energy is expressed in terms of *N* orbitals.

Now taking the variation of energy in equation (2.35) with respect to the one-electron orbital ψ_i, along with the constraint that these orbitals are orthonormal to each other:

$$\int \psi_i^* \psi_j d\vec{x} = \delta_{ij} \tag{2.36}$$

We get,

$$\delta\left[E[\rho] - \sum_i^N \sum_j^N \varepsilon_{ij} \int \psi_i^*(\vec{x}) \psi_i(\vec{x}) d\vec{x} \right] = 0 \tag{2.37}$$

In equation (2.37) ε_{ij} are the Lagrange multipliers. Let us now consider the variation in the energy $E[\rho]$ given by the equation (2.35),

$$\delta E[\rho] = \left[\frac{\delta}{\delta \psi_i^*} \sum_i^N \int \psi_i^* \left(-\frac{1}{2}\nabla^2 \right) \psi_i d\vec{r} + \frac{\delta J}{\delta \psi_i^*} + \frac{\delta E_{xc}}{\delta \psi_i^*} + \frac{\delta}{\delta \psi_i^*} \int v(\vec{r}) \left(\sum_i^N |\psi_i|^2 \right) d\vec{r} \right] \delta \psi_i^* \tag{2.38}$$

Using chain rule for functional derivative, the first term in the right hand side gives,

$$\frac{\delta}{\delta \psi_i^*} \sum_i^N \int \psi_i^* \left(-\frac{1}{2}\nabla^2 \right) \psi_i d\vec{r} = \frac{\partial \psi_i^*}{\partial \psi_i^*} \left(-\frac{1}{2}\nabla^2 \right) \psi_i + \psi_i^* \frac{\partial}{\partial \psi_i^*} \left\{ \left(-\frac{1}{2}\nabla^2 \right) \psi_i \right\}$$

$$= -\frac{1}{2}\nabla^2 \psi_i \tag{2.39}$$

where derivative in the second term is zero. Similarly the last term in the variation of energy in equation (2.38) gives,

$$\frac{\delta}{\delta \psi_i^*} \int v(\vec{r}) \left(\sum_i^N |\psi_i|^2 \right) d\vec{r} = v(\vec{r}) \psi_i \tag{2.40}$$

So from equation (2.37), for any arbitrary variation of $\delta \psi_i^*$, we get using equations (2.39) and (2.40),

$$h_{eff}\psi_i = \left[-\frac{1}{2}\nabla^2 + \frac{\delta J[\rho]}{\delta\rho} + \frac{\delta E_{xc}[\rho]}{\delta\rho} + v(\vec{r})\right]\psi_i = \sum_j^N \varepsilon_{ij}\psi_j$$

$$\Rightarrow h_{eff}\psi_i = \left[-\frac{1}{2}\nabla^2 + v_{eff}(\vec{r})\right]\psi_i = \sum_j^N \varepsilon_{ij}\psi_j \tag{2.41}$$

Where $v_{eff}(\vec{r})$ is defined by equation (2.33). Now in equation (2.41) the Hamiltonian h_{eff} is a Hermitian operator, hence ε_{ij} is a Hermitian matrix which can be diagonalize by unitary transformation, which leads to the Kohn-Sham equations:

$$\left[-\frac{1}{2}\nabla^2 + v_{eff}(\vec{r})\right]\psi_i = \varepsilon_i\psi_i \tag{2.42}$$

Equation (2.42) (or equation (2.41)) is the central equation in the application of density function theory. These equations are usually solved by self-consistent methods which can be represented by the following flow-chart:

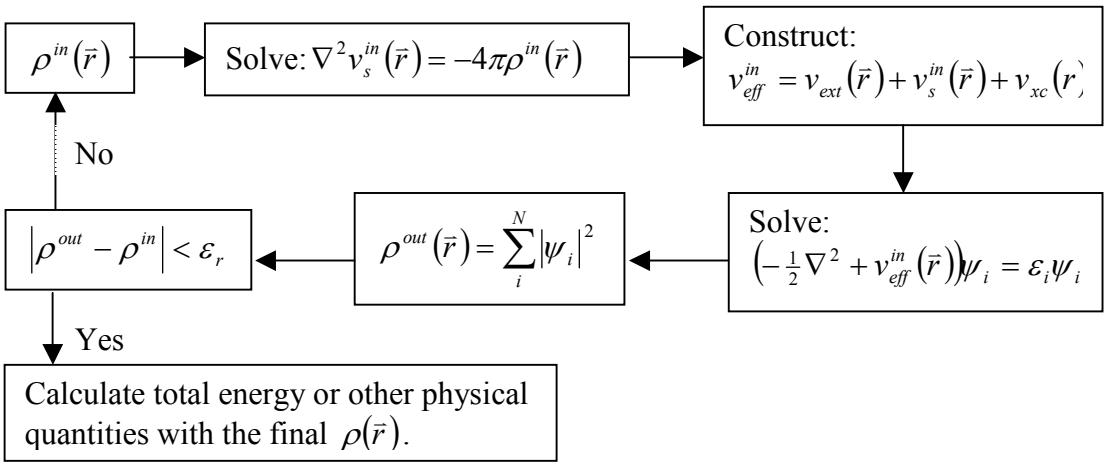

Figure 2.1 Flow-chart for DFT self-consistency loop

The solution of Kohn-sham equation is in principle is exact, but as can be seen from the above discussion of the Kohn-Sham procedure that, it does not give any prescription of obtaining the exchange-correlation functionals. Depending on the system at hand, different levels of approximations were made to deal with this functional. In the following, we will describe the local and generalized density approximations to these functionals.

2.1.4 The Local Density Approximations: LDA

Historically local density approximation to the functionals is the most used approach in the condensed matter physics. In this approximation the functionals are local, that is they depend only on the local variable. Formally, a functional *F* is local if,

$$F[\rho] = \int f(\rho(\vec{r}))d\vec{r} \tag{2.43}$$

where the functional *F* depends on $\vec{r}$ only through the density $\rho(\vec{r})$. Physically this approximation would be correct in the limit where the charge density is a slowly varying function with respect to the spatial variable, $\vec{r}$. Within the LDA the exchange and correlation energy becomes,

$$E_{xc}^{LDA}[\rho] = \int \rho(\vec{r})\varepsilon_{xc}(\rho)d\vec{r} \tag{2.44}$$

where $\varepsilon_{xc}(\rho)$ is the exchange and correlation energy per particle of a uniform electron gas of density $\rho(\vec{r})$. The exchange-correlation potential then is given by,

$$v_{xc}^{LDA}(\vec{r}) = \frac{\delta E_{xc}^{LDA}}{\delta\rho(\vec{r})} = \varepsilon_{xc}(\rho(\vec{r})) + \rho(\vec{r})\frac{\partial\varepsilon_{xc}}{\partial\rho} \tag{2.45}$$

Then the Kohn-Sham equation can be written as,

$$\left[-\frac{1}{2}\nabla^2 + v(\vec{r}) + \int \frac{\rho(\vec{r})}{|\vec{r}-\vec{r}'|} d\vec{r}' + v_{xc}^{LDA}(\vec{r})\right]\psi_i = \varepsilon_i \psi_i \tag{2.46}$$

Now the function $\varepsilon_{xc}(\rho)$ can be divided into exchange and correlation contribution [17],

$$\varepsilon_{xc}(\rho) = \varepsilon_x(\rho) + \varepsilon_c(\rho) \tag{2.47}$$

where $\varepsilon_x(\rho)$ is the Dirac exchange energy,

$$\varepsilon_x(\rho) = -\frac{3}{4}\left(\frac{3}{\pi}\right)^{1/3} \rho(\vec{r})^{1/3} \tag{2.48}$$

and $\varepsilon_c(\rho)$ is the correlation energy per particle of a homogeneous electron gas,

$$\varepsilon_c(\rho) = \begin{cases} 0.0311 \ln r_s - 0.048 + r_s(A \ln r_s + C) & \text{for } r_s << 1 \\ \frac{1}{2}\left(\frac{g_0}{r_s} + \frac{g_1}{r_s^{3/2}} + \frac{g_2}{r_s^2} + \cdots\right) & \text{for } r_s >> 1 \end{cases} \tag{2.49}$$

where r_s is the Wigner_seitz radius,

$$\frac{4}{3}\pi r_s^3 = \frac{1}{n} \tag{2.50}$$

We can extend the LDA to include spin for so-called unrestricted calculations. We can divide the total electronic density in two parts for spin up density (ρ_α) and spin down (ρ_β), so that,

$$\rho_\alpha(\vec{r}) + \rho_\beta(\vec{r}) = \rho(\vec{r}). \tag{2.51}$$

Then in the local spin density approximation the exchange-correlation functional can be written as,

$$E_{xc}^{LSD}\left[\rho_\alpha,\rho_\beta\right]=\int\rho(\vec{r})\varepsilon_{xc}\left(\rho_\alpha(\vec{r}),\rho_\beta(\vec{r})\right)d\vec{r} \tag{2.52}$$

As mentioned earlier, LDA (or LSD) is based upon the idealization that the system is a homogeneous electron gas with equal (or slowly varying) density. It is obvious that any real system could behave in a drastically different manner. However, the success and importance of the local density approximation in condensed matter physics is noteworthy. It gives results comparable or better than the Hartree-Fock approximation.

2.1.5 Generalized Gradient Approximation: GGA

Logically the first step to improve upon the LDA is to take into account the spatial change in electronic density, i.e., the gradient of the density, $\nabla\rho(\vec{r})$, to take into account the non-homogeneity of the true electron density. This method is named as the gradient expansion approximation (GEA). This can be done by a Taylor series expansion of the exchange-correlation functional,

$$E_{xc}^{GEA}\left[\rho_\alpha,\rho_\beta\right]=\int\rho(\vec{r})\varepsilon_{xc}\left(\rho_\alpha,\rho_\beta\right)d\vec{r}+\sum_{\sigma,\sigma'}\int C_{xc}^{\sigma,\sigma'}\left(\rho_\alpha,\rho_\beta\right)\frac{\nabla\rho_\sigma}{\rho_\sigma^{2/3}}\frac{\nabla\rho_\beta}{\rho_{\sigma'}^{2/3}}d\vec{r}+\cdots \tag{2.53}$$

The coefficient $C_{xc}^{\sigma,\sigma'}$ in equation (53) was found to be proportional to $1/\rho^{4/3}$. Unfortunately, GEA did not give a systematic improvement on the LDA approximation. The reason is that the exchange correlation interaction was not found physically very meaningful in this definition. In addition to it, higher order corrections of $\nabla\rho$'s are exceedingly difficult to calculate. However, a more sophisticated approach to include the gradient of densities was proposed by Perdew and others [76-81] called generalized

gradient approximation (GGA), which defines the exchange-correlation functional in the following manner,

$$E_{xc}^{GGA}\left[\rho_\alpha,\rho_\beta\right]=\int f\left(\rho_\alpha,\rho_\beta,\nabla\rho_\alpha,\nabla\rho_\beta\right)d\vec{r} \tag{2.54}$$

In practice, E_{xc}^{GGA} is divided into its exchange and correlation contributions,

$$E_{xc}^{GGA}=E_x^{GGA}+E_c^{GGA}, \tag{2.55}$$

and the approximations for the functionals are usually made individually.

Several suggestions for the explicit dependence of *f* on the densities and their gradient have been proposed over the year, including the functionals which include the parameters which are calibrated against some reference systems. Among the most widely used functionals are the 1986 Perdew functions [76], where the correlation functional contained on empirical parameter. The Perdew-Wang 1991 [77 -79] functional (PW91) incorporates no empirical parameters and is determined from the uniform electron gas approximations and with exact constraints. A refinement on PW91 was done by Perdew, Burke and Ernzerhof, the PBE functional [80]. Another popular functional for correlation is due to Lee, Yang and Parr (LYP) [81], which is not based on uniform electron gas, and obtained the correlation energy as an explicit functional of the density, its gradient. The LYP functional contained one empirical parameter. This correlation functional is often combined with Becke's exchange functional [82] and is known as BLYP.

It should be mentioned in here that GGA does not provide a complete non-local functional. In true mathematical sense, $\rho(\vec{r})$, and its gradient $\nabla\rho(\vec{r})$ depends only on $\vec{r}$,

and is independent of any $\rho(\vec{r}')$, where $\vec{r}' \neq \vec{r}$. Only advantage GGA achieved is that it includes the local variation of the densities. Also GGA in its original form does not produce the simultaneous asymptotic behavior for both the energy and the potentials. In the modern day functionals, a cut-off procedure on density is used to produce the satisfactory results. However, GGA functionals does show improvements over LDA functionals in many systems in condensed matter physics and quantum chemistry, with the exception in the long range weakly bound system, for instance in van der Waals interaction.

CHAPTER 3

STABILITY OF $Si_{60}C_{2n}$ FULLERENE LIKE NANOSTRUCTURES (n=1, 2)

3.1 Results and Discussions on $Si_{58}C_2$, $Si_{60}C_2$, $Si_{56}C_4$ and $Si_{60}C_4$ Nanostructures

One of the primary concerns for an *ab initio* study of the type reported here is the selection of the basis set and the type of the exchange-correlation used for calculation. The theoretical formalism of generalized gradient approximation to density functional theory has been used with Perdew-Wang (PW91) [76-80] exchange-correlation functional. The selection of proper basis set is a trade-off between the computational cost and the accuracy. Keeping this in mind, we have decided to represent a fairly large system like the novel carbon based silicon fullerenes by the LANL2DZ basis set [83]. For the silicon atom, the Hay-Wadt pseudo-potential with the associated basis set are used for the core electrons and the valence electrons, respectively. For the carbon atom, the Dunning/Huzinaga double zeta basis set [84] is employed. The Hay-Wadt effective core potentials and the associated basis set for silicon atom is shown in Table 3.1 and Table 3.2. The Dunning/Huzinaga basis set for the carbon atom is shown in Table 3.3. The basis set has been tested for silicon and carbon at atomic level for ionization potential (IP) and electron affinity (EA) with the experimental values. This basis set has also been tested for SiC dimer's optimized bond length, ionization potential (IP), electron affinity (EA) and binding energy per atom

(BE) with the known experimental values. The values of IP, EA for the silicon and the carbon atom are shown in Tables 3.4 and 3.5 and the values of bond length, IP, EA , BE for SiC dimer are given in Table 3.6. These results clearly indicate that the choice of basis set does a good job for system studied in this work. Full geometry optimization of the cages has been performed without any symmetry constraints with the LANL2DZ basis set and Gaussian 03 suite of programs [85]. All computations have been performed at the supercomputing facilities at the University of Texas at Arlington.

Table 3.1: Hay-Wadt pseudopotentials for silicon atom

n_k	ζ_k	d_k
d potential		
1	505.3138	-10.0000
2	103.2221	-84.9236
2	23.4569	-30.3299
2	6.7506	-12.1049
2	2.1603	-1.8945
s-d potential		
0	689.4911	3.0000
1	114.1729	60.5207
2	35.7424	201.3086
2	9.4530	65.9400
2	2.2544	19.0301
p-d potential		
0	88.9379	5.0000
1	76.7774	6.6414
2	56.1481	247.5972
2	21.1874	129.3715
2	6.8277	47.4617
2	2.1001	11.7377

Table 3.2: Basis functions for silicon atom

Exponents(α_i)	**Coefficients(c_i)**
s orbitals	
1.2220000	0.274462
0.2595000	0.616689
0.0931100	0.558086
p orbitals	
2.5800000	-0.039785
0.2984000	0.521997
0.0931100	0.587382

Table 3.3: Dunning /Huzinaga basis set for carbon atom

Exponents(α_i)	**Coefficients(c_i)**
s orbitals	
4232.6100	0.002029
634.8820	0.015535
146.0970	0.075411
42.4974	0.257121
14.1892	0.596555
1.9666	0.242517
5.1477	1.000000
0.4962	0.542048
0.1533	0.517121
p orbitals	
18.1557	0.018534
3.9864	0.115442
1.1429	0.386206
0.3594	0.640089
0.1146	1.000000

Table 3.4: Ionization potentials (eV) for Si and C

Element	This work	Experimental[86]
Si	8.558	8.151
C	11.654	11.26

Table 3.5: Electron affinities (eV) for Si and C

Element	This work	Experimental[86]
Si	1.073	1.385
C	0.969	1.262

Table 3.6: Optimized Bond length (Å), IP, EA and BE /atom (all in eV) for SiC dimer

	This work				Experimental[87-90]			
Dimer	Opt BL	IP	EA	BE/atom	Opt BL	IP	EA	BE/atom
Si-C	1.77	9.368	2.228	2.155	1.719	9.2 +/- 0.4	-----	2.325 to 2.339

3.1.1 Bare Si_{60} cage

As is known, Si_{60} fullerene like cage has 12 pentagons and 20 hexagons. The optimized Si_{60} fullerene cage at GGA-DFT level of theory has binding energy/ atom of 3.61 eV and the structure is shown in Fig 3.1.

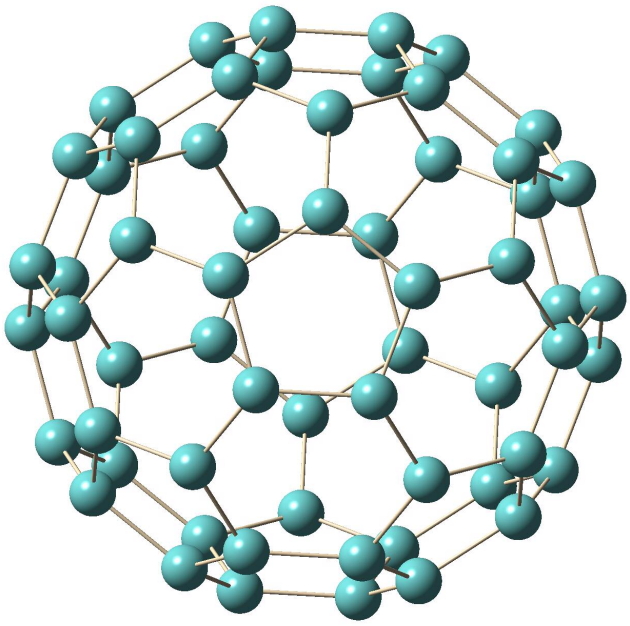

Binding energy/atom = 3.61 eV
(GGA-DFT)

Figure 3.1: Bare Si_{60} cage

In the first step, silicon atoms on the surface of the cage have been replaced by two and four carbon atoms at various symmetry orientations. In the second step, two and four carbon atoms have been put inside the Si_{60} cage at various possible orientations with

carbon atoms parallel and perpendicular to the pentagonal and hexagonal faces. In the third step, as a test of the SiC bond strength, we also put the carbon dimers and tetramers close to the surface, with the same surface orientation, at an initial optimized SiC dimer bond length of 1.77 Å and optimized the structures. For C_4 ground state structure, theoretical and experimental studies have reported that there are two structures almost degenerate in energy, one being a rhombus singlet D_{2h} and the other being triplet linear chain structure [91-98]. For this reason, carbon tetramers in rhombus, linear chain (as separated dimers) and also in trigonal planar arrangement optimized at GGA-DFT level of theory have been added inside the cage at various orientations.

In the results to follow, we report the electronic states, binding energies per atom (BE), highest occupied –lowest unoccupied molecular orbital (HOMO-LUMO) gaps, vertical ionization potentials (VIPs) , vertical electron affinities (VEAs) and total dipole moments of the stable fullerene-like $Si_{58}C_2$, $Si_{60}C_2$, $Si_{56}C_4$, and $Si_{60}C_4$ optimized structures [99] with their corresponding average Si-C and C-C bond lengths. Binding energies per atom of the clusters are calculated as the relative energies of these clusters in the separated atom limit, with the atoms in their respective ground states. VIP and VEA are calculated as the difference in the total energies between the neutral clusters and the corresponding positively and negatively charged clusters at the neutral optimized geometries. Harmonic frequencies were also calculated to make sure that the cage structures obtained were not the local minima. Bonding between the atoms,

especially Si-C and C-C for all the stable structures were analyzed using NBO (Natural Bonding Orbital) program and NBO View [100].

For the set of optimized $Si_{58}C_2$, fullerene like nanostructures are reported in Table 3.7 where the column under the structures refers to the positions of the carbon atoms substituting silicon atoms on the surface of the Si_{60} cage. The optimized geometries of all three structures in Table 3.7 are reported in Figure 3.2. The structure Maindiag (a) has two carbon atoms at diagonally opposite ends of the cage. The structure Penta-hexa (b) has two carbon atoms along the common side of a pentagon and a hexagon. The structure Hexa-hexa (c) has two carbon atoms along the common side of two hexagons. The first structure Maindiag has the highest BE per atom of 3.721eV in this set. The HOMO-LUMO gap of 0.733eV is also the highest. The total dipole moment of this structure is zero, indicating a highly symmetric charge distribution and strong covalent bonding nature contributing to its increased stability. The average Si-C bond length for this structure is 1.85 Å, which is the smallest in this group indicating stronger Si-C interaction. There is no C-C bonding in this structure. NBO σ and π bonds between Si-C for this structure are shown in Figure 3.16. The Penta-hexa structure has the highest VIP and VEA in this group, but the BE per atom and the HOMO-LUMO gap are slightly lower than the Maindiag structure. The average Si-C bond length for this structure is slightly higher compared to the Maindiag structure. The total dipole moment for this structure is 0.83D. The last structure Hexa-hexa has the lowest BE per atom of 3.712eV and the HOMO-LUMO gap is also the lowest in this set. The C-C bond length for this structure is 1.44 Å, indicating stronger

C-C interaction. However the average Si-C bond length is 1.91 Å, indicating the weakest Si-C interaction for this set. From NBO analysis, the numbers of Si-C bonds in these three structures are found to be 8, 6 and 4 respectively, which clearly follow the trend of stability. The vibrational frequencies for the most stable Maindiag structure in this set are listed in Table 3.15.

The second set of optimized structures, $Si_{60}C_2$ with carbon atoms inside the Si_{60} cage are listed in Table 3.9 and the corresponding geometries are presented in Figures 3.3 and 3.4. Here also the column under the structures represents the orientations of the carbon atoms inside the Si_{60} cage. The Penta-hexa structure (Fig 3.3 a) has the carbon dimer parallel to the common side of a pentagon and a hexagon at Si-C bond length. The Heper structure (Fig 3.3 b) has the carbon dimer closer to the surface in a plane perpendicular to the hexagonal face of the cage. The Maindiag structure (Fig 3.3 c) has two carbon atoms along the two ends of the perpendicular diagonal at Si-C bond length distance. The Hexa-hexa structure (Fig 3.3 d) has the carbon dimer parallel to the common side of two hexagons at Si-C bond length distance. The Peper structure (Fig 3.4 a) has the carbon dimer placed closer to the surface in a plane perpendicular to the pentagonal face of the cage. The Hepar structure (Fig 3.4 b) has the carbon dimer closer to the surface in a plane parallel to the hexagonal face of the cage. The structure Pepar (Fig 3.4 c) has the carbon dimer placed closer to the surface in a plane parallel to the pentagonal face of the cage.

The Penta-hexa structure in this set has the highest BE per atom of 3.700eV. The total dipole moment for this structure is 2.08D. NBO analysis of this structure yielded 4

Si-C σ bonds and one C-C double bond. For the next six structures in Table 3.9, the difference in binding energies per atom is at the meV level, maximum difference being 7 meV. A common feature in these six structures is that all have a C-C triple bond, except Maindiag where there is no C-C bond. It is interesting to note that in general, VEAs for $Si_{60}C_2$ structures are higher, whereas the VIPs and HOMO-LUMO gaps are lower than those of the $Si_{58}C_2$ structures. This indicates relatively higher chemically reactive characteristics for the $Si_{60}C_2$ structures. Particularly for Maindiag structure, it has the highest VEA, the lowest VIP and the smallest HOMO-LUMO gap. From Figure 3.7, we note that the two loosely bound silicon atoms may be responsible for these characteristics. Removal of those two silicon atoms makes this structure similar to the $Si_{58}C_2$ Maindiag structure, which is highly stable and relatively less reactive. The Hepar structure has the highest HOMO-LUMO gap and the Hexa-hexa structure has the highest VIP in this set. The vibrational frequencies of the most stable Penta-hexa structure in this set are listed in Table 3.16.

The third set of optimized structures is $Si_{56}C_4$ cages, which have four carbon atoms substituting the silicon atoms on the surface of the Si_{60} cage. These are reported in Table 3.11 and their corresponding geometries are presented in Figures 3.5 and 3.6. The structure Hex (Fig 3.5 a) has four carbon atoms at opposite sides of the hexagon. This has the highest BE per atom of 3.819eV in this set. The total dipole moment of this structure is 1.41D. NBO analysis of this structure yielded 10 Si-C bonds (8 σ bonds, 2 π bonds), 2 C-C σ bonds and 1 C-C π bond. NBO σ and π bonds between C-C and Si-C for this Hex structure are shown in Figure 3.17. The vibrational frequencies for this

most stable structure of this set are listed in Table 3.17. The structure Inpenta (Fig 3.5 b), which has four carbon atoms at four corners of a pentagon, has almost the same stability as the Hex structure. It has BE per atom of 3.817eV, 0.002eV less than the hex structure. The dipole moment of this structure is 0.52D indicating a slightly less ionic contribution to mixed ionic-covalent bonding. NBO analysis of this structure yielded 8 Si-C bonds with 6 σ bonds and 2 π bonds, 3 C-C σ bonds and 1 C-C π bond. The structure Hexa (Fig 3.5 c) has four carbon atoms at four corners of a hexagon adjoining two pentagons. The BE per atom is 0.005 eV less than the Hex structure. The VIP, VEA and the HOMO-LUMO gap for this structure is higher than the Hex and Inpenta structures. NBO analysis of this structure yielded 6 Si-C bonds (all σ bonds), 3 C-C σ bonds and 2 C-C π bonds. The number of Si-C bonds in this structure is lower than the Hex and Inpenta structures. Here again, from the above three structures it might be suggested that the decreasing number of Si-C bonds lowers the binding energy. However, one exception needs to be mentioned. Though the Maindiag structure (Fig 3.5 d) has 16 Si-C bonds (12 σ bonds and 4 π bonds), the binding energy per atom is 0.008eV less than the most stable structure of this set. As the four carbon atoms are situated at the opposite end of two perpendicular diagonals of this cage, there is no C-C bonding. This indicates that C-C bonding also contributes to the stability, absence of which might be the reason for Maindiag's lower binding energy. Zero dipole moment of this structure indicates a highly symmetric charge distribution and a strong covalent bonding. The Penta-hexa structure (Fig 3.6 b), which has four carbon atoms along the common side of pentagon and hexagon at two ends of the cage, has the highest HOMO-

LUMO gap and VIP in this set. The Hexa-hexa structure has the lowest BE in this set, 3.791eV per atom. In this structure the two carbon dimers are along the common side of two hexagons at opposite end of the cage. The total dipole moment for this structure is 0.01D indicating a very negligible ionic contribution to predominantly covalent bonding. This structure has the lowest VIP and highest VEA in this set. NBO analysis of this structure yielded 8 Si-C bonds (all σ bonds). The number of Si-C bonds in this structure is equal to the Inpenta structure and higher than the Hexa structure. This also shows that the C-C interactions and their arrangement affect the stability of the cage.

The last set of optimized nanostructures is $Si_{60}C_4$ cages which have four carbon atoms inside the Si_{60} cage. Here also before relaxation all the carbon atoms were placed inside the cage closer to the cage surface and also at Si-C bond length distance. These are reported in Table 3.13 and their corresponding geometries in Figures 3.21 to 3.40. From the table it can be found that some of the structures are degenerate in energy. For the sake of brevity, only few energetically most favorable structures will be discussed here. There are several structures which are comparable in stability as we increase the number of carbon atoms inside the cage from two to four. For example binding energies per atom for the first three structures in table 4 are within 6 meV. The structure Triangle (Fig 3.7 a) has four carbon atoms in trigonal planar arrangement closer to the surface in a plane parallel to a hexagonal face of the cage. This structure has the highest BE per atom of 3.787eV in the $Si_{60}C_4$ set. The dipole moment is 1.67D. The vibrational frequencies for this structure were all found to be positive, and these are listed in Table 3.18. Next the structure Hexa (Fig 3.7 b) has four carbon atoms parallel to the four

corners of a hexagon adjoining two pentagons. The BE per atom is 0.004eV less than the Triangle structure. The HOMO-LUMO gap of this structure is lower, but the VEA is higher than the Triangle structure. The dipole moment of this structure indicates a slight increase in the asymmetric charge distribution compared to the Triangle structure. The average Si-C bond length and C-C bond length for this structure are almost the same as before. However the HOMO-LUMO gap is almost half of the Triangle structure's gap. The structure Inpenta (Fig 3.7 c) has four carbon atoms along the four corners of a pentagon. The Si-C and C-C average bond lengths are comparable to the previous two structures. The Inpenta structure's BE per atom is 0.002eV less than the Hexa structure. It can be noted from Table 4 that the dipole moments of all these three structures are higher than the previously discussed structures. Particularly for Inpenta it is the highest, 3.80D. The highly asymmetric structure for these cages is responsible for this increased dipole moment.

A common feature of the above $Si_{60}C_4$ structures is that the carbon atoms pushed a few silicon atoms outside the cage, and as a result those silicon atoms become loosely bound to the cage. This is one of the main reason for the lower binding energy of these set compared to $Si_{56}C_4$ cages. For example, the structure Maindiag (Fig 3.9 c) in this set has no C-C bonding and has a low dipole moment indicating a strong covalent bonding and a highly symmetric charge distribution, but the BE per atom is 0.041eV less than the most stable Triangle structure. Absence of C-C bonding might be one of the reasons for the lower binding energy, but the primary reason is that the four silicon atoms, which are pushed out by the carbon atom, are loosely bound to the cage.

It is interesting to compare this structure with the $Si_{56}C_4$ Maindiag structure. Both the structures are similar provided the four loosely bound silicon atoms are removed from the $Si_{60}C_4$ cage, which resulted in 0.065eV per atom increase in binding energy and become more stable than the most stable structure of $Si_{60}C_4$ set, the Triangle structure. In addition to this the difference between the binding energy of $Si_{56}C_4$ Hex structure, highest in that group, and Maindiag structure is 0.008eV per atom. This example suggests that the mere presence of the C-C bonding would not significantly increase the binding energy; it is the Si-C interaction that is important. The most stable Triangle structure has 8 Si-C bonds, all of which are σ bonds. The next two structures, Hexa and Inpenta have each 6 Si-C bonds, which is less than the Triangle structure. This again might indicate that Si-C interaction is important for the stability.

In addition to above structures, several other possibilities were also tried. It was mentioned above that, carbon atoms (2 and 4) put inside the Si_{60} cage at various orientations closer to the cage surface, move closer to the surface and bond with silicon atoms, thereby pushing one or two silicon atoms outside the surface of the fullerene like cage. Silicon atoms those are pushed out of the $Si_{60}C_4$ and $Si_{60}C_2$ cage were removed and the corresponding structures were re-optimized. Re-optimized structures showed higher stability as expected from the removal of silicon atoms but were barely as stable as $Si_{56}C_4$ and $Si_{58}C_2$ clusters. We also tried to put carbon atoms at the center of the Si_{60} cages, but the structures were not stable. From Tables 3.7, 3.9, 3.11, and 3.13, it is clear that there is a general tendency of the increase in the binding energy per atom with the increase in the number of carbon atoms. In general, all the optimized structures

considered here are stable nanostructures with higher binding energies per atom compared to the bare Si_{60} cage which has a binding energy per atom of 3.61eV at GGA-DFT level of theory. Also, the carbon atoms substituting silicon atoms on the surface of the Si_{60} fullerene cage gives higher binding energies than carbon atoms put inside the Si_{60} cage. Thus, the stability of the nanostructures is found to be dependent on the number of carbon atoms and their orientations inside or on the surface of fullerene like cage.

As mentioned before that for most part the carbon-carbon interaction does not contribute significantly to the cage stability. It is the Si-C interaction that is important. For example, from Table 3.7 we note that for the most stable structure there is no C-C interaction, while in Table 3.9, the Maindiag ($Si_{60}C_2$), where there is no C-C bonding, is only 0.016eV/atom less stable than the highest stable one in that group. Similar conclusions can be made from the $Si_{56}C_4$ group (Table 3.11). In fact a part of the C-C interaction sometimes slightly offset the increased stability of the cages due to the fact that carbon atoms usually acquire some charges and their mutual Coulomb interaction is repulsive. However, for the $Si_{60}C_4$ group (Table 3.13), the difference between the B. E. of the most stable one and the one where there is no C-C bond is slightly higher, 0.041eV/atom, which is approximately 1 per cent of the total binding energy.

Considering the fact that inclusion of carbon atoms increased the Si_{60} cage binding energy by almost 5 per cent for this structure, 1 per cent is a significant contribution. The asymmetric charge distribution on the carbon atoms and the cage is responsible for this (Figure 3.15) increase in total binding energy in Triangle structure. In this structure,

the four carbon atoms are arranged in a planar triangular form, where the carbon atom at the center of the triangle is positively charged, and has no bonding with the silicon atoms. So the increased C-C attractive Coulomb interaction is added to the binding energy, and is responsible for the above fact. However it should be noted that despite this increased attractive C-C interaction, $Si_{60}C_4$ structures are less stable than the $Si_{56}C_4$ Maindiag structure, where C-C interactions do not play any significant role.

Table 3.7: Binding energy per atom (BE), HOMO-LUMO gap, VEA, VIP (all in eV), Dipole moment (Debye), Average Si-C bond length (Å) and C-C bond length (Å) for optimized $Si_{58}C_2$ fullerene like nanostructures.

Structures	**State**	**BE per atom (eV)**	**HOMO-LUMO gap (eV)**	**VEA (eV)**	**VIP (eV)**	**Dipole Moment (Debye)**	**Avg Si-C BL (Å)**	**C-C BL (Å)**
Maindiag	^1A	3.721	0.733	3.637	6.414	0.00	1.85	--
Penta- hexa	^1A	3.715	0.687	3.683	6.419	0.83	1.87	1.48
Hexa-hexa	^1A	3.712	0.652	3.646	6.364	0.89	1.91	1.44

Table 3.8: NBO σ bonds and π bonds between C-C and Si-C for the $Si_{58}C_2$ fullerene like nanostructures.

Structures	C-C σ bonds	C-C π bonds	Si-C σ bonds	Si-C π bonds
Maindiag	------	-------	6	2
Penta-hexa	1	-------	4	2
Hexa-hexa	1	1	4	------

Table 3.9: Binding energy per atom (BE), HOMO-LUMO gap, VEA, VIP (all in eV), Dipole moment (Debye), Average Si-C bond length (Å) and C-C bond length (Å) for optimized $Si_{60}C_2$ fullerene like nanostructures.

Structures	State	BE per atom (eV)	HOMO-LUMO gap (eV)	VEA (eV)	VIP (eV)	Dipole Moment (Debye)	Avg Si-C BL (Å)	Avg C-C BL (Å)
Penta-hexa	^{1}A	3.700	0.252	3.959	6.260	2.08	1.95	1.43
Heper	^{1}A	3.685	0.357	3.888	6.289	3.06	1.91	1.29
Maindiag	^{3}A	3.684	0.157	4.044	6.197	0.57	1.91	--
Hexa-hexa	^{1}A	3.683	0.389	3.854	6.306	1.67	1.93	1.29
Peper	^{1}A	3.682	0.441	3.783	6.286	2.78	1.91	1.28
Hepar	^{1}A	3.679	0.496	3.678	6.223	2.16	1.87	1.33
Pepar	^{1}A	3.678	0.335	3.890	6.273	1.99	1.89	1.29

Table 3.10: NBO σ bonds and π bonds between C-C and Si-C for the $Si_{60}C_2$ fullerene like nanostructures.

Structures	C-C σ bonds	C-C π bonds	Si-C σ bonds	Si-C π bonds
Penta-hexa	1	1	4	------
Heper	1	2	2	------
Maindiag	------	------	8	------
Hexa-hexa	1	2	2	------
Peper	1	2	2	------
Hepar	1	2	2	------
Pepar	1	2	2	------

Table 3.11: Binding energy per atom (BE), HOMO-LUMO gap, VEA, VIP (all in eV), Dipole moment (Debye), Average Si-C bond length (Å) and C-C bond length (Å) for optimized $Si_{56}C_4$ fullerene like nanostructures.

Structures	State	BE per atom (eV)	HOMO-LUMO Gap (eV)	VEA (eV)	VIP (eV)	Dipole Moment (Debye)	Avg Si-C BL (Å)	Avg C-C BL (Å)
Hex	^{1}A	3.819	0.616	3.645	6.342	1.41	1.87	1.45
Inpenta	^{1}A	3.817	0.501	3.646	6.244	0.52	1.85	1.48
Hexa	^{1}A	3.814	0.665	3.655	6.392	1.36	1.88	1.47
Maindiag	^{1}A	3.811	0.645	3.654	6.369	0.00	1.85	--
Tetra	^{1}A	3.808	0.576	3.690	6.358	0.95	1.85	1.49
Diag	^{1}A	3.807	0.456	3.742	6.285	0.67	1.86	1.46
Hexb	^{1}A	3.807	0.601	3.648	6.327	1.18	1.90	1.47
Penta-hexa	^{1}A	3.805	0.715	3.681	6.457	0.00	1.87	1.48
Hexa-hexa	^{3}A	3.791	0.255	4.075	5.893	0.01	1.89	1.45

Table 3.12: NBO σ bonds and π bonds between C-C and Si-C for the $Si_{56}C_4$ fullerene like nanostructures.

Structures	**C-C σ bonds**	**C-C π bonds**	**Si-C σ bonds**	**Si-C π bonds**
Hex	2	1	8	2
Inpenta	3	1	6	2
Hexa	3	2	6	------
Maindiag	------	------	12	4
Tetra	3	------	6	------
Diag	2	1	8	------
Hexb	3	1	6	------
Penta-hexa	2	1	8	------
Hexa-hexa	2	1	8	------

Table 3.13: Binding energy per atom (BE), HOMO-LUMO gap, VEA, VIP (all in eV), Dipole moment (Debye), Average Si-C bond length (Å) and C-C bond length (Å) for optimized $Si_{60}C_4$ fullerene like nanostructures.

Structures	State	BE per atom (eV)	HOMO-LUMO gap (eV)	VEA (eV)	VIP (eV)	Dipole Moment (Debye)	Avg Si-C BL (Å)	Avg C-C BL (Å)
Triangle	^{1}A	3.787	0.453	3.752	6.262	1.67	1.95	1.47
Hexa	^{1}A	3.783	0.252	3.982	6.253	2.16	1.92	1.44
Inpenta	^{1}A	3.781	0.454	3.696	6.242	3.80	1.87	1.46
Triangle-pepar	^{3}A	3.771	0.177	4.048	6.276	1.03	1.92	1.43
Rho-pepar	^{1}A	3.768	0.506	3.778	6.316	0.62	1.91	1.49
Tetra	^{1}A	3.762	0.364	3.836	6.248	1.50	1.90	1.45
Rho-heper	^{1}A	3.761	0.258	4.036	6.311	0.30	1.96	1.43
Hexb	^{1}A	3.758	0.457	3.810	6.310	1.79	1.93	1.46
Triangle-heper	^{1}A	3.756	0.512	3.669	6.245	2.39	1.96	1.44
Triangle-peper	^{1}A	3.755	0.234	4.024	6.310	2.58	1.95	1.43
Rho-peper	^{3}A	3.747	0.089	4.096	6.228	0.97	1.99	1.44
Rho-hepar	^{3}A	3.746	0.139	3.948	6.139	1.14	1.96	1.49
Maindiag	^{3}A	3.746	0.101	4.058	6.171	0.35	1.91	--
Lin-pepar	^{1}A	3.742	0.128	4.131	6.261	0.00	1.91	1.29
Diag	^{1}A	3.741	0.398	3.756	6.212	2.16	1.87	1.29
Lin-hepar	^{1}A	3.735	0.427	3.787	6.238	0.01	1.92	1.29
Hexa-hexa	^{1}A	3.735	0.372	3.826	6.236	3.52	1.92	1.29
Hex	^{1}A	3.734	0.217	4.088	6.315	1.31	1.90	1.30
Lin-heper	^{1}A	3.730	0.555	3.748	6.340	0.47	1.94	1.30
Penta-hexa	^{1}A	3.729	0.437	3.787	6.243	0.37	1.89	1.29

Table 3.14: NBO σ bonds and π bonds between C-C and Si-C for the $Si_{60}C_4$ fullerene like nanostructures.

Structures	**C-C σ bonds**	**C-C π bonds**	**Si-C σ bonds**	**Si-C π bonds**
Triangle	3	1	8	------
Hexb	3	3	6	------
Inpenta	3	2	6	------
Triangle-pepar	4	3	4	------
Rho-pepar	4	------	4	------
Tetra	3	1	8	------
Rho-heper	3	2	5	------
Hexa	3	1	8	------
Triangle-heper	4	2	3	------
Triangle-peper	4	2	3	------
Rho-peper	4	3	2	------
Rho-hepar	4	------	4	------
Maindiag	------	------	16	------
Lin-pepar	2	4	4	------
Diag	2	4	4	------
Lin-hepar	2	4	4	------
Hexa-hexa	2	4	4	------
Hex	2	4	4	------
Lin-heper	2	4	3	------
Penta-hexa	2	4	4	------

Table 3.15: Harmonic vibrational frequencies (in cm^{-1}) for the most stable Maindiag ($Si_{58}C_2$) structure

67.2528	68.9506	69.4892	71.5099	73.7224	75.7825
76.6665	78.2681	80.1385	83.6655	85.6104	86.2467
87.0711	88.1825	89.6015	89.8317	90.7293	91.6518
93.1846	97.1953	98.6862	100.5930	102.3428	103.5402
106.8975	107.3933	108.5157	109.6754	110.3648	112.6120
116.2148	116.5164	121.0070	122.6653	124.1451	125.1779
126.4958	128.9342	130.2034	131.5681	133.7737	136.5532
137.8029	138.0258	138.8841	139.6383	143.4462	147.7625
149.1803	150.3291	150.6827	152.3468	153.2762	153.5670
153.7882	154.8712	156.4148	157.8551	158.4162	160.2066
160.7908	163.1541	166.0594	166.3533	168.5544	173.7858
177.4844	177.6144	178.9859	182.6495	185.0177	188.5466
192.2359	192.5990	194.7615	195.8585	199.2020	199.6121
201.6535	201.9579	214.2247	218.8931	223.0151	230.5475
252.9123	255.7660	256.8913	263.5158	267.2846	304.4610
309.5043	312.4917	321.2037	322.2484	326.6787	336.7827
339.3550	346.4768	347.9267	353.6435	361.4630	363.0975
372.4991	375.5892	378.7841	379.1540	385.3190	387.1092
392.7387	393.2580	394.1669	399.9481	419.6895	427.0512
430.4219	434.0461	434.7724	437.6593	449.5708	455.3821
456.6676	458.2275	463.0661	464.6311	467.0505	467.4373
471.7322	473.0874	474.7745	476.6368	476.8719	477.2810
480.7753	483.3967	483.9850	485.2348	487.7770	488.5815
499.1633	501.0921	512.3206	512.3542	520.4046	526.6416
527.5680	528.4857	530.6444	530.9885	531.9342	533.7724
535.6391	539.7646	540.0453	540.8056	542.2616	542.5298
544.3493	546.4828	548.2918	548.9984	550.9888	554.2582
556.9954	557.3913	559.0929	563.0583	563.0767	563.8918
804.9617	808.0488	899.3156	903.4599		

Table 3.16: Harmonic vibrational frequencies (in cm^{-1}) for the most stable Penta-hexa ($Si_{60}C_2$) structure

61.4380	65.6871	67.1141	69.0670	70.3458	72.3324
73.8313	78.6247	79.3951	81.8368	82.3542	85.5154
86.8146	87.4857	88.0980	89.3450	90.6143	92.5326
92.8308	94.4205	96.4967	98.0016	101.5959	103.8825
104.7959	106.8864	107.0518	107.7585	108.4389	112.9797
114.5146	115.4591	117.0905	118.7266	119.3513	119.8236
123.7903	126.5110	127.3642	129.7329	131.3478	132.7710
135.4870	137.3848	138.4942	139.1971	141.5049	141.6681
143.8370	144.1454	145.1267	147.2058	148.7125	149.5239
150.4265	151.9951	153.0452	153.5576	154.9936	155.8489
156.2479	157.5863	159.1715	159.6298	161.3190	163.0284
164.1997	165.5267	172.4387	176.6239	180.7312	183.2489
184.1647	187.6388	189.0732	191.4760	192.4742	194.7349
195.5769	198.2387	199.8880	201.5446	206.1449	218.7464
229.4978	233.2395	242.9628	251.0135	252.8370	257.5168
260.0644	276.7017	279.2264	294.2308	306.0848	308.5169
311.5759	315.3881	323.1498	325.9094	332.1018	332.9843
349.0772	350.2729	351.2290	354.2351	360.1856	363.1294
367.6935	372.8973	379.8572	381.2812	385.5637	387.6370
392.6505	402.7018	407.2736	415.3283	422.2473	423.9157
428.2365	430.8320	434.7051	446.3945	447.7801	449.2103
452.7068	453.5500	456.9786	458.4316	460.8712	462.3906
464.3924	465.9921	468.8249	472.9853	475.1949	476.7964
478.4831	480.4061	483.5290	484.1373	485.3403	488.0372
491.7920	493.2359	502.4448	512.5161	514.2632	517.1332
519.6858	521.5957	523.5515	523.7473	526.8102	527.9181
529.2305	529.9793	530.1559	532.4767	535.7952	538.3100
540.4330	541.9555	542.9837	546.9465	550.3744	553.6866
554.5299	556.5974	558.5449	561.9541	563.3650	566.8807
602.0848	629.0248	741.1496	1182.5890		

Table 3.17: Harmonic vibrational frequencies (in cm^{-1}) for the most stable Hex ($Si_{56}C_4$) structure

55.8971	64.8758	67.4576	68.8136	70.1043	70.6354
76.0272	76.7145	79.3358	84.5322	85.4243	86.2111
86.6987	88.4220	90.8561	92.0461	93.4135	94.4081
95.9415	97.9270	100.3234	101.7886	106.1511	106.4578
108.5754	108.8234	109.8548	112.2919	112.7577	117.2513
117.8666	121.1488	121.9427	123.6936	126.2278	128.0834
130.0498	132.8628	134.5980	137.1598	138.8212	142.1625
144.5175	145.3037	146.2073	147.2587	148.2423	149.1042
149.9379	150.6858	151.3585	153.7104	154.4117	155.4954
157.6244	159.2372	161.7054	163.0248	163.1543	164.0207
165.7153	167.0740	171.2112	173.1026	177.7388	180.1959
181.4158	183.6016	186.1420	188.6784	189.3223	189.5684
200.7452	202.4702	205.3420	205.4491	206.4818	210.4183
222.7128	224.2411	251.5649	256.0932	259.4522	262.5135
266.1600	266.7312	274.0572	305.9623	307.6404	315.7169
319.4978	322.7541	325.0004	328.2235	332.2382	333.9206
345.1230	357.7753	358.7861	361.2270	363.3338	367.1075
374.7993	378.7277	385.1335	390.7282	392.5863	395.3141
412.9346	420.0545	423.9183	426.4257	432.8939	433.8715
446.8141	452.2418	455.6517	456.4768	459.5258	461.8868
464.2376	466.6832	468.3824	469.9848	472.2045	473.5322
475.6338	475.9617	478.5850	481.6462	483.1754	484.3756
488.4980	489.1455	496.9158	498.4706	504.9393	509.1182
511.6436	513.4332	518.1884	518.8939	519.6976	522.2381
523.3524	526.2855	528.2145	528.7358	530.9120	532.3983
534.2779	535.5277	539.0244	540.8196	546.0233	547.7202
551.8715	552.9817	554.3657	556.7204	561.4914	562.8507
563.9161	576.9557	678.9798	705.4701	737.1673	847.2127
864.5097	942.9391	1128.0110	1260.2130		

Table 3.18: Harmonic vibrational frequencies (in cm^{-1}) for the most stable Triangle ($Si_{60}C_4$) structure

49.7552	58.9743	60.1120	66.0902	66.8694	67.9457
69.1863	72.1076	73.7615	75.3259	81.7274	82.0819
82.9210	84.3885	86.2289	87.0282	88.0398	89.0461
90.2648	91.5501	91.6918	94.8985	95.5058	95.9930
97.3068	102.2961	104.5481	104.7198	107.8555	110.2392
110.8057	113.1303	113.5005	114.8453	115.5529	117.2166
120.7915	121.6276	124.2676	124.8945	127.2579	129.8385
129.9245	131.6173	135.3745	137.1226	138.0591	139.8121
140.3117	141.6199	143.9036	145.1952	146.5855	146.8078
147.4073	148.3879	148.9918	150.0588	150.9102	152.0497
153.1739	154.5320	155.9713	158.0597	158.8518	162.1844
163.6115	165.5331	167.5378	171.7991	173.9596	176.5456
180.4647	182.9086	184.9349	188.5154	189.3309	190.0572
192.0811	193.2621	193.9098	196.9885	199.3039	203.1191
208.3694	212.4788	236.4997	237.3201	246.1291	247.8152
250.3185	258.0734	259.9359	271.3593	288.7121	297.3005
298.3099	306.4778	317.2833	320.2421	324.1934	331.8038
333.2665	341.7561	345.6608	350.1541	353.9437	356.7321
363.3244	365.9202	376.9841	380.5235	381.1953	382.6007
388.8660	390.9662	405.4569	409.4178	416.1382	421.5773
422.8883	427.9403	437.3735	440.4580	443.0314	450.3516
452.8411	453.6226	455.4769	456.9585	458.9745	462.1194
464.4722	465.1663	470.0218	472.1717	473.5199	474.8560
477.3087	479.8247	482.7303	483.5643	485.1619	488.7785
491.9932	494.8849	500.9976	507.2206	512.1353	516.3337
519.7814	520.9690	522.1977	522.4916	524.9228	525.0532
526.3849	527.6935	529.9200	532.7044	533.2465	535.9315
536.7555	538.7476	542.0027	545.2748	546.8995	548.8837
550.3002	554.4512	559.2945	561.7528	563.5512	564.7733
566.7559	567.8880	629.4694	685.7000	703.1022	743.5396
1003.3810	1010.5070	1174.6650	1255.1420		

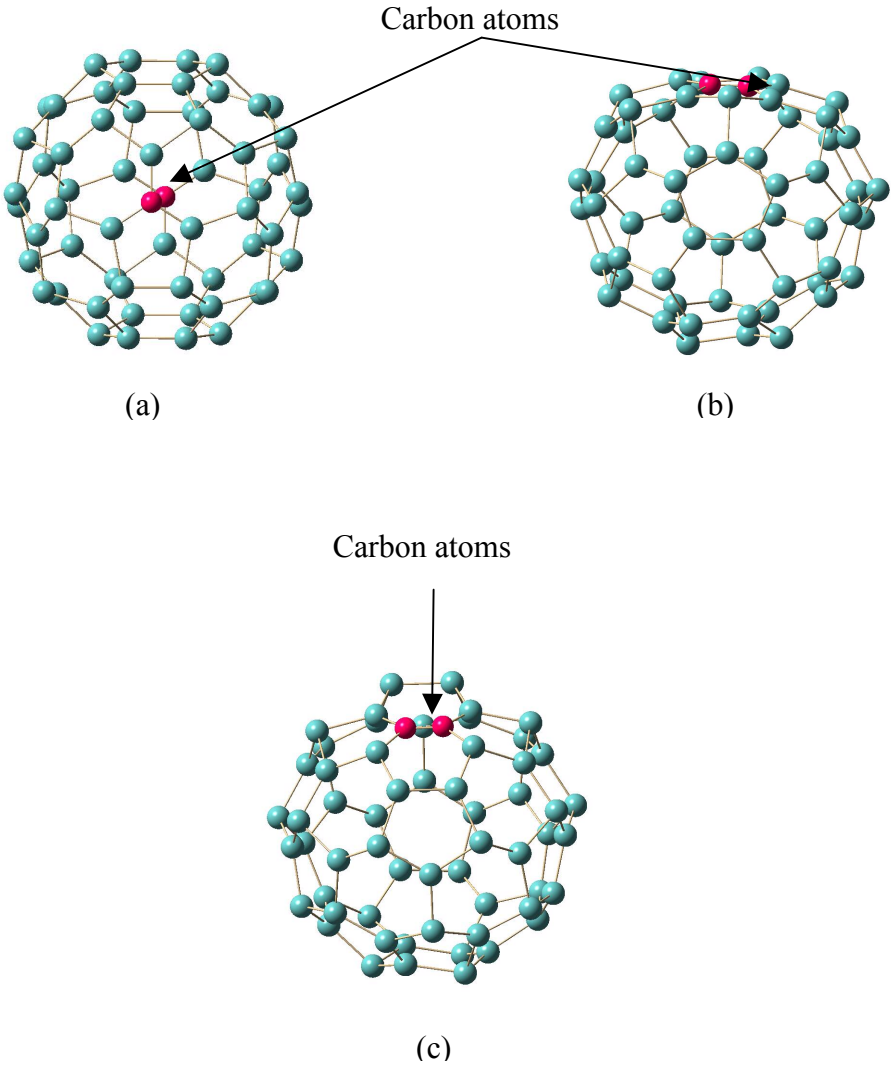

Figure 3.2: Optimized structures of $Si_{58}C_2$ silicon-carbon fullerene like nanostructures (a) Maindiag (b) Penta-hexa (c) Hexa-hexa (Carbon atoms denoted by dark pink color)

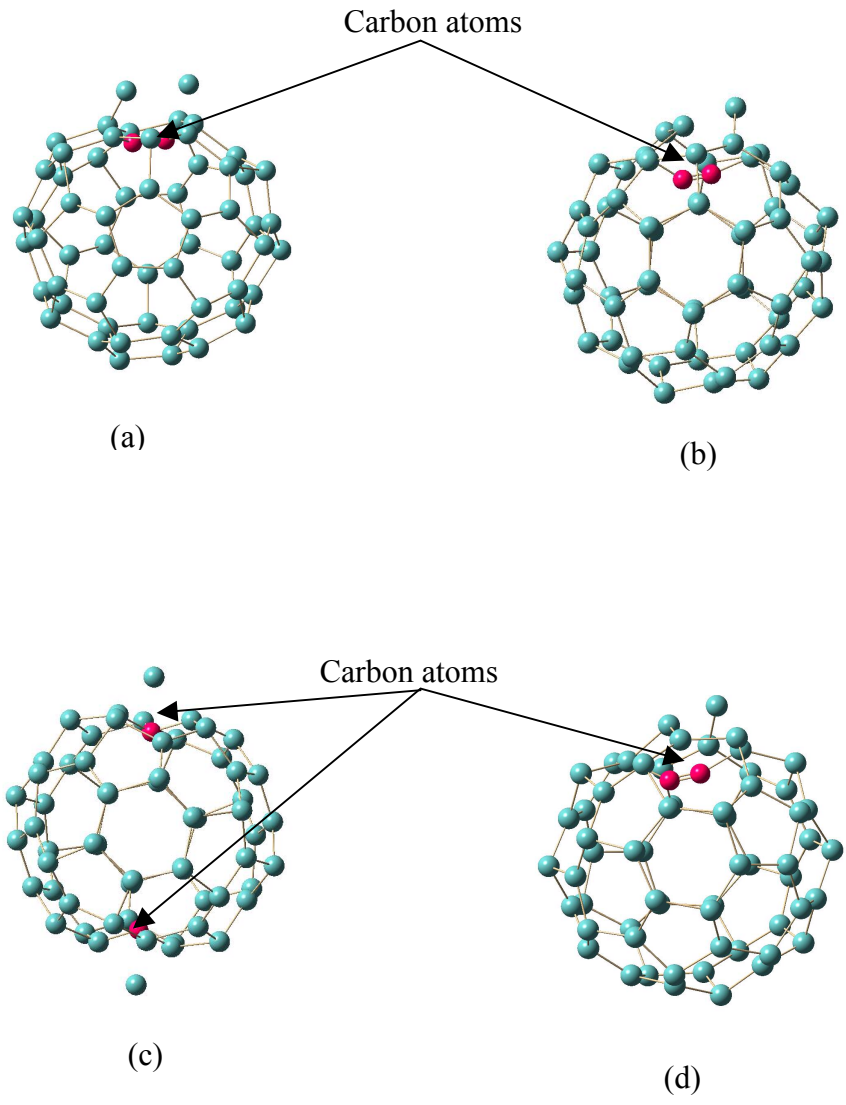

Figure 3.3: Optimized structures of $Si_{60}C_2$ silicon-carbon fullerene like nanostructures (a) Penta-hexa (b) Heper (c) Maindiag (d) Hexa-hexa (Carbon atoms denoted by dark pink color)

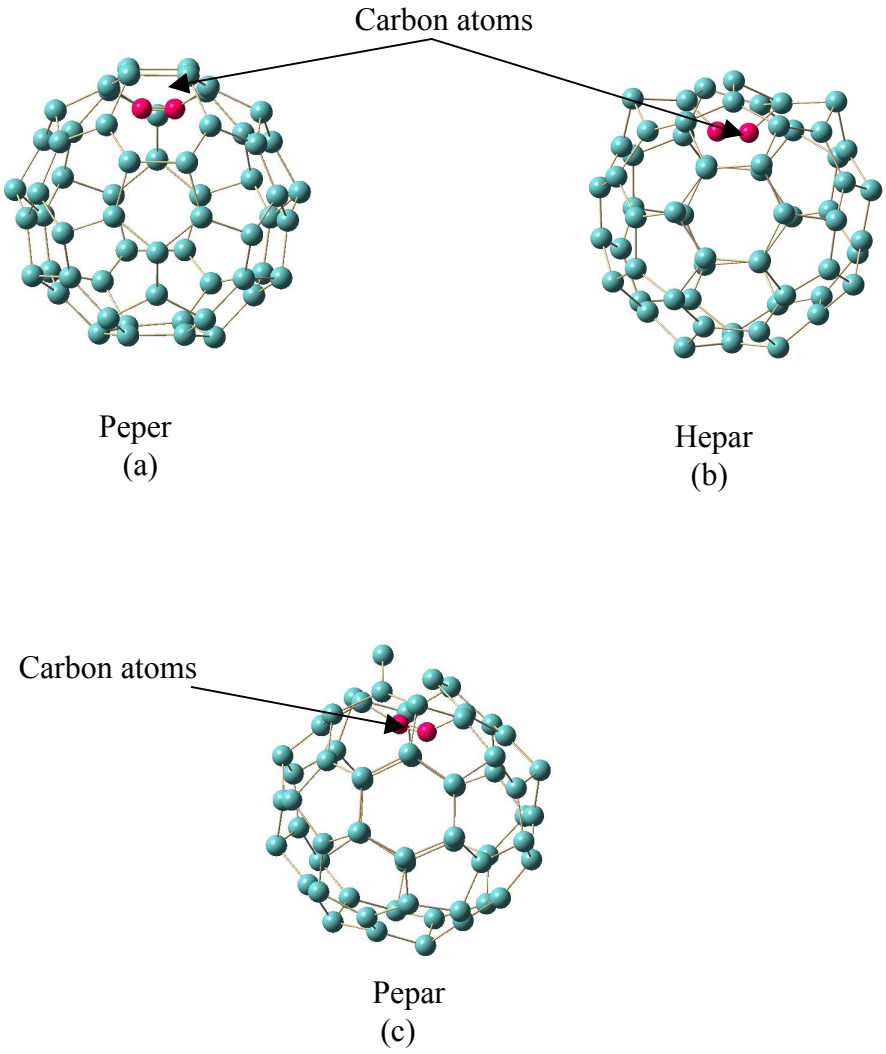

Figure 3.4: Optimized structures of $Si_{60}C_2$ silicon-carbon fullerene like nanostructures (a) Peper b) Hepar (c) Pepar (Carbon atoms denoted by dark pink color)

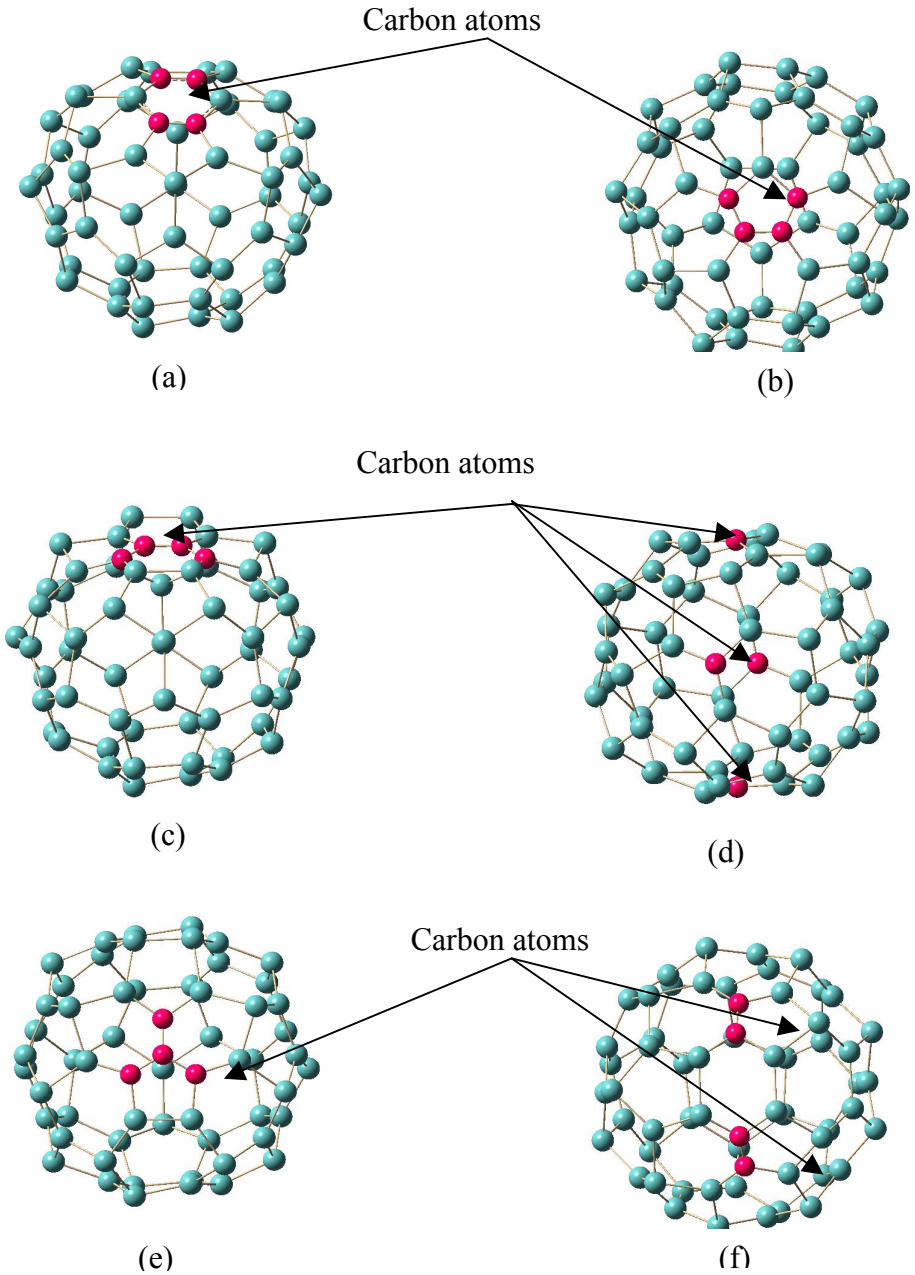

Figure 3.5: Optimized structures of $Si_{56}C_4$ silicon-carbon fullerene like nanostructures (a) Hex (b)Inpenta (c)Hexa (d)Maindiag (e) Tetra (f) Diag (Carbon atoms denoted by dark pink color)

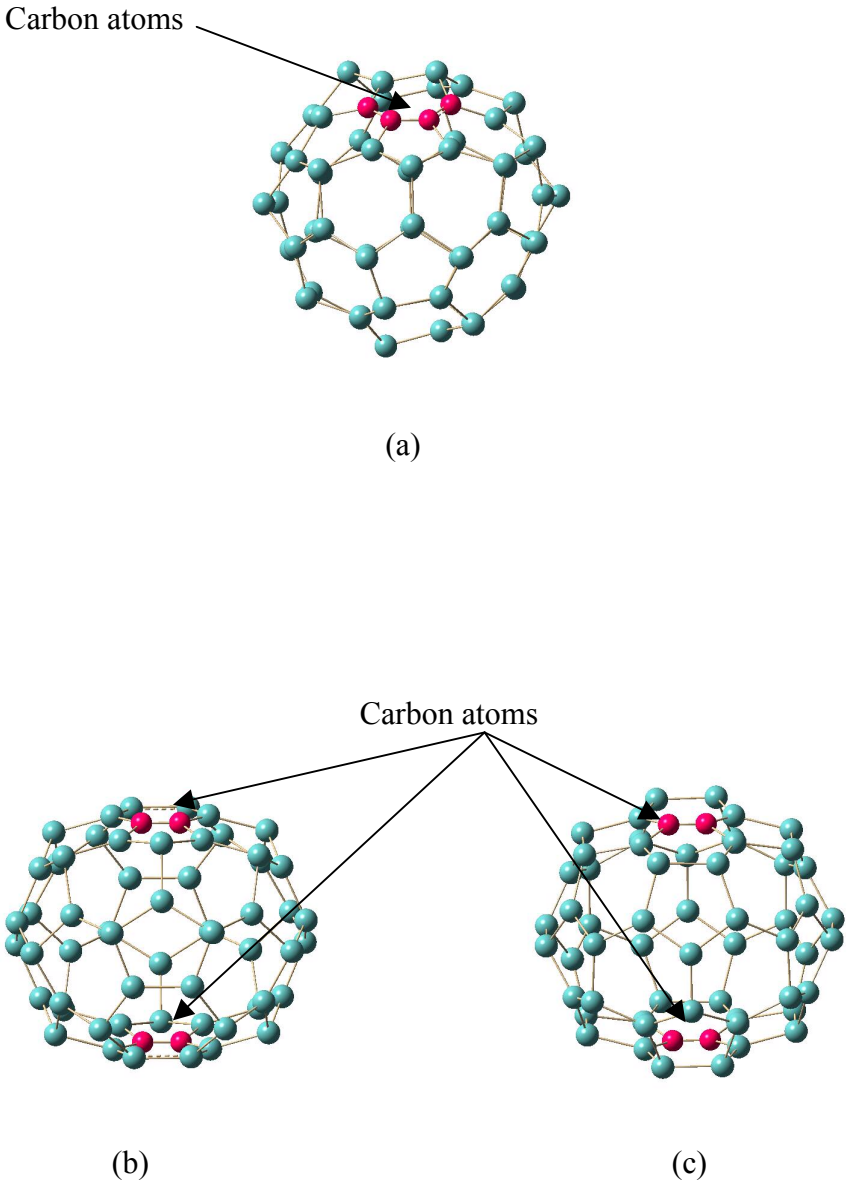

Figure 3.6: Optimized structures of $Si_{56}C_4$ silicon-carbon fullerene like nanostructures (a) Hexb (b) Penta-hexa (c) Hexa-hexa
(Carbon atoms denoted by dark pink color)

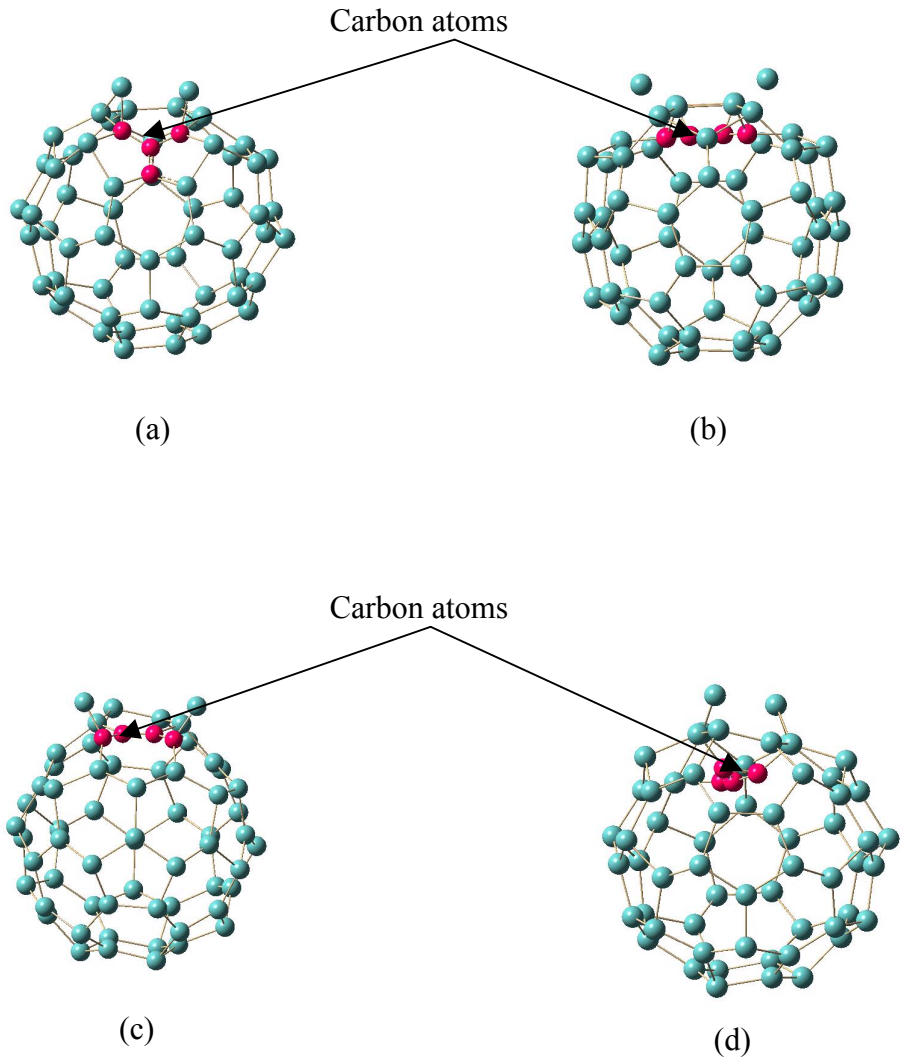

Figure 3.7: Optimized structures of $Si_{60}C_4$ silicon-carbon fullerene like nanostructures (a) Triangle (b) Hexa (c) Inpenta (d) Triangle-pepar (Carbon atoms denoted by dark pink color)

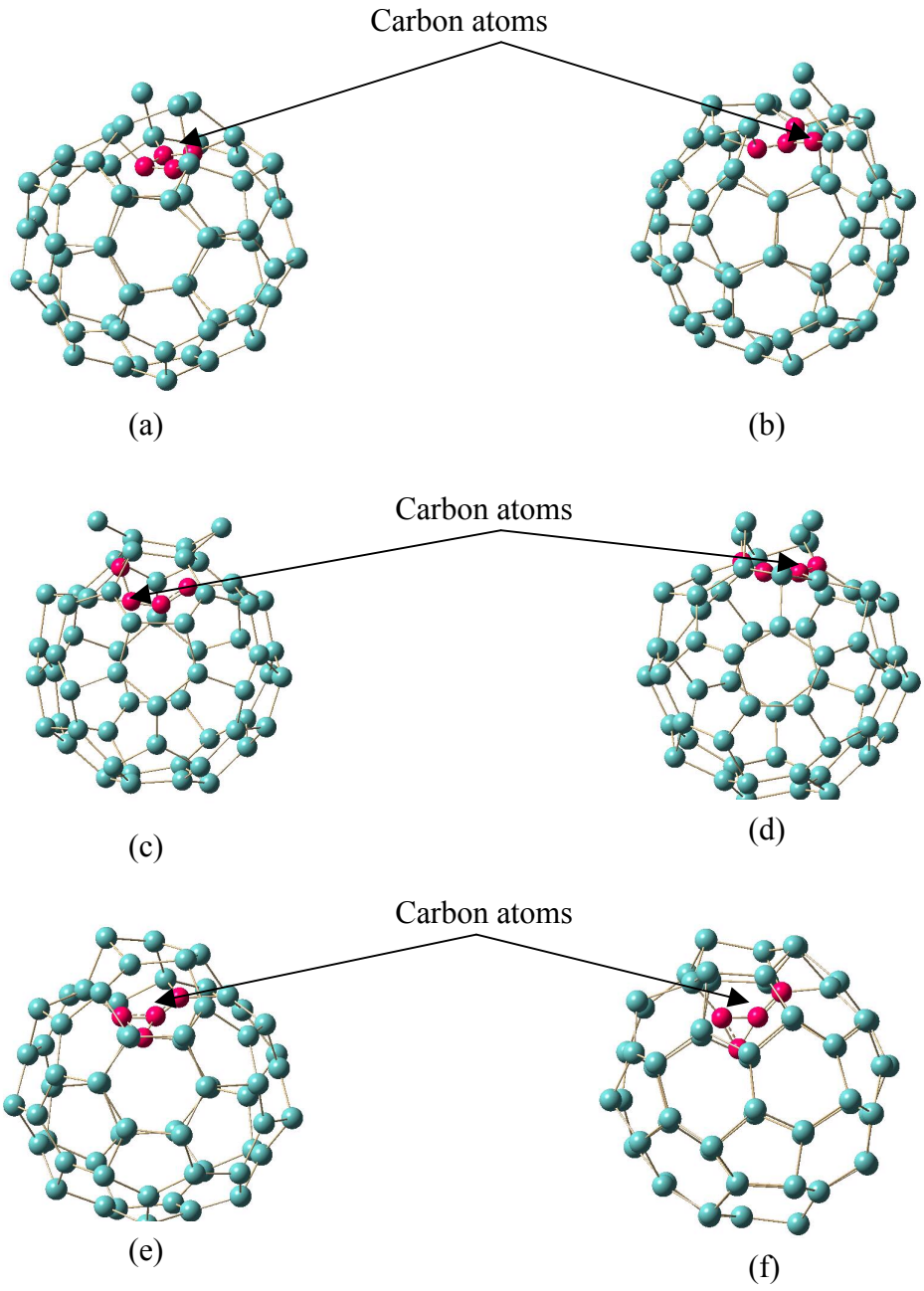

Figure 3.8: Optimized structures of $Si_{60}C_4$ silicon-carbon fullerene like nanostructures (a) Rho-pepar (b) Tetra (c) Rho-heper (d) Hexb (e) Triangle-heper (f) Triangle-peper
(Carbon atoms denoted by dark pink color)

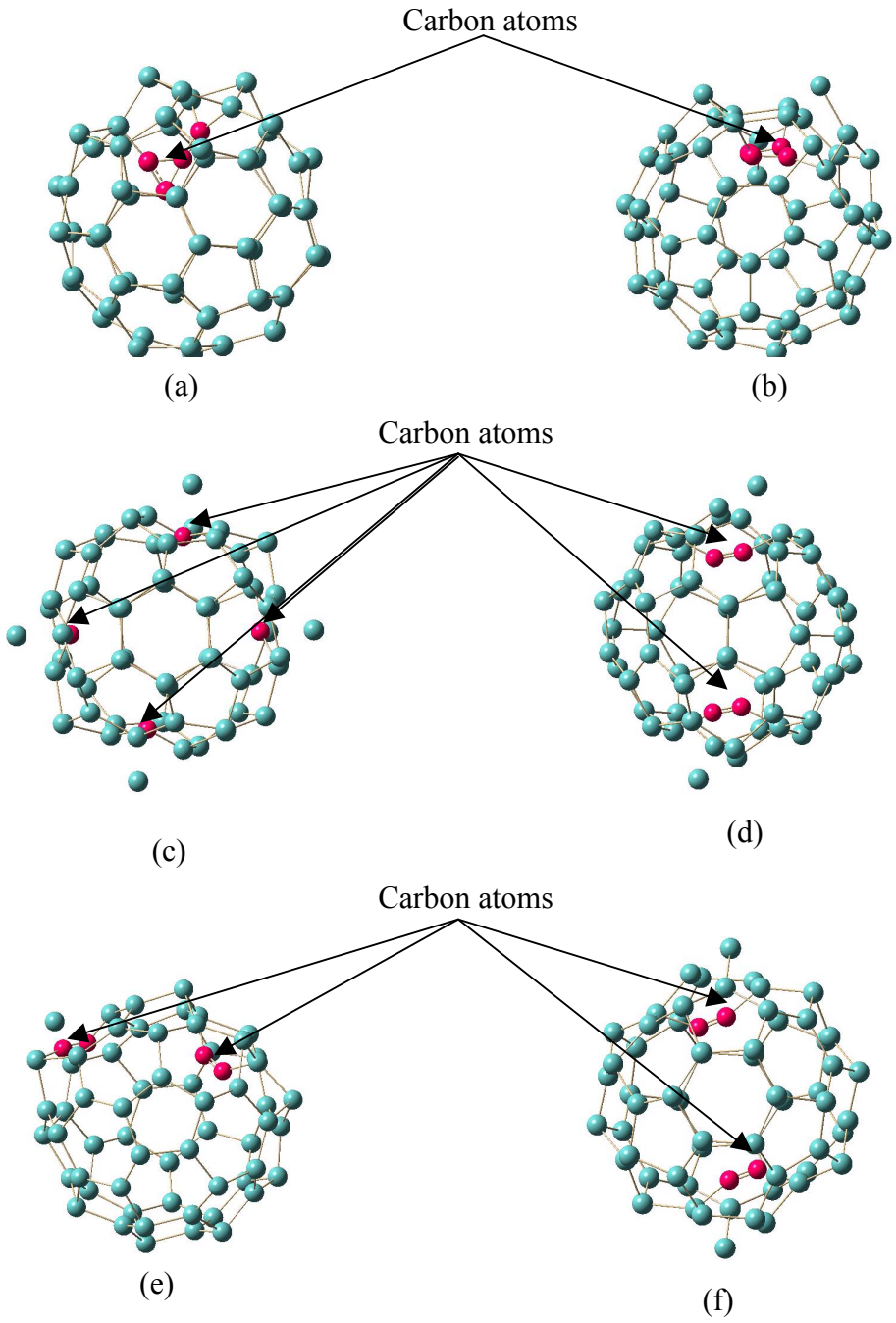

Figure 3.9: Optimized structures of $Si_{60}C_4$ silicon-carbon fullerene like nanostructures (a) Rho-peper (b) Rho-hepar (c) Maindiag (d) Lin-pepar (e) Diag (f) Lin-hepar
(Carbon atoms denoted by dark pink color)

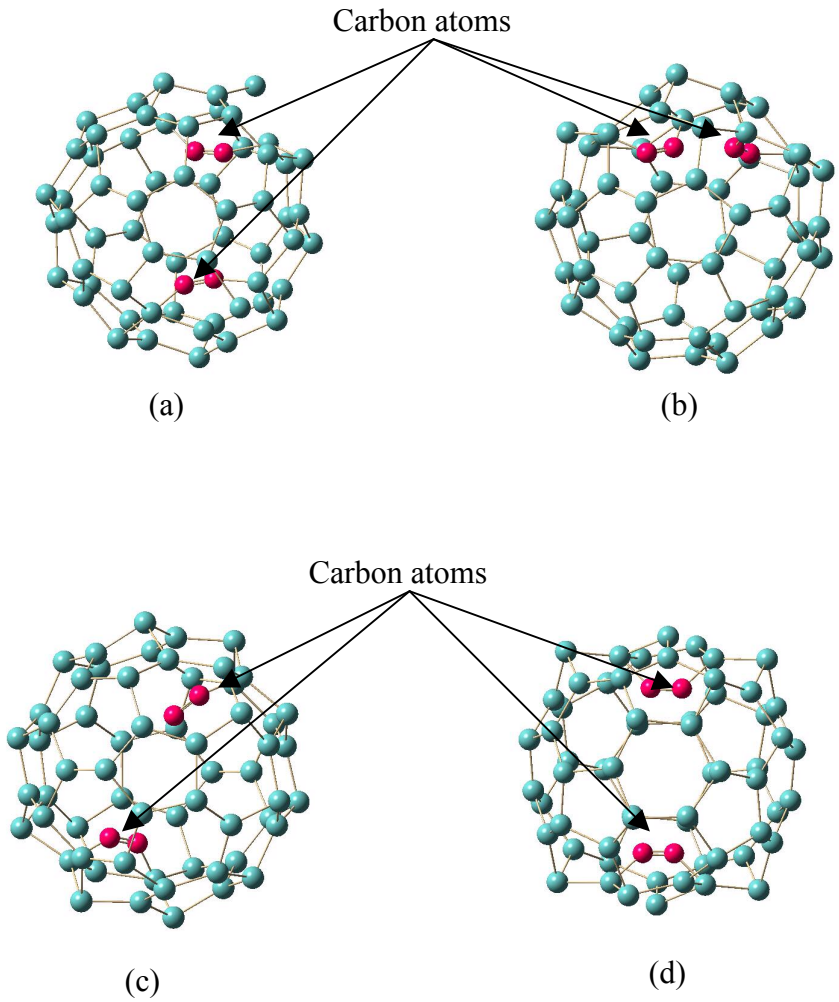

Figure 3.10: Optimized structures of $Si_{60}C_4$ silicon-carbon fullerene like nanostructures (a) Hexa-hexa (b) Hex (c) Lin-heper (d) Penta-hexa (Carbon atoms denoted by dark pink color)

3.2 Charge distributions for the most stable $Si_{58}C_2$, $Si_{60}C_2$, $Si_{56}C_4$ and $Si_{60}C_4$ Nanostructures

In general, Mulliken charge analysis [101-103] for all the structures clearly indicate that carbon atoms gain charge and the silicon atoms lose charge, as expected from their electro-negativity. Mulliken charge distribution diagrams for the four most stable structures in each set generated using Gaussian 03 along with the electronic charges for selective group of atoms are reported in Figures 3.12 to 3.15. Mulliken electronic charges for these structures are reported in Tables 3.19 to 3.22. All the charges are noted in electronic charge unit. In general these structures have mostly covalent and partly ionic bonding between the silicon and carbon atoms. For example, in the $Si_{56}C_4$ Hex structure (Fig 3.14), four carbon atoms (labels 16, 17, 35 and 36) along the opposite corners of the hexagon have electronic charges of -0.68,-0.67,-0.67 and -0.67 respectively and they are bonded to six silicon atoms (labels 15, 18, 34, 37, 51 and 53) having electronic charges of 0.43, 0.42, 0.68, 0.67, 0.14 and 0.14, which clearly indicating mixed ionic and covalent bonding, with covalent being more prominent. From Figure 3.15, we notice an exception in the Mulliken charge distribution for the Triangle structure ($Si_{60}C_4$) as the center carbon atom for C_4 trigonal planar arrangement inside the cage did lose charge to three other nearby carbon atoms. Carbon atom labels (61, 62, 63, 64) and their Mulliken electronic charges (-1.45, 0.92, -0.72, -1.39) clearly shows positive electronic charges for a carbon atom indicating an attractive Coulomb interaction between the four carbon atoms. As mentioned earlier, this adds to the cage

stability, but may not result in fullerene type structures because of its ionic nature. The VIP's and the VEA's for all the optimized nanostructures reported in this work are considerably higher indicating stability. The VIP's and the VEA's do not follow any specific pattern with the number of carbon atoms in Si_{60} cage. In general Mulliken charge analysis for the novel silicon-carbon fullerene like nanostructures indicates more covalent bonding nature, except for the last one $Si_{60}C_4$ where ionic contribution also becomes significant.

Table 3.19: Mulliken electronic charges for the atoms in most stable Maindiag ($Si_{58}C_2$) structure

1	Si	0.05	31	Si	0.13
2	Si	0.32	32	Si	-0.16
3	C	-1.15	33	Si	0.15
4	Si	0.32	34	Si	-0.03
5	Si	0.04	35	Si	-0.03
6	Si	-0.11	36	Si	0.15
7	Si	0.17	37	Si	-0.16
8	Si	-0.12	38	Si	0.11
9	Si	0.17	39	Si	-0.09
10	Si	-0.19	40	Si	-0.10
11	Si	0.17	41	Si	0.17
12	Si	0.30	42	Si	-0.19
13	Si	0.17	43	Si	0.17
14	Si	-0.19	44	Si	-0.12
15	Si	0.17	45	Si	0.17
16	Si	-0.12	46	Si	-0.12
17	Si	0.17	47	Si	0.00
18	Si	-0.12	48	Si	-0.03
19	Si	-0.01	49	Si	-0.11
20	Si	-0.02	50	Si	0.17
21	Si	0.13	51	Si	-0.12
22	Si	-0.16	52	Si	0.17
23	Si	0.15	53	Si	-0.19
24	Si	-0.03	54	Si	0.17
25	Si	-0.03	55	Si	0.30
26	Si	0.15	56	C	-1.15
27	Si	-0.16	57	Si	0.32
28	Si	0.11	58	Si	0.05
29	Si	-0.09	59	Si	0.04
30	Si	-0.10	60	Si	0.32

Table 3.20: Mulliken electronic charges for the atoms in most stable Penta-hexa ($Si_{60}C_2$) structure

1	Si	-0.09	32	Si	0.14
2	Si	0.14	33	Si	-0.11
3	Si	-0.15	34	Si	-0.03
4	Si	0.15	35	Si	-0.02
5	Si	-0.06	36	Si	-0.11
6	Si	0.02	37	Si	0.13
7	Si	-0.15	38	Si	-0.01
8	Si	0.17	39	Si	-0.04
9	Si	-0.16	40	Si	0.14
10	Si	0.16	41	Si	-0.14
11	Si	-0.16	42	Si	0.20
12	Si	0.15	43	Si	0.01
13	Si	-0.10	44	Si	0.28
14	Si	0.15	45	Si	0.07
15	Si	-0.15	46	Si	-0.07
16	Si	0.14	47	Si	0.15
17	Si	-0.15	48	Si	-0.11
18	Si	0.15	49	Si	0.16
19	Si	-0.11	50	Si	-0.16
20	Si	0.09	51	Si	0.14
21	Si	-0.16	52	Si	-0.15
22	Si	0.21	53	Si	0.15
23	Si	-0.05	54	Si	-0.10
24	Si	0.22	55	Si	0.13
25	Si	0.06	56	Si	-0.10
26	Si	-0.10	57	Si	0.02
27	Si	0.17	58	Si	0.15
28	Si	-0.15	59	Si	-0.17
29	Si	0.16	60	Si	0.16
30	Si	-0.05	61	C	-0.56
31	Si	-0.02	62	C	-0.45

Table 3.21: Mulliken electronic charges for the atoms in most stable Hex ($Si_{56}C_4$) structure

1	Si	-0.05	31	Si	0.16
2	Si	-0.09	32	Si	-0.21
3	Si	0.17	33	Si	0.23
4	Si	-0.17	34	Si	0.68
5	Si	0.16	35	C	-0.66
6	Si	-0.14	36	C	-0.66
7	Si	0.04	37	Si	0.67
8	Si	-0.07	38	Si	0.23
9	Si	0.16	39	Si	-0.21
10	Si	-0.16	40	Si	0.13
11	Si	0.14	41	Si	-0.01
12	Si	-0.16	42	Si	-0.05
13	Si	0.16	43	Si	0.15
14	Si	-0.20	44	Si	-0.15
15	Si	0.43	45	Si	0.16
16	C	-0.68	46	Si	-0.15
17	C	-0.67	47	Si	0.12
18	Si	0.42	48	Si	-0.09
19	Si	-0.20	49	Si	-0.10
20	Si	0.17	50	Si	0.23
21	Si	-0.14	51	Si	0.14
22	Si	0.09	52	Si	0.15
23	Si	-0.09	53	Si	0.14
24	Si	0.14	54	Si	0.22
25	Si	-0.09	55	Si	-0.13
26	Si	0.15	56	Si	0.16
27	Si	-0.11	57	Si	-0.15
28	Si	-0.01	58	Si	0.08
29	Si	-0.04	59	Si	0.06
30	Si	-0.11	60	Si	-0.16

Table 3.22: Mulliken electronic charges for the atoms in most stable Triangle ($Si_{60}C_4$) structure

1	Si	0.21	33	Si	0.08
2	Si	0.50	34	Si	-0.10
3	Si	0.41	35	Si	0.16
4	Si	-0.17	36	Si	-0.11
5	Si	0.14	37	Si	0.13
6	Si	-0.10	38	Si	-0.14
7	Si	0.16	39	Si	0.12
8	Si	-0.12	40	Si	-0.15
9	Si	0.17	41	Si	0.15
10	Si	-0.17	42	Si	-0.15
11	Si	0.16	43	Si	0.14
12	Si	0.18	44	Si	-0.10
13	Si	0.22	45	Si	0.13
14	Si	0.26	46	Si	-0.01
15	Si	0.45	47	Si	-0.11
16	Si	0.34	48	Si	0.15
17	Si	-0.03	49	Si	-0.16
18	Si	-0.05	50	Si	0.16
19	Si	0.13	51	Si	-0.15
20	Si	-0.09	52	Si	0.14
21	Si	0.15	53	Si	-0.04
22	Si	-0.16	54	Si	-0.01
23	Si	0.15	55	Si	-0.11
24	Si	-0.04	56	Si	0.15
25	Si	-0.02	57	Si	-0.10
26	Si	0.13	58	Si	-0.04
27	Si	-0.15	59	Si	0.15
28	Si	0.13	60	Si	-0.16
29	Si	-0.13	61	C	-1.45
30	Si	0.15	62	C	0.92
31	Si	-0.10	63	C	-0.72
32	Si	-0.09	64	C	-1.39

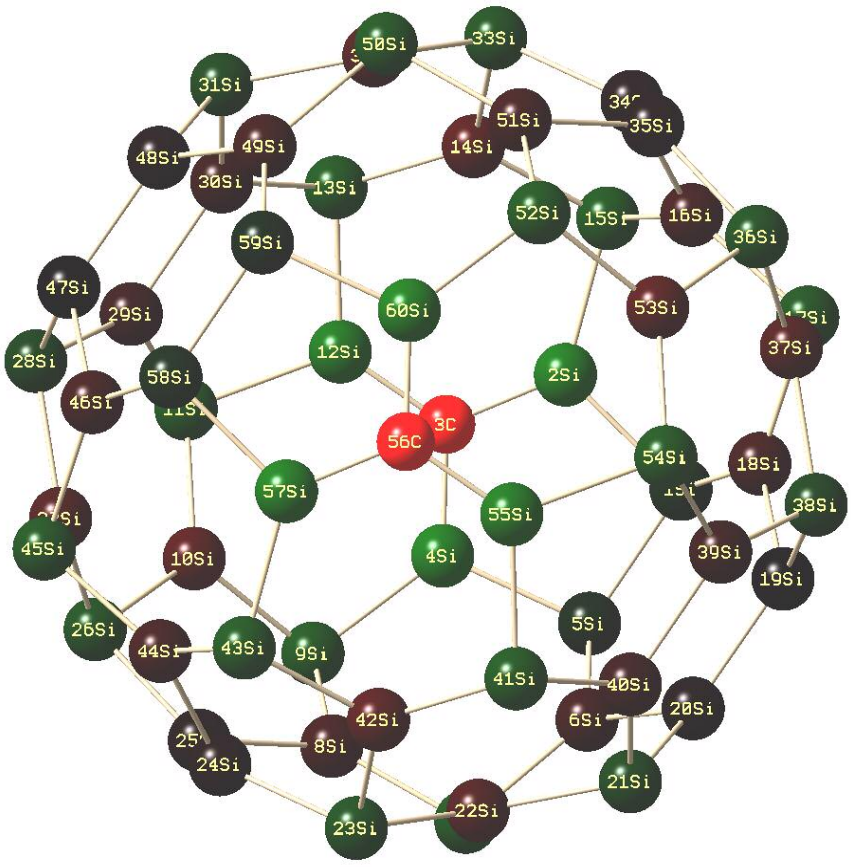

Figure 3.11: Mulliken charge distribution for the most stable Maindiag ($Si_{58}C_2$) structure.

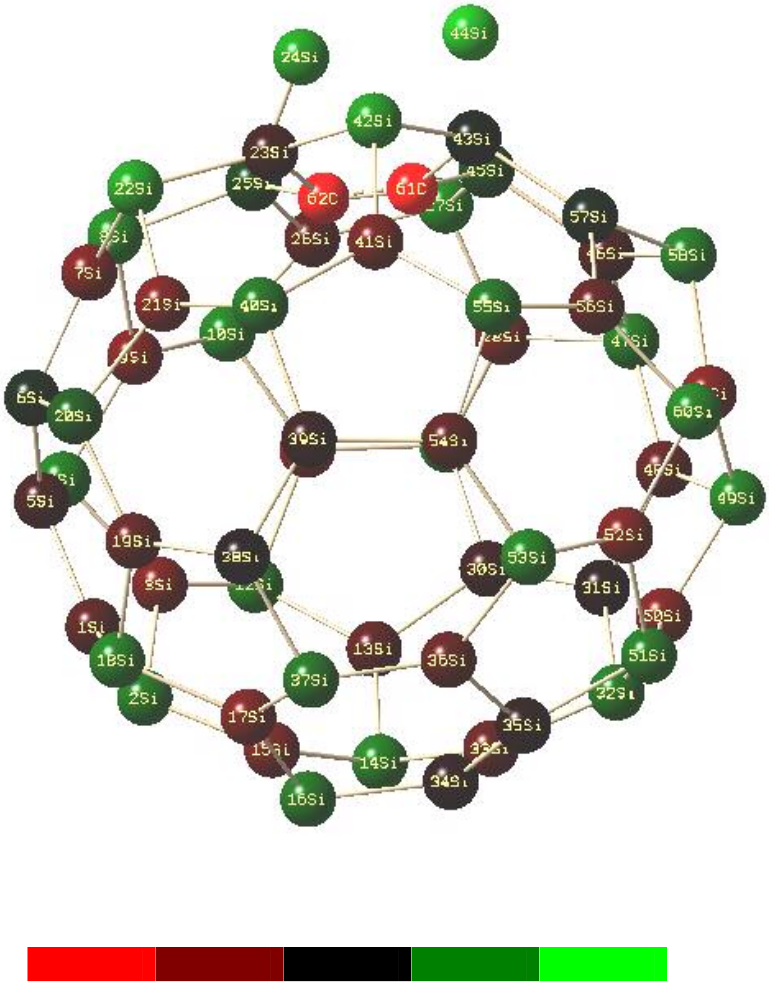

Figure 3.12: Mulliken charge distribution for the most stable Penta-hexa ($Si_{60}C_2$) structure.

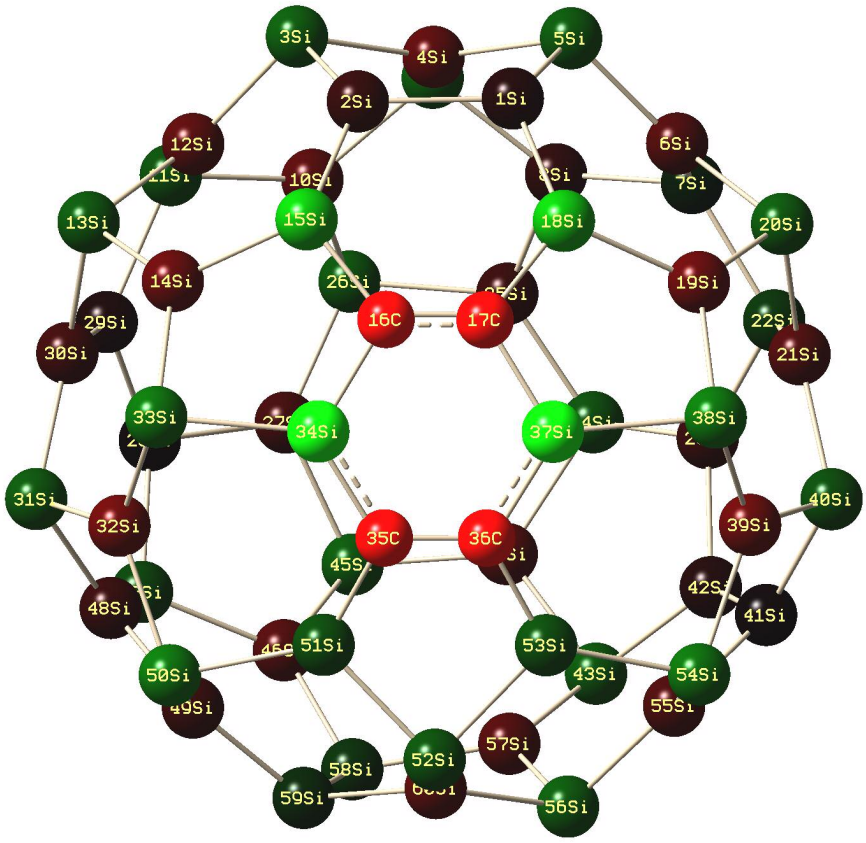

Figure 3.13: Mulliken charge distribution for the most stable Hex ($Si_{56}C_4$) structure.

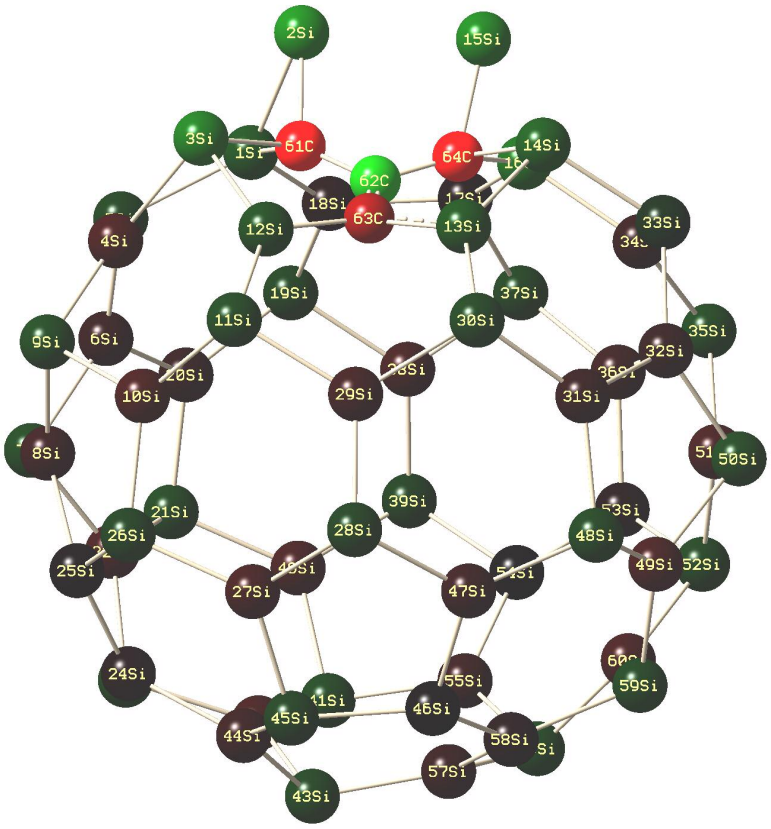

Figure 3.14: Mulliken charge distribution for the most stable Triangle ($Si_{60}C_4$) structure.

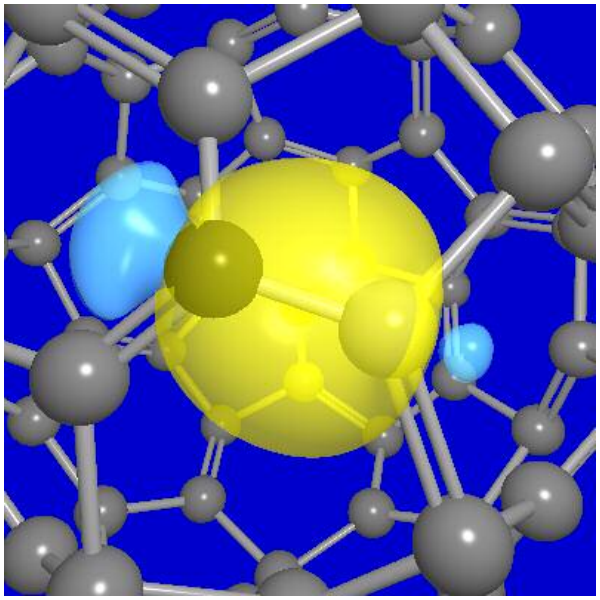

(a)

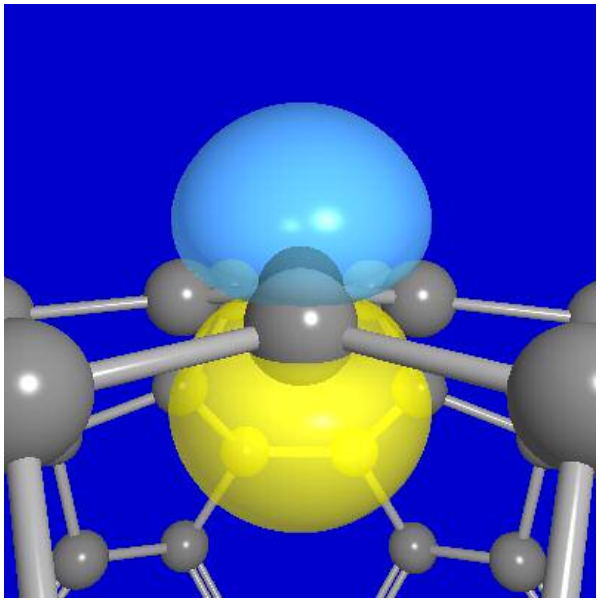

(b)

Figure 3.15: Natural Bond Orbital (NBO) plots generated using NBO program & NBO View for the most stable Maindiag structure ($Si_{58}C_2$) (a) σ bond between Si-C (b) π bond between Si –C.

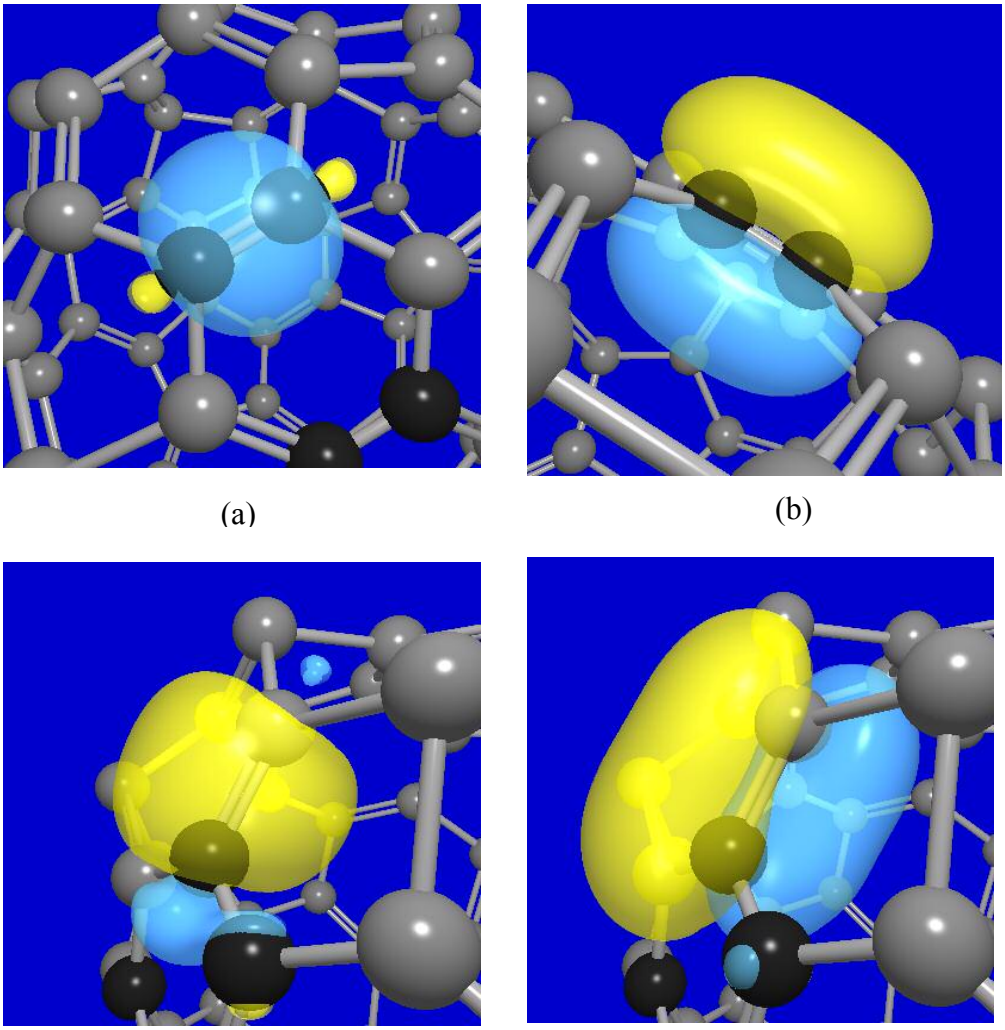

Figure 3.16: Natural Bond Orbital (NBO) plots generated using NBO program& NBO View for the most stable Maindiag structure ($Si_{56}C_4$) (a) σ bond between C-C (b) π bond between C –C (c) σ bond between Si-C (d) π bond between Si –C.

CHAPTER 4

STABILITY OF $Si_{60}C_{2n}$ FULLERENE LIKE NANOSTRUCTURES (n=3)

4.1 Results and Discussions on $Si_{54}C_6$ and $Si_{60}C_6$ Nanostructures

As is known, Si_{60} fullerene like cage has 12 pentagons and 20 hexagons. In the first step, six silicon atoms on the surface of the cage have been replaced by six carbon atoms at various symmetry orientations. In the second step, six carbon atoms have been put inside the Si_{60} cage at various possible orientations with carbon atoms parallel and perpendicular to the pentagonal and hexagonal faces. In the third step, as a test of the SiC bond strength, we also put the six carbon atoms close to the surface, with the same surface orientation, at an initial optimized SiC dimer bond length of 1.77 Å and optimized the structures. For C_6 ground state structure, theoretical and experimental studies have reported that there are two possible structures close in stability, one being a cyclic singlet structure (D_{3h} planar, resembling a distorted hexagon or benzene) and the other being triplet linear chain structure [91-98, 104]. For this reason, six carbon atoms in cyclic and linear chain arrangement optimized at GGA-DFT level of theory have been added inside the cage at various orientations.

In the results to follow, we report the electronic states, binding energies per atom (BE), highest occupied – lowest unoccupied molecular orbital (HOMO-LUMO) gaps, vertical ionization potentials (VIPs) , vertical electron affinities (VEAs) and total

dipole moments of the stable fullerene-like $Si_{54}C_6$ and $Si_{60}C_6$ optimized structures [105] with their corresponding average Si-C and C-C bond lengths. Binding energies per atom of the clusters are calculated as the relative energies of these clusters in the separated atom limit, with the atoms in their respective ground states, with a positive binding energy indicating stability. VIPs and VEAs have been calculated as the difference in the total energies between the neutral clusters and the corresponding positively and negatively charged clusters at the neutral optimized geometries. For the two most $Si_{54}C_6$ and $Si_{60}C_6$ stable structures harmonic frequencies are also reported. Bonding between the atoms, especially Si-C and C-C for all the stable structures were analyzed using the NBO (Natural Bonding Orbital) program and NBO View [100].

For the set of optimized $Si_{54}C_6$ fullerene like nanostructures reported in Table 4.1, the column under the structures refers to the positions of the carbon atoms substituting silicon atoms on the surface of the Si_{60} cage. The optimized geometries of all the structures in Table 4.1 are reported in Figures 4.1 to 4.3. The most stable structure Hexa (Fig 4.1 a) has six carbon atoms at six corners of the hexagon. The structure Penta (Fig 4.1 b) has five carbon atoms at the five corners of a pentagon and one carbon atom along the common side of two hexagons. The structure Hexa1 (Fig 4.1 c) has five carbon atoms at five corners of a hexagon and one carbon atom along the common side of a pentagon and hexagon. The Ditri1 structure (Fig 4.1 d) has six carbon atoms along the six corners of two hexagons adjoining two pentagons of the cage. As different combinations are possible for six carbon atoms along the corners of two pentagons and two hexagons, the set of structures Hexa2 (Fig 4.1 e), Hexa3 (Fig 4.2

a), Hexa4 (Fig 4.2 b), Ditri (Fig 4.2 c), Hexa5 (Fig 4.3 d), Hexa6 (Fig 4.3 a) were tried out. The Penta1 (Fig 4.2 d) structure has six carbon atoms along the common sides between four hexagons surrounding a pentagon. The structure Penta-Hexa-tb1 (Fig 4.3 b) has three carbon atoms at three corners of a pentagon surrounding two hexagons, at two ends of the cage. For the Penta-Hexa-tb (Fig 4.3 c), the three carbon atoms are at three corners of a hexagon surrounding a hexagon and a pentagon, at two ends of the cage.

As seen from Table 4.1, there are several almost degenerate structures comparable in stability in the set of $Si_{54}C_6$ structures. The first structure Hexa has the highest BE per atom of 3.923 eV in this set. The dipole moment of this structure has a value of 1.22 Debye indicating mixed ionic-covalent bonding nature contributing to its increased stability. The average Si-C and C-C bond lengths for this structure are 1.93 Å and 1.45 Å, respectively. NBO analysis of this structure yielded 6 Si-C σ bonds, 6 C-C σ bonds and 3 C-C π bonds (alternate carbon single bond and double bond similar to the benzene structure). NBO σ and π bonds for this structure are shown in Figure 4.11. Important thing to be noted in this structure is the strong covalent bonding between the carbon atoms. The Penta structure BE per atom is only 0.001 eV less than the previous structure. NBO analysis yielded 6 Si-C σ bonds, 1 Si-C π bond, 6 C-C σ bonds and 2 C-C π bonds. One of the C-C π bonds in the Hexa structure is replaced by the Si-C π bond whose occupancy (1.51) is less compared to C-C π bond (1.69), indicating a weaker Si-C π bond contributing to its slightly lower stability. Dipole moment of this structure is 0.49 Debye indicating a lower ionic contribution in the bonding. The BE per atom of

the Hexa1 structure is 0.004 eV less than the most stable Hexa structure. NBO analysis of this structure yielded 8 Si-C σ bonds, 3 Si-C π bonds, 5 C-C σ bonds and 1 C-C π bond. The number of C-C bonds is less in this structure compared to the previous two structures and the number of Si-C bonds is higher indicating that less carbon bonds contribute to its lower stability. The Ditri1 and Hexa2 structures have the same BE per atom of 3.918 eV, 0.005 eV less than the most stable Hexa structure. The Ditri1 structure has the highest HOMO-LUMO gap and VIP in this set. NBO analysis for the Ditri1 structure yielded 8 Si-C σ bonds, 2 Si-C π bonds, 5 C-C σ bonds, 2 C-C π bonds and for Hexa2 structure yielded 8 Si-C σ bonds, 4 Si-C π bonds, 5 C-C σ bonds, 1 C-C π bond clearly indicating that Si-C interactions are also important for the stability in addition to C-C bonding (binding energies were lower even with significant C-C interactions). Average Si-C bond length of 1.85 Å and average C-C bond length 1.49 Å for these structures indicates slightly stronger Si-C bonding and weaker C-C bonding compared to Hexa structure. The Hexa3 structure has the highest VEA in this set. NBO analysis for this structure yielded 8 Si-C σ bonds, 2 Si-C π bonds, 5 C-C σ bonds and 3 C-C π bonds clearly indicating an increase in C-C bonding compared to Ditri1 and Hexa2 but the average occupancies of Si-C σ bonds, Si-C π bonds and C-C π bonds were low indicating weaker Si-C and C-C bonding contributing to its lower binding energy. The structures Penta-Hexa-tb1 and Penta-Hexa-tb have zero dipole moment indicating a highly symmetric charge distribution and strong covalent bonding. These two structures have the highest number of Si-C bonds (10 σ bonds and 2 π bonds) but owing to the orientation of 3 carbon atoms at two ends of the cage, the number of C-C

bonds is lower compared to the other structures in this set contributing to lower binding energy. The vibrational frequencies for the most stable Hexa structure in this set are listed in Table 4.5.

The second set of optimized structures, $Si_{60}C_6$ with carbon atoms inside the Si_{60} cage are listed in Table 4.3 and the corresponding geometries are presented in Figures 4.4 to 4.8. Here also the column below the structures denotes the orientations of carbon atoms inside the Si_{60} cage. Before relaxation, C_6 distorted cyclic structure (resembling distorted hexagon) was added inside the cage closer to the surface and C_6 linear structure put inside the cage symmetrically with respect to its center. The structures Dhex-pepar (Fig 4.4 a), Dhex-hepar (Fig 4.4 b), Dhex-heper (Fig 4.4 c) and Dhex-peper (Fig 4.7 d) have six carbon atoms in distorted cyclic structure in a plane parallel to pentagonal face, parallel to hexagonal face , perpendicular to hexagonal face and perpendicular to the pentagonal face of the cage respectively. The structures Lin-hepar (Fig 4.5 b), Lin-peper (Fig 4.5 c), Lin-heper (Fig 4.5 d) have six carbon atoms in linear arrangement in a plane parallel to hexagonal face, perpendicular to pentagonal face and perpendicular to the hexagonal face of the cage, respectively. The structure Hexa (Fig 4.4 d) has six carbon atoms inside the cage along the six corners of a hexagonal face of the cage at Si-C bond length distance. This structure is similar to the Hexa structure (Fig 4.1 a) but the carbon atoms are at Si-C bond length distance inside the cage. All other optimized structures reported in the Table 4.3 are similar to their corresponding surface orientations, repeated inside the Si_{60} cage at Si-C test bond length distance.

For this set also, there are a significant number of almost degenerate structures comparable in stability. For the sake of brevity, we discuss in detail only a few structures in Table 4.3. The Dhex-pepar structure is the most stable in the $Si_{60}C_6$ set with a BE per atom of 3.896 eV. The total dipole moment of 1.85 Debye indicates a mixed ionic-covalent bonding nature contributing to its stability. The vibrational frequencies for this structure are listed in Table 4.6. Binding energies per atom for the first four structures in the Table 2 are within 7meV. NBO analysis for the first three structures yielded the same number of Si-C bonds (6 σ bonds) and C-C bonds (6 σ bonds and 3 π bonds). For Dhex-hepar, the average C-C σ bond occupancy is slightly lower than the Dhex-pepar structure with the C-C π bond, Si-C σ and π bond average occupancies similar for the two structures. This could be one of the reasons for the reduction in BE per atom by 0.001 eV. The Dhex-hepar structure's VIP and HOMO-LUMO gap are higher than the Dhex-pepar structure but its VEA is lower. For Dhex-heper, Si-C σ bond average occupancies were lower than the previous two structures indicating a slightly weaker Si-C bonding contributing to its lower binding energy. NBO analysis of the Hexa structure yielded the same number of Si-C and C-C bonds as the three previous structures but the Si-C σ bonds and C-C π bonds were weaker resulting in lower binding energy. The set of structures Lin-hepar, Lin-peper and Lin-heper have the strongest C-C interactions in this set as evident from their average C-C bond lengths. NBO analysis for these structures yielded 2 C-C single bonds and 3 C-C triple bonds for Lin-hepar and Lin-peper, 2 C-C single bonds, 1 C-C double bond and 2 C-C triple bonds for Lin-heper. These structures have the minimum Si-C interactions (3

σ bonds for Lin-hepar and Lin-heper, 4 σ bonds for Lin-peper) which results in lower binding energy. The structure Penta-hexa-tb1 with 3 carbon atoms at two ends of cage has a negligible ionic contribution to predominantly covalent bonding. This structure has the maximum Si-C bonds (10 σ bonds) but the C-C interactions are lower (2 single bonds and 2 double bonds) which results in lower binding energy. The Dhex-hepar structure has the highest VIP in this set. The Ditri1 structure has the highest HOMO-LUMO gap of 0.547 eV and the Lin-heper structure has the highest VEA in this set.

A common feature of the above $Si_{60}C_6$ structures is that the carbon atoms put inside the Si_{60} cage move closer to the surface of the cage thereby pushing a few silicon atoms outside the surface of fullerene like cage, and as a result those silicon atoms are loosely bounded to the cage. This might be one of the reasons for the lower binding energy of these set compared to $Si_{54}C_6$ cages. For example, the structure Hexa's (Fig 4.4 d) BE per atom in this set is 0.007 eV lower than the most stable structure in this set. As discussed before the number of Si-C bonds and C-C bonds in this structure are the same as the most stable in this set. The only difference is the average occupancies of the Si-C σ bonds and C-C π bonds which are lower than the most stable structure in this set thus contributing to lower binding energy. This might indicate that Si-C interactions and C-C interactions together are important for the stability. This structure has six silicon atoms loosely bound to the cage and the removal of these six silicon atoms leads to structure which is almost similar to Hexa structure (Fig 4.1 a) in the $Si_{54}C_6$ set and the BE per atom increases by 0.034 eV. As discussed before, the NBO analysis of this most stable Hex structure ($Si_{54}C_6$) yielded the same number of Si-C bonds and the C-C bonds

as in $Si_{60}C_6$ set but the average C-C π bond and Si-C σ bond average occupancies are little higher at the surface. This might again indicate that Si-C interactions and C-C interactions are important for the stability. We also tried to put six carbon atoms in distorted cyclic structure at the center of the cage but the structures were not stable. This might again indicate that Si-C interactions are also important for stability.

In general, all the optimized structures considered here are stable nanostructures with higher binding energies per atom compared to the bare Si_{60} cage which has a binding energy per atom of 3.61eV at GGA-DFT level of theory. In chapter 3,[28] we have seen that binding energies per atom for the $Si_{58}C_2$, $Si_{60}C_2$, $Si_{56}C_4$, $Si_{60}C_4$ fullerene like nanostructures were higher compared to the bare Si_{60} cage and they increase with the number of carbon atoms from two to four. Also, the structures with carbon atoms substituting silicon atoms on the surface of the Si_{60} fullerene cage give higher binding energies compared to the structures with carbon atoms put inside the Si_{60} cage. Here too, the binding energies of $Si_{54}C_6$ and $Si_{60}C_6$ nanostructures were higher compared to the results for two and four carbon atoms which agree with the trend of increasing binding energies with increase in carbon atoms. The stability of the nanostructures here is found to be dependent on the orientations of carbon atoms inside or on the surface of fullerene like cage. All the optimized nanostructures tend to be distorted and not a smoother fullerene like silicon nanostructures.

As mentioned before that for the most part carbon-carbon interactions and the Si-C interactions contribute to the cage stability. For example, we note that for the most stable structure in Table 4.1, there is a mixture of ionic and covalent bonding

contributing to its stability. As discussed before, it has the maximum number of C-C bonds with alternate single and double bonds (similar to benzene structure) .Strong covalent bonding between the carbon atoms and slight ionic interaction between silicon and carbon atoms also contribute to its increased stability. Similar conclusions can be made for the most stable structure in Table 4.3. Here too, the number of Si-C and C-C bonds is the same as in Hexa ($Si_{54}C_6$) but they were weaker contributing to lower binding energy. This could be due to the fact that silicon atoms bonded with carbon atoms gain charge similar to the carbon atoms and this might have offset the increased C-C interaction, as Si-C interactions might be repulsive. This again indicates that Si-C interactions and C-C interactions are important for stability. In fact the increase in the Si-C bonding for the structures in both sets at the expense of C-C bonding were not as stable compared to the most stable structure in both sets ($Si_{54}C_6$ and $Si_{60}C_6$), indicating that Si-C bonding and C-C bonding together are important for the stability.

For the $Si_{54}C_6$ group (Table 4.1), the difference between the BE of the most stable one which has the maximum number of C-C bonds (3 single bonds and 3 double bonds), 6 Si-C bonds and the least stable one which has the minimum number of C-C bonds (1 single bond, 1 double bond and 1 triple bond) and more Si-C bonds (7 single bonds and 1 double bond) is 0.078 eV/atom which indicates a difference in BE of 2.2% . Considering the fact that inclusion of six carbon atoms on the surface increased the BE per atom by 8.7% compared to the bare Si_{60} cage, 2.2% difference is significant. For the $Si_{60}C_6$ group, the difference between the BE of the most stable one (with the same bonding nature as most stable in $Si_{54}C_6$ set) and the least stable one which had less C-C

bonds (3 single bonds and 1 double bond) and more Si-C bonds (10 σ bonds) is 0.058 eV/atom, which is approximately 1.6 % difference in the binding energy. This indicates that Si-C and C-C interactions are stronger at the surface than inside the cage. This could be evident from the fact that carbon atoms put inside the cage move closer to surface of the cage but are loosely bonded with the surface silicon atoms of the cage.

Table 4.1: Binding energy per atom (BE), HOMO-LUMO gap, VEA, VIP (all in eV), Dipole moment (Debye), Average Si-C bond length (Å) and C-C bond length (Å) for optimized $Si_{54}C_6$ fullerene like nanostructures.

Structures	State	BE per atom (eV)	HOMO-LUMO gap (eV)	VEA (eV)	VIP (eV)	Dipole Moment (Debye)	Avg Si-C BL (Å)	Avg C-CBL (Å)
Hexa	^{1}A	3.923	0.502	3.674	6.282	1.22	1.93	1.45
Penta	^{1}A	3.922	0.467	3.712	6.284	0.49	1.86	1.47
Hexa1	^{1}A	3.919	0.629	3.666	6.395	1.01	1.86	1.47
Ditri1	^{1}A	3.918	0.662	3.648	6.414	0.41	1.85	1.48
Hexa2	^{1}A	3.918	0.570	3.625	6.301	0.76	1.85	1.49
Hexa3	^{1}A	3.906	0.406	3.852	6.376	0.97	1.87	1.48
Hexa4	^{1}A	3.905	0.539	3.733	6.381	1.19	1.87	1.49
Ditri	^{1}A	3.904	0.543	3.765	6.406	0.51	1.85	1.50
Penta1	^{1}A	3.901	0.443	3.787	6.341	0.71	1.89	1.48
Hexa6	^{1}A	3.899	0.605	3.685	6.379	1.00	1.89	1.48
Penta-Hexa-tb1	^{1}A	3.896	0.586	3.677	6.351	0.00	1.89	1.47
Penta-Hexa-tb	^{1}A	3.894	0.415	3.678	6.181	0.00	1.87	1.49
Hexa5	^{3}A	3.845	0.500	3.735	6.383	1.07	1.86	1.33

Table 4.2**:** NBO σ and π bonds between C-C and Si-C for $Si_{54}C_6$ nanostructures

Structures	**C-C σ bonds**	**C-C π bonds**	**Si-C σ bonds**	**Si-C π bonds**
Hexa	6	3	6	-----
Penta	6	2	6	1
Hexa1	5	1	8	3
Ditri1	5	2	8	2
Hexa2	5	1	8	4
Hexa3	5	3	8	2
Hexa4	5	3	8	1
Ditri	5	2	8	2
Penta1	5	3	8	-----
Hexa6	5		8	-----
Penta-Hexa-tb1	4	2	10	2
Penta-Hexa-tb	4	2	10	2
Hexa5	3	3	8	1

Table 4.3: Binding energy per atom (BE), HOMO-LUMO gap, VEA, VIP (all in eV), Dipole moment (Debye), Average Si-C bond length (Å) and C-C bond length (Å) for optimized $Si_{60}C_6$ fullerene like nanostructures.

Structures	State	BE per atom (eV)	HOMO-LUMO gap (eV)	VEA (eV)	VIP (eV)	Dipole Moment (Debye)	Avg Si-C BL (Å)	Avg C-C BL (Å)
Dhex-pepar	^{1}A	3.896	0.177	4.056	6.304	1.85	1.99	1.45
Dhex-hepar	^{1}A	3.895	0.447	3.666	6.749	3.68	1.98	1.44
Dhex-heper	^{1}A	3.891	0.335	3.858	6.240	2.23	1.95	1.44
Hexa	^{1}A	3.889	0.331	3.869	6.268	2.14	1.98	1.44
Penta	^{1}A	3.878	0.373	3.783	6.221	0.77	1.90	1.46
Lin-hepar	^{1}A	3.876	0.434	3.786	6.286	3.78	1.94	1.30
Lin-peper	^{1}A	3.873	0.119	4.101	6.246	0.08	2.02	1.30
Lin-heper	^{3}A	3.870	0.171	4.147	6.267	0.66	1.95	1.26
Hexa4	^{1}A	3.866	0.419	3.761	6.232	0.81	1.93	1.34
Hexa3	^{1}A	3.864	0.198	3.970	6.220	1.91	1.99	1.35
Hexa1	^{1}A	3.862	0.204	3.965	6.192	2.40	1.94	1.40
Hexa5	^{1}A	3.860	0.403	3.782	6.200	2.17	1.89	1.45
Ph-tb1	^{1}A	3.855	0.329	3.888	6.177	0.01	1.87	1.46
Penta1	^{1}A	3.855	0.260	3.877	6.139	2.11	1.90	1.44
Ditri1	^{1}A	3.854	0.547	3.704	6.289	2.39	1.91	1.48
Dhex-peper	^{1}A	3.848	0.408	3.828	6.284	2.28	1.96	1.40
Hexa6	^{1}A	3.845	0.291	3.845	6.159	4.73	1.94	1.46
Ditri	^{1}A	3.845	0.333	3.860	6.226	2.66	1.96	1.46
Hexa2	^{3}A	3.839	0.143	3.977	6.144	1.76	1.92	1.46
Penta-hexa-tb	^{3}A	3.838	0.133	3.988	6.015	0.75	1.92	1.45

Table 4.4**:** NBO σ and π bonds between C-C and Si-C for $Si_{60}C_6$ nanostructures

Structures	**C-C σ bonds**	**C-C π bonds**	**Si-C σ bonds**	**Si-C π bonds**
Dhex-pepar	6	3	6	-----
Dhex-hepar	6	3	6	-----
Dhex-heper	6	3	6	-----
Hexa	6	3	6	-----
Penta	6	2	6	-----
Lin-hepar	5	6	3	-----
Lin-peper	5	6	4	-----
Lin-heper	5	5	3	-----
Hexa4	5	5	4	-----
Hexa3	5	5	4	-----
Hexa1	5	4	6	-----
Hexa5	4	2	10	-----
Ph-tb1	4	2	12	-----
Penta1	5	3	8	-----
Ditri1	6	2	8	-----
Dhex-peper	6	4	6	-----
Hexa6	5	1	10	-----
Ditri	5	2	10	-----
Hexa2	4	3	10	-----
Ph-tb	4	2	10	-----

Table 4.5: Harmonic vibrational frequencies (in cm^{-1}) for the most stable Hexa ($Si_{54}C_6$) structure

51.6066	53.6670	62.3425	64.4699	66.1706	67.5942
69.2840	71.2338	74.3528	76.9013	79.4822	82.8037
84.3902	86.9733	87.2549	88.5844	89.8825	91.9561
93.8196	94.6499	97.7534	99.9689	104.4714	107.0917
107.9672	110.1528	110.3677	112.5283	113.6029	115.0407
117.8613	119.5923	119.9442	122.9739	123.5558	126.7850
128.9872	132.1208	134.8681	137.3268	138.9504	139.9010
141.7933	142.9868	144.5780	145.9414	148.9365	149.6441
150.2276	151.3420	152.5980	153.7540	154.0280	156.1107
156.8233	157.7831	159.2920	161.1541	162.3279	163.2833
166.9380	167.2361	170.5793	174.8860	181.3600	181.7086
184.4003	184.9295	187.9456	188.4284	189.1316	189.6335
203.3944	205.3896	205.5822	207.7545	212.3159	216.9288
229.6824	241.5313	243.9611	259.6436	260.9012	266.4025
270.2382	274.9693	275.5735	312.0548	312.8775	324.7209
326.5496	328.9947	333.2084	336.0153	343.2868	348.6645
352.0465	355.8704	363.9089	366.8892	372.9602	378.8973
379.5664	383.1387	386.5132	390.6564	412.8396	416.3196
420.2995	426.5265	429.8828	431.4706	433.1138	442.6118
446.6550	450.6666	453.0689	455.4501	457.5894	459.3614
463.3220	465.1685	465.4681	468.2222	472.3147	474.7594
477.3736	478.9231	480.9315	487.0616	491.6377	493.9546
495.5355	497.5622	500.6095	500.8958	506.6402	513.6511
517.8133	518.8240	521.4553	522.9376	526.1510	526.9739
531.0034	533.4883	534.4340	536.4425	538.1040	540.6188
541.5989	544.8776	546.6124	547.0680	550.2673	552.2657
559.3025	563.6539	571.3961	579.5507	586.1379	590.9676
595.4452	597.2620	766.6615	772.6892	841.5563	961.6884
1010.1259	1120.9099	1128.9283	1238.9936	1324.7767	1331.4695

Table 4.6: Harmonic vibrational frequencies (in cm^{-1}) for the most stable Dhex-pepar ($Si_{60}C_6$) structure

48.0104	54.4610	63.2262	64.8817	66.9340	70.2927
75.2598	75.7797	79.1278	79.6186	81.5180	85.9226
87.4066	89.8294	90.3869	91.3196	92.8914	93.8078
94.4392	95.9884	98.3453	99.1704	99.9141	102.4280
103.5847	105.7260	108.8515	109.8580	112.4889	113.0755
114.0309	117.5268	118.7530	120.2885	122.0914	122.9736
125.4096	126.8385	130.3497	131.3191	134.7606	136.0373
138.6142	139.2111	140.8205	142.4800	144.0638	144.9304
145.2712	146.6092	147.6541	149.4390	150.0287	151.6920
152.6425	153.6297	154.8296	156.1907	157.2649	159.5351
161.0842	162.1196	164.3902	166.3427	167.7696	169.6001
171.5228	173.2481	175.0931	179.3261	181.0863	182.3557
184.7743	186.6925	187.9277	188.9440	191.7097	194.8619
196.0787	198.9965	201.7185	206.7772	211.5627	215.1459
224.4828	230.9784	233.2299	244.9014	247.0703	253.1913
263.1425	264.2855	270.1472	278.5265	282.1440	295.5148
302.8809	306.9920	310.0736	312.8386	317.9597	320.2429
325.8890	328.0364	333.8930	338.4243	342.0895	344.9279
347.4840	354.2319	358.2418	360.6354	363.5151	369.5996
372.1887	379.8025	380.8133	381.5163	387.4256	393.9491
403.9621	405.2798	412.8501	414.4996	419.3373	423.3057
425.6977	429.6442	432.3469	435.9125	436.9609	439.5228
442.6969	446.2311	449.5497	450.6020	455.7289	456.9454
458.6002	462.6334	465.7578	466.3718	468.6699	470.5858
475.7853	476.0236	478.3146	478.4717	484.0034	485.0182
489.7694	493.0806	498.6518	504.2676	508.1725	511.9767
512.9776	515.6333	517.2627	519.9383	521.5607	522.5366
524.2985	525.5530	527.0766	529.4400	530.3168	531.1632
535.5751	536.7232	539.2073	540.3118	545.6558	546.9955
549.7297	550.2936	551.4860	556.1531	559.7381	562.8541
564.3654	567.8690	708.4315	719.2559	731.7504	951.0004
979.9193	1121.2007	1146.1703	1218.9516	1310.3426	1348.1393

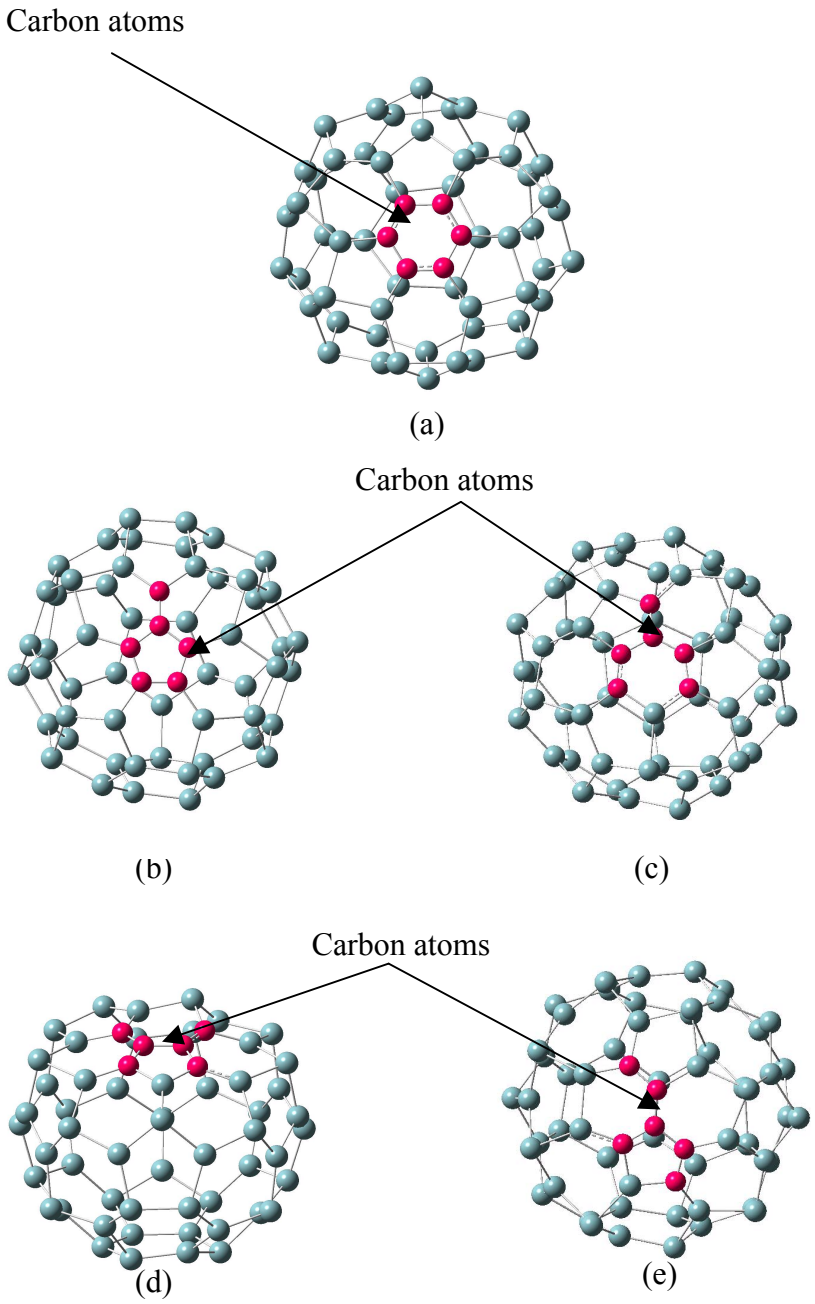

Figure 4.1: Optimized structures of $Si_{54}C_6$ stable silicon-carbon fullerene like nanostructures (a) Hexa (b) Penta (c) Hexa1 (d) Ditri1 (e) Hexa2 (Carbon atoms denoted by dark pink color)

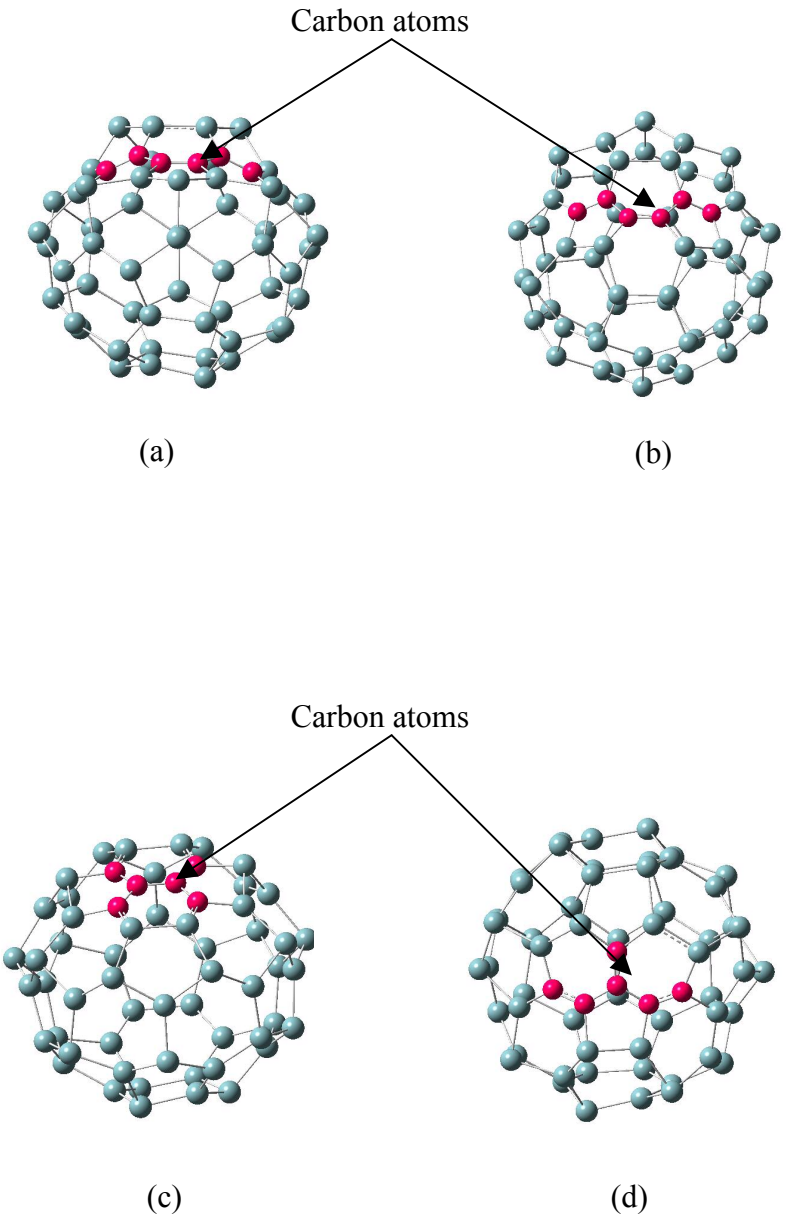

Figure 4.2: Optimized structures of $Si_{54}C_6$ stable silicon-carbon fullerene like nanostructures (a) Hexa3 (b) Hexa4 (c) Ditri (d) Penta1
(Carbon atoms denoted by dark pink color)

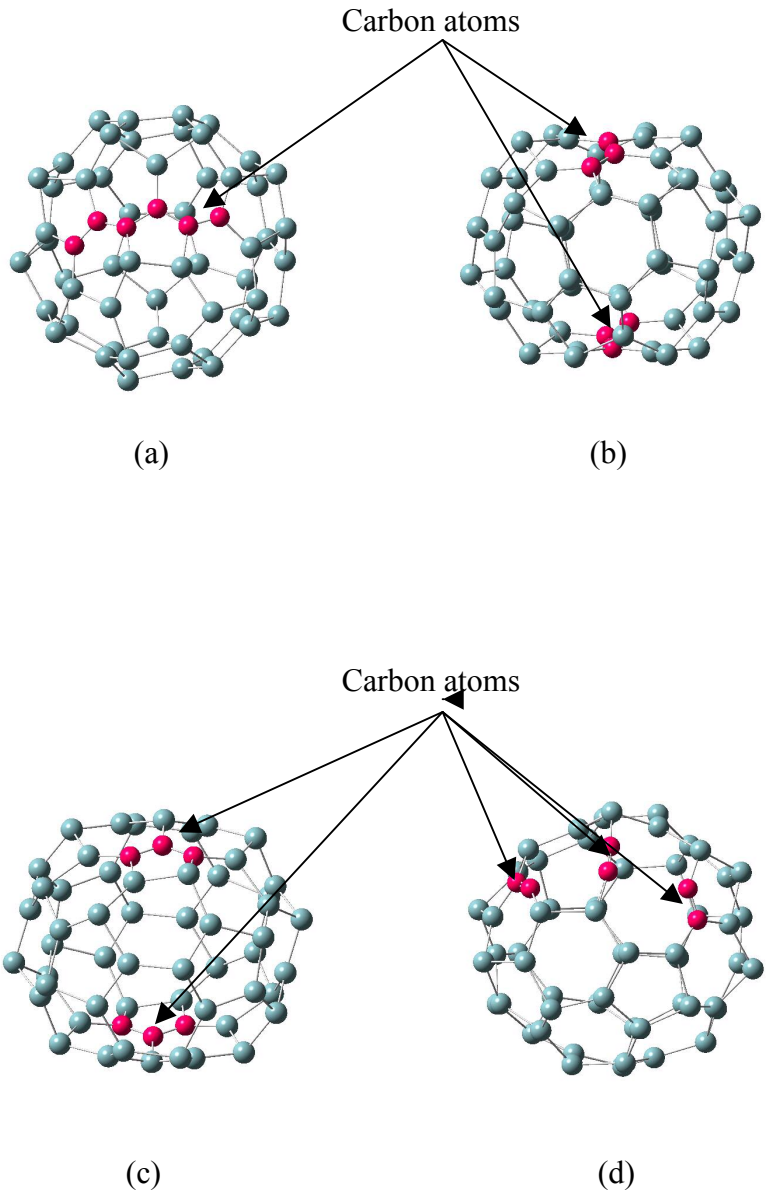

Figure 4.3: Optimized structures of $Si_{54}C_6$ stable silicon-carbon fullerene like nanostructures (a) Hexa6 (b) Penta-Hexa-tb1 (c) Penta-Hexa-tb (d) Hexa5 (Carbon atoms denoted by dark pink color)

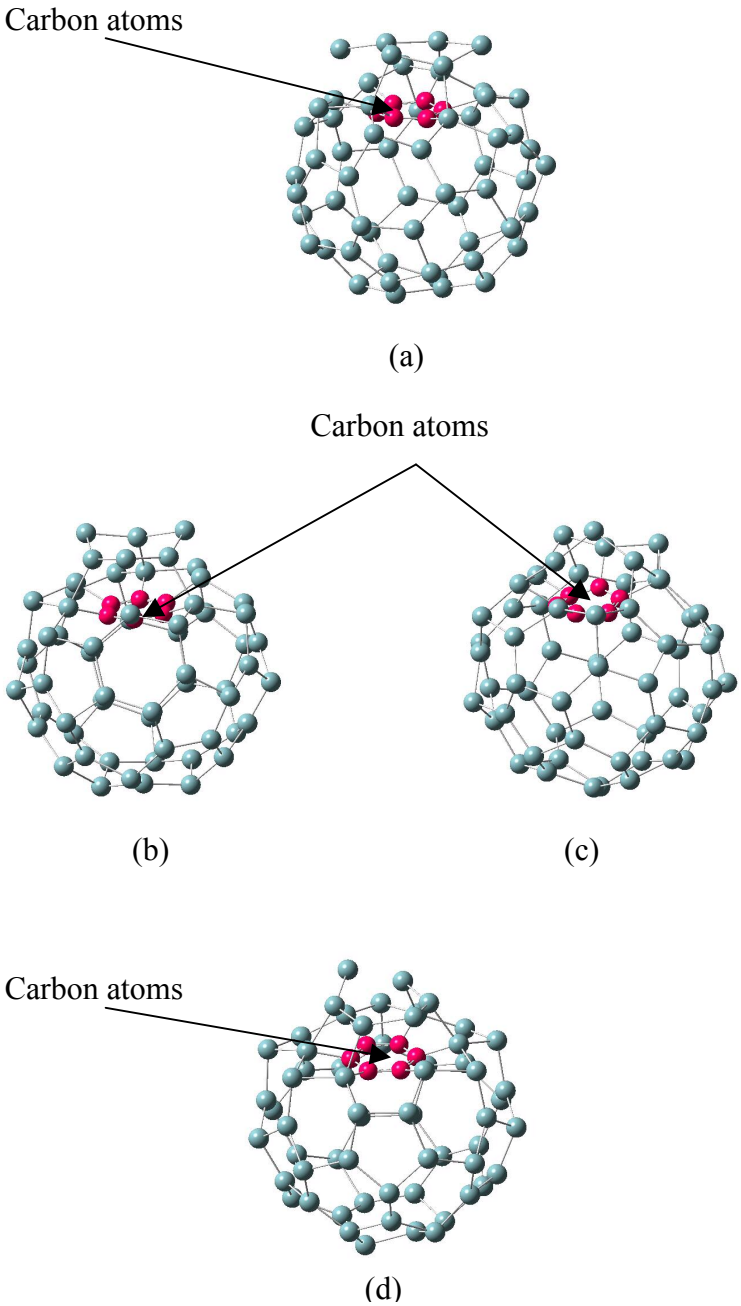

Figure 4.4: Optimized structures of $Si_{60}C_6$ stable silicon-carbon fullerene like nanostructures (a) Dhex-pepar (b) Dhex-hepar (c) Dhex-heper (d) Hexa (Carbon atoms denoted by dark pink color)

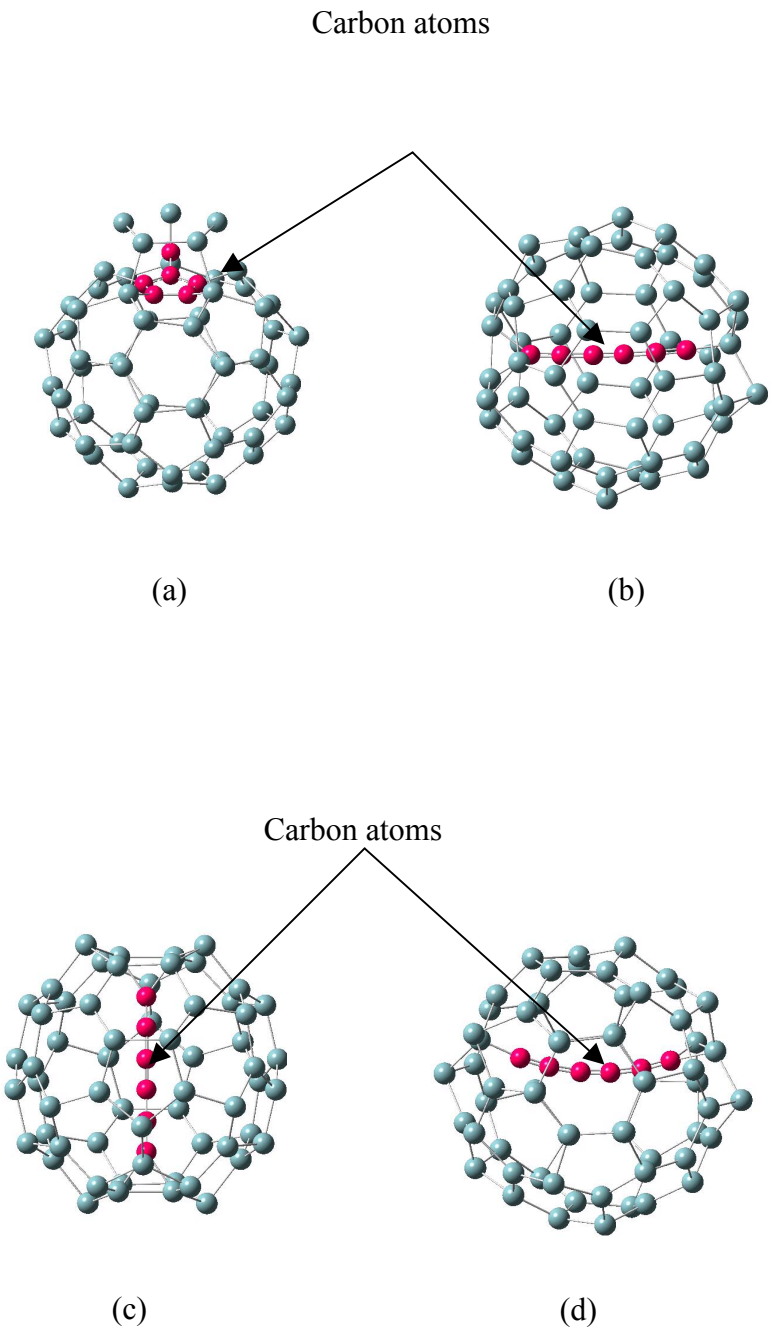

Figure 4.5: Optimized structures of $Si_{60}C_6$ stable silicon-carbon fullerene like nanostructures (a) Penta (b) Lin-hepar (c) Lin-peper (d) Lin-heper (Carbon atoms denoted by dark pink color)

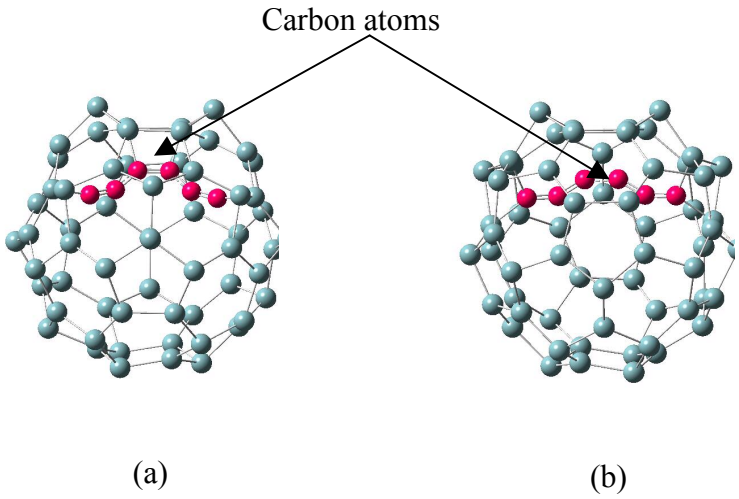

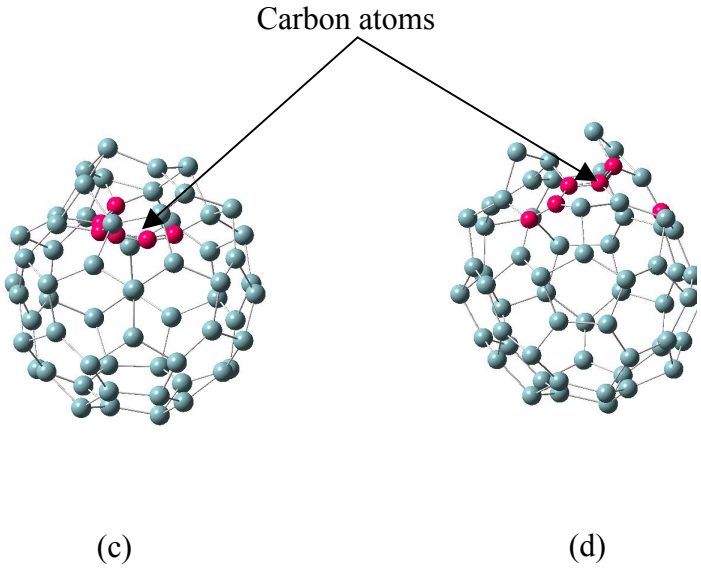

Figure 4.6: Optimized structures of $Si_{60}C_6$ stable silicon-carbon fullerene like nanostructures (a) Hexa4 (b) Hexa3 (c) Hexa1 (d) Hexa5
(Carbon atoms denoted by dark pink color)

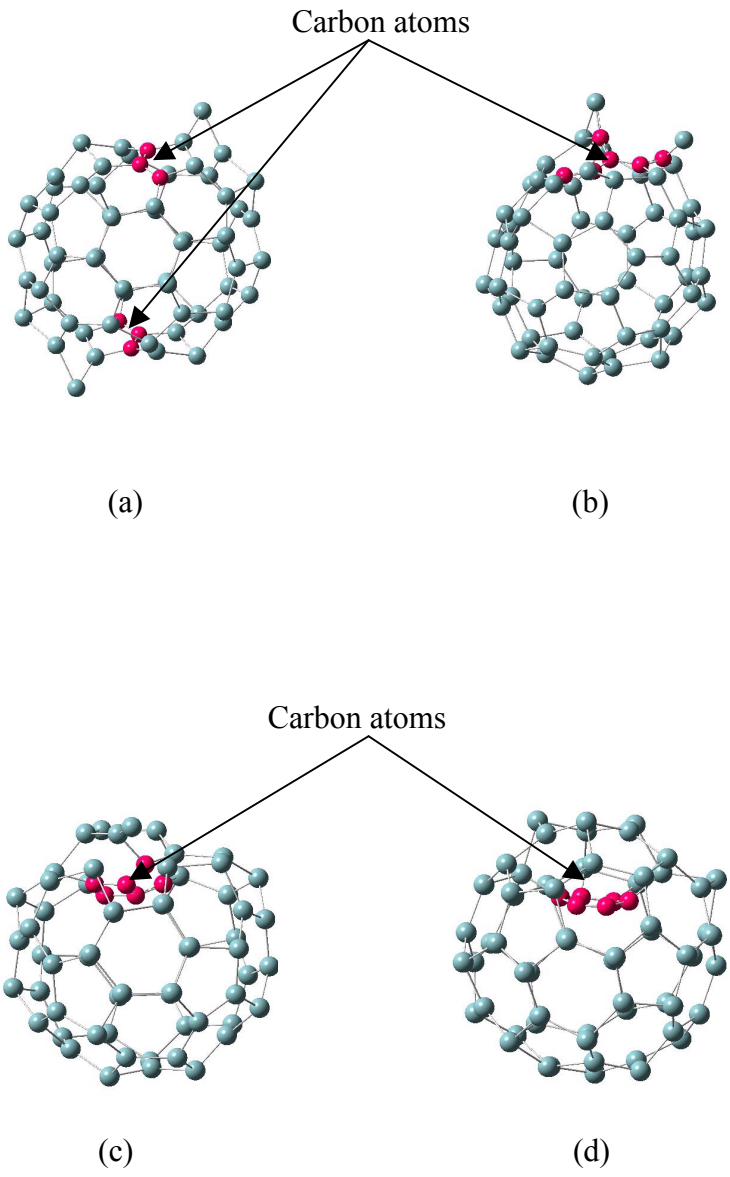

Figure 4.7: Optimized structures of $Si_{60}C_6$ stable silicon-carbon fullerene like nanostructures (a) Penta-Hexa-tb1 (b) Penta1 (c) Ditri1 (d) Dhex-peper (Carbon atoms denoted by dark pink color)

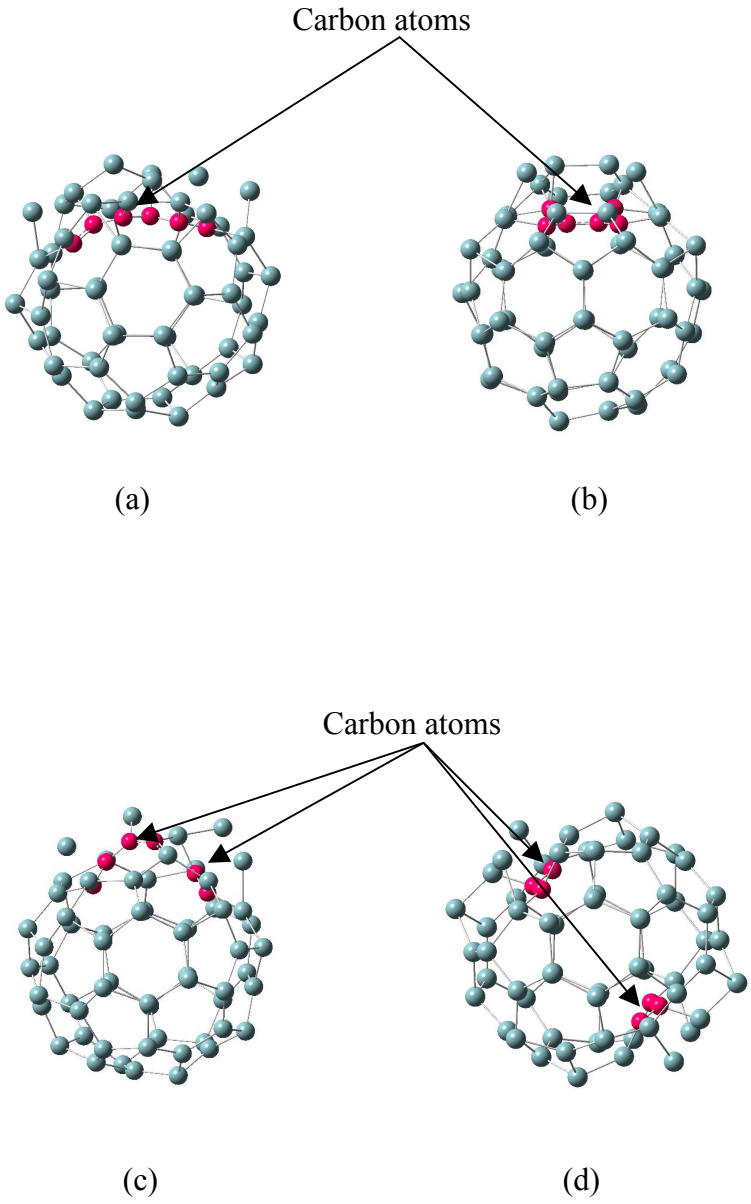

Figure 4.8: Optimized structures of $Si_{60}C_6$ stable silicon-carbon fullerene like nanostructures (a) Hexa6 (b) Ditri (c) Hexa2 (d) Penta-Hexa-tb (Carbon atoms denoted by dark pink color)

4.2 Charge distributions for the most stable $Si_{54}C_6$ and $Si_{60}C_6$ fullerene like Nanostructures

We also performed detailed Mulliken charge population [101-103] analysis for the clusters reported here. In general, Mulliken charge analysis for all the structures indicates that carbon atoms gain charge and the silicon atoms lose charge, as expected from their electro-negativities. Some exceptions were noted in which carbon atoms lose charge and silicon atoms gain charge indicating asymmetric charge distribution and total dipole moment values for the structures. Mulliken charge distribution diagrams for the two most stable structures in each set along with the electronic charges for all atoms are reported in Figs 4.9, 4.10 and Tables 4.7, 4.8 respectively. All the charges are noted in electronic charge unit. In general these structures have mostly covalent and partly ionic bonding between the silicon and carbon atoms. For example, in the $Si_{54}C_6$ Hexa structure (Fig 4.9) six carbon atoms (labels 28, 29, 30, 31, 47 and 48) along the six corners of the hexagon have electronic charges of -0.17, -0.29, -0.30, -0.17, -0.23 and -0.23 respectively and they are bonded to six silicon atoms (labels 11, 13, 27, 32, 46 and 49) having electronic charges of (0.34, 0.33, 0.06, 0.07, 0.07 and 0.07), which clearly indicates mixed ionic and covalent bonding, with covalent being more prominent. The ionic character of bonding results from the Si-C interactions with C-C interactions being predominantly covalent in nature. From Figure 4.10, we notice exceptions in the Mulliken charge distribution for the Dhex-pepar structure ($Si_{60}C_6$) as the 6 silicon atoms bonded to the carbon atoms gain charge. Silicon atom labels (16, 33, 37, 50, 54 and 60) and their Mulliken electronic charges (-0.19, -0.25, -0.07, -0.31, -0.27, and -0.06) show

negative electronic charges for all six silicon atoms and all the carbon atoms have negative electronic charges which results in a repulsive type of interaction between silicon and carbon atoms offsetting the increased C-C interaction. The VIPs and the VEAs for all the optimized nanostructures reported in this work are considerably high indicating stability. In general Mulliken charge analysis for the novel silicon-carbon fullerene like nanostructures indicates a mixed ionic-covalent bonding with covalent being more prominent for $Si_{54}C_6$ nanostructures and increased ionic contribution for $Si_{60}C_6$ nanostructures.

Table 4.7: Mulliken electronic charges for the atoms of most stable Hexa ($Si_{54}C_6$) structure

1	Si	0.13	31	C	-0.17
2	Si	-0.17	32	Si	0.07
3	Si	0.17	33	Si	0.26
4	Si	-0.13	34	Si	-0.13
5	Si	-0.02	35	Si	0.17
6	Si	-0.02	36	Si	-0.11
7	Si	0.13	37	Si	0.11
8	Si	-0.10	38	Si	-0.15
9	Si	0.18	39	Si	0.13
10	Si	-0.20	40	Si	-0.15
11	Si	0.33	41	Si	0.16
12	Si	-0.16	42	Si	-0.16
13	Si	0.33	43	Si	0.18
14	Si	-0.21	44	Si	-0.15
15	Si	0.18	45	Si	0.19
16	Si	-0.06	46	Si	0.07
17	Si	0.01	47	C	-0.23
18	Si	-0.12	48	C	-0.23
19	Si	0.15	49	Si	0.07
20	Si	-0.11	50	Si	0.19
21	Si	0.16	51	Si	-0.19
22	Si	-0.15	52	Si	0.18
23	Si	0.09	53	Si	-0.05
24	Si	0.05	54	Si	-0.02
25	Si	-0.09	55	Si	-0.11
26	Si	0.26	56	Si	0.14
27	Si	0.06	57	Si	-0.16
28	C	-0.17	58	Si	0.15
29	C	-0.29	59	Si	0.16
30	C	-0.30	60	Si	-0.17

Table 4.8: Mulliken electronic charges for the atoms of most stable Dhex-pepar ($Si_{60}C_6$) structure

1	Si	0.09	34	Si	0.29
2	Si	0.03	35	Si	-0.10
3	Si	-0.13	36	Si	0.10
4	Si	0.15	37	Si	-0.07
5	Si	-0.14	38	Si	-0.04
6	Si	0.15	39	Si	0.23
7	Si	-0.10	40	Si	-0.16
8	Si	0.14	41	Si	0.17
9	Si	-0.15	42	Si	-0.13
10	Si	0.14	43	Si	0.15
11	Si	-0.16	44	Si	-0.15
12	Si	0.15	45	Si	0.15
13	Si	-0.11	46	Si	-0.17
14	Si	0.19	47	Si	0.16
15	Si	0.02	48	Si	-0.10
16	Si	-0.19	49	Si	0.25
17	Si	0.27	50	Si	-0.30
18	Si	-0.14	51	Si	0.20
19	Si	0.15	52	Si	0.01
20	Si	-0.16	53	Si	0.26
21	Si	0.14	54	Si	-0.27
22	Si	-0.05	55	Si	-0.07
23	Si	0.00	56	Si	0.23
24	Si	0.13	57	Si	-0.17
25	Si	-0.10	58	Si	0.17
26	Si	-0.03	59	Si	-0.08
27	Si	-0.03	60	Si	-0.06
28	Si	-0.12	61	C	-0.25
29	Si	0.13	62	C	-0.06
30	Si	-0.01	63	C	-0.14
31	Si	-0.04	64	C	-0.17
32	Si	0.27	65	C	-0.09
33	Si	-0.25	66	C	-0.06

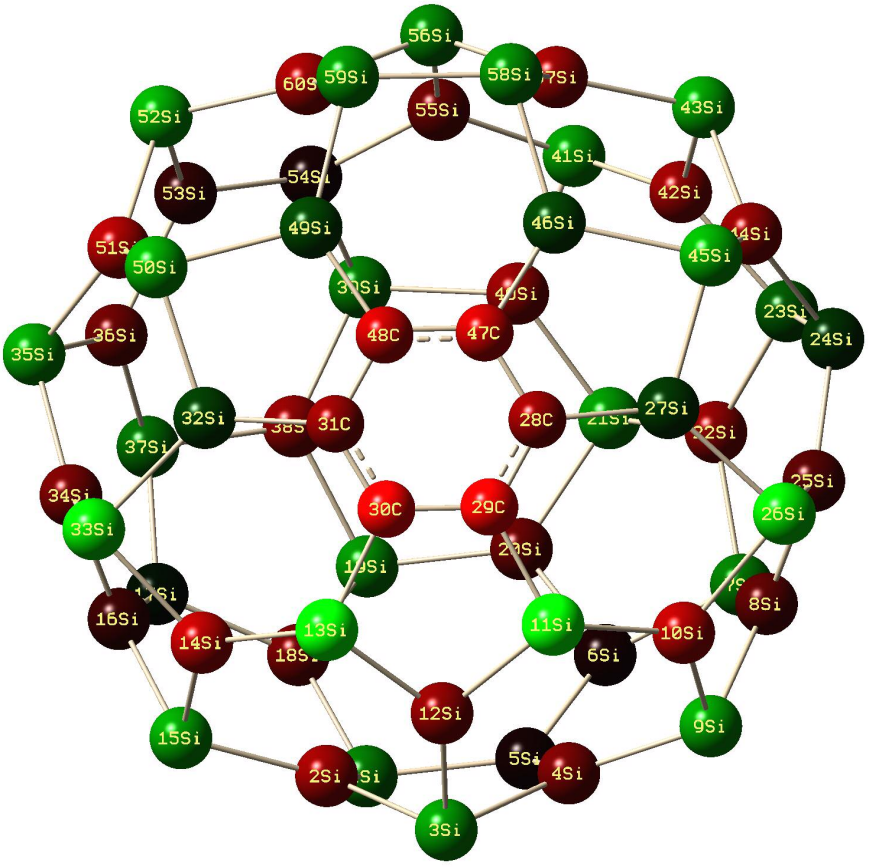

Figure 4.9: Mulliken charge distributions for the most stable Hexa ($Si_{54}C_6$) structure.

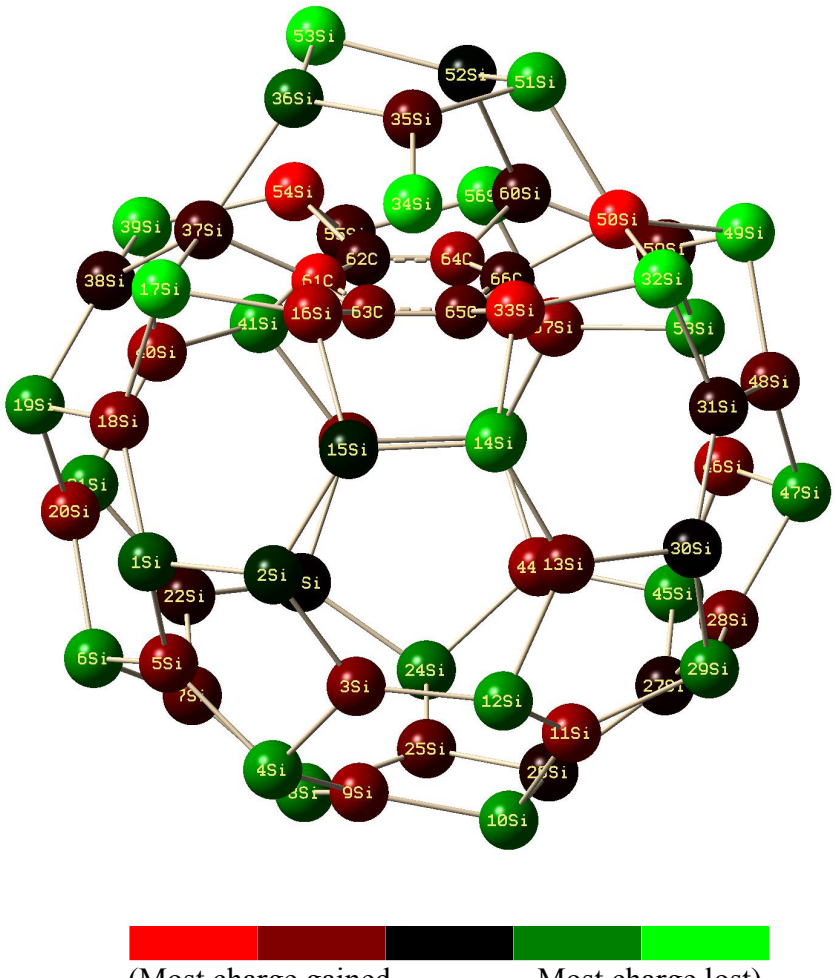

Figure 4.10: Mulliken charge distributions for the most stable Dhex-pepar ($Si_{60}C_6$) structure.

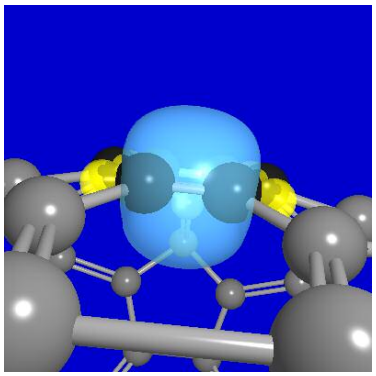

(a)

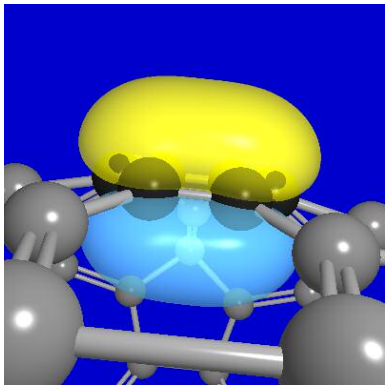

(b)

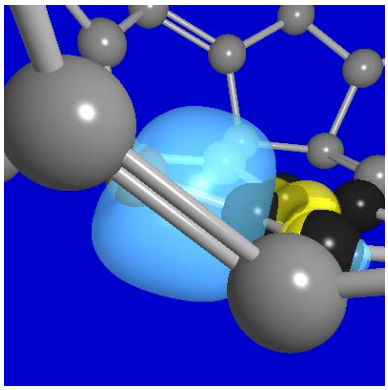

(c)

Figure 4.11: Natural Bond Orbital (NBO) plots generated using NBO program & NBO View for the most stable Hexa structure ($Si_{54}C_6$) (a) σ bond between C-C (b) π bond between C –C (c) σ bond between Si-C.

CHAPTER 5

STABILITY OF $Si_{60}C_{2n}$ FULLERENE LIKE NANOSTRUCTURES (n=10, 12)

5.1 Results and Discussions on $Si_{40}C_{20}$, $Si_{60}C_{20}$, $Si_{36}C_{24}$ and $Si_{60}C_{24}$ Nanostructures

As is known, Si_{60} fullerene like cage has 12 pentagons and 20 hexagons. In the first step, silicon atoms on the surface of the cage have been replaced by twenty and twenty four carbon atoms at various symmetry orientations. In the second step, C_{20} and C_{24} clusters are put inside the Si_{60} cage symmetrically with respect to its center. For C_{20} clusters, theoretical and experimental studies have reported possible structures as the bowl, fullerene, ring, bow-tie and planar sheet like structures [23-25, 91-98, 106 -110]. For this reason, C_{20} clusters in bowl, fullerene like cage, ring, bow-tie and two planar sheets like structures optimized at GGA-DFT level of theory have been added inside the cage. For C_{24} clusters, theoretical and experimental studies have reported possible structures as the flat graphitic sheet, one pentagon bowl, three pentagon bowl, ring, fullerene and a cage structure with square, pentagonal and hexagonal faces [91-98, 106-110]. For this reason, C_{24} clusters in graphitic sheet, one pentagon bowl, three pentagonal bowl, ring, fullerene and a square faced cage optimized at GGA-DFT level of theory have been added inside the cage.

In the results to follow, we report the electronic states, binding energies per atom (BE), highest occupied – lowest unoccupied molecular orbital (HOMO-LUMO)

gaps, vertical ionization potentials (VIPs) , vertical electron affinities (VEAs) and total dipole moments of the stable fullerene-like $Si_{40}C_{20}$, $Si_{60}C_{20}$, $Si_{36}C_{24}$ and $Si_{60}C_{24}$ optimized structures with their corresponding average Si-C and C-C bond lengths. Binding energies per atom of the clusters are calculated as the relative energies of these clusters in the separated atom limit, with the atoms in their respective ground states, with a positive binding energy indicating stability. VIPs and VEAs have been calculated as the difference in the total energies between the neutral clusters and the corresponding positively and negatively charged clusters at the neutral optimized geometries. For the four most $Si_{40}C_{20}$, $Si_{60}C_{20}$, $Si_{36}C_{24}$ and $Si_{60}C_{24}$ stable structures harmonic frequencies are also reported. Bonding between the atoms, especially Si-C and C-C for all the stable structures were analyzed using the NBO (Natural Bonding Orbital) program and NBO View [100].

For the set of optimized $Si_{40}C_{20}$ fullerene like nanostructures reported in Table 5.1, the column under the structures refers to the positions of the carbon atoms substituting silicon atoms on the surface of the Si_{60} cage. The optimized geometries of all the structures in Table 5.1 are reported in Figure 5.1 The most stable structure Sur1 (a) has twenty carbon atoms in an arrangement of one pentagon surrounded by five hexagons. The structure Sur2 (b) has twenty carbon atoms in an arrangement of one hexagon surrounded by three hexagons and three pentagons. The structure Sur3 (c) denotes the other possible way of arranging twenty carbon atoms in a hexagon surrounded by three hexagons and three pentagons. The structure Tb1 (d) has ten carbon atoms along the corners of two hexagons at two ends of the cage. The structure Tb2 (e)

has ten carbon atoms along the corners of two pentagons at two ends of the cage. For the Dia (f) structure, the twenty carbon atoms are in an arrangement which dissects the cage in to two sections of Si_{20} (one pentagon surrounded by five hexagons).

As seen from Table 5.1, the first three structures are almost degenerate structures comparable in stability in the set of $Si_{40}C_{20}$ structures. The first structure Sur1 has the highest BE per atom of 4.748 eV in this set. The dipole moment of this structure has a value of 1.36 Debye indicating mixed ionic-covalent bonding nature contributing to its increased stability. The average Si-C and C-C bond lengths for this structure are 1.91 Å and 1.45 Å, respectively. This structure has the highest HOMO-LUMO gap of 0.528 eV in this set. NBO analysis of this structure yielded 25 C-C σ bonds, 10 C-C π bonds and 10 Si-C σ bonds. NBO σ bonds and π bonds between C-C and Si-C for this structure are shown in Figure 5.10. Important thing to be noted in this structure is the strong covalent bonding between the C-C σ bonds and a slight increase in the asymmetric charge distribution among the C-C π bonds. The Sur2 structure BE per atom is only 0.001 eV less than the previous structure. NBO analysis yielded 24 C-C σ bonds, 8 C-C π bonds 10 Si-C σ bonds and 3 Si-C π bonds. The number of C-C bonds is less compared to the previous structure, contributing to its small difference in binding energy. The BE per atom of the Sur3 structure is 0.004 eV less than the most stable Sur1 structure. NBO analysis of this structure yielded 25 C-C σ bonds, 10 C-C π bonds and 10 Si-C σ bonds similar to the Sur1 structure but the average occupancies of the C-C π bonds and the Si-C σ bonds were slightly lower, indicating weaker C-C interaction and Si-C interaction contributing to its lower binding energy. NBO analysis of the Tb1

structure yielded 22 C-C σ bonds, 8 C-C π bonds and 16 Si-C σ bonds clearly indicating that increase in the Si-C bonding at the expense of the C-C bonding contributes to lower binding energy. NBO analysis of the Tb2 structure yielded the same number of C-C bonds and Si-C bonds compared to the Tb1 structure but its average occupancies were lower indicating weaker Si-C and C-C interaction contributing to its lower binding energy. NBO analysis of Dia structure yielded the maximum number of 20 Si-C σ bonds but the number of C-C bonds were lower (20 C-C σ bonds and 10 C-C π bonds), contributing to its lower binding energy. The Dipole moment value of 0.02 Debye indicates a very negligible ionic contribution to strong covalent bonding. This structure has the highest VIP in this set. The Tb1 structure has the highest VEA in this set. The vibrational frequencies for the most stable Sur1 structure are listed in Table 5.9.

The second set of optimized structures, $Si_{60}C_{20}$ with C_{20} clusters inside the Si_{60} cage are listed in Table 5.3 and the corresponding geometries are presented in Figure 5.2. Here also the column below the structures denotes the orientations of carbon atoms inside the Si_{60} cage. The bowl structure (a) has C_{20} bowl (one pentagon surrounded by five hexagons) inside the Si_{60} cage. The Sheet2 structure (b) has two twenty carbon atoms in four hexagons and one heptagon (in a flat sheet like arrangement) inside the Si_{60} cage. For the Sheet1 structure (c), there are twenty carbon atoms in five hexagons (in a flat sheet like arrangement) inside the Si_{60} cage. The Cage (d) has C_{20} cluster in fullerene like cage arrangement and the Ring (e) has C_{20} cluster in ring arrangement inside the Si_{60} cage. As a test of Si-C bond strength, we also put the carbon atoms closer

to the surface, with the same surface orientations in Table 5.1, at an initial optimized SiC dimer bond length of 1.77 Å (at GGA-DFT) but the optimized structures were energetically unfavorable.

The bowl structure has the highest BE per atom of 4.482 eV and also has highest VIP in this set. The dipole moment value of 2.73 Debye indicates a mixed ionic-covalent bonding contributing to its increased stability. NBO analysis of this structure yielded 25 C-C σ bonds, 11 C-C π bonds and 10 Si-C σ bonds. This structure has the maximum number of C-C bonds, which might be the reason for its increased stability. As a test for true ground state, the C_{20} bowl was rotated by 30, 60 and 90 degrees inside the Si_{60} cage and the variation in binding energies of the optimized structures were very low ranging from -0.2% to +0.06%. NBO analysis of Sheet2 structure yielded 24 C-C σ bonds, 10 C-C π bonds and 12 Si-C σ bonds clearly indicating that decrease in the number of C-C bonds contributes to its lower binding energy. NBO analysis of Sheet1 structure yielded the same number of C-C and Si-C bonds as Sheet2 structure but their average occupancies were lower contributing to its lower binding energy. NBO analysis of the Cage structure yielded the maximum number of 30 C-C σ bonds and 6 C-C π bonds but the number of Si-C σ bonds were four and also weaker as evident from the average Si-C bond length, clearly indicating that lesser and weaker Si-C interaction contributing to its lower stability. NBO analysis of the Ring structure yielded the maximum number of 18 Si-C σ bonds, 20 C-C σ bonds and 12 C-C π bonds. The average occupancies of Si-C bonds were also lower compared to all previous structures, indicating that less C-C interactions and weaker Si-C interactions contributed to its

lower stability. The Cage structure has the highest VEA and the Ring structure has the highest HOMO-LUMO gap in this set. The vibrational frequencies for the most stable Bowl structure are reported in Table 5.10.

The third set of optimized structures is $Si_{36}C_{24}$ fullerene like nanostructures, which have twenty four carbon atoms substituting the silicon atoms on the surface of the Si_{60} cage. These are reported in Table 5.5 and their corresponding geometries are presented in Figures 5.3 and 5.4. The structure Sur4 (Fig 5.3 a) has twenty four carbon atoms arranged along the corners in four pentagons and four hexagons. The structures Sur1 (Fig 5.3 b), Sur2 (Fig 5.3 c) and Sur3 (Fig 5.3 d) have basic prototype of one pentagon surrounded by five hexagons for twenty carbon atoms, differing in the arrangement of other four carbon atoms. For the structure Sur5 (Fig 5.3 e), there are twenty four carbon atoms along the corners of three pentagons and five hexagons. The rest of the structures Tb4 (Fig 5.4 a), Tb2 (Fig 5.4 b), Tb3 (Fig 5.4 c), Tb1 (Fig 5.4 d) and Tb5 (Fig 5.4 e) have twelve carbon atoms in different arrangements along the two ends of the cage.

For the first five structures in Table 5.5, the binding energies are within 10 meV. This indicates that the structures are almost degenerate and comparable in stability. The Sur4 structure has the highest BE per atom of 4.977 eV and has highest HOMO-LUMO gap of 0.557 eV in this set. The dipole moment value of 1.41 Debye indicates a mixed ionic-covalent bonding nature contributing to its stability. NBO analysis of this structure yielded 31 C-C σ bonds, 10 C-C π bonds, 10 Si-C σ bonds and 4 Si-C π bonds. NBO σ and π bonds between C-C and Si-C for this Sur4 structure are shown in Figure

5.11. The next two structures Sur1 and Sur5 differ in BE per atom by 0.002 eV compared to Sur4 structure. NBO analysis for Sur1 structure yielded 30 C-C σ bonds, 11 C-C π bonds, 12 Si-C σ bonds and 2 Si-C π bonds. One of the reasons for its lower binding energy might be the substitution of one C-C σ bond by C-C π bond having lower occupancy. NBO analysis of Sur5 structure yielded 31 C-C σ bonds, 11 C-C π bonds, 10 Si-C σ bonds and 2 Si-C π bonds. The number of C-C bonds is one more than the Sur4 structure but the Si-C interactions were lower, contributing to its lower stability. This might indicate Si-C interactions are also important for stability. This structure has the highest VIP and VEA in this set. For Sur2 structure, NBO analysis yielded 30 C-C σ bonds, 12 C-C π bonds and 12 Si-C σ bonds but the Si-C interactions were weaker (Average Si-C bond length of 1.90 Å) contributing to its lower stability. The set of structures Tb4, Tb2, Tb3, Tb1 and Tb5 have twelve carbon atoms along two ends of the cage, indicating that the number of Si-C interactions is higher and the number of C-C interactions are less compared to previous structures. Less C-C interactions contribute to their low binding energies. Except for Tb2 structure, the dipole moment values for rest of them indicate very negligible ionic contribution to strong covalent bonding. Important thing to be noted in Tb4 structure is that the optimized structure shows significant reconstructions from its original fullerene like geometry to a flat tube like geometry. The vibrational frequencies for the most stable Sur4 structure are reported in Table 5.11.

The last set of optimized structures is $Si_{60}C_{24}$ fullerene like nanostructures, which has C_{24} clusters inside the Si_{60} cage. These are reported in Table 5.7 and their

corresponding geometries in Figure 5.5. The Sheet structure (a) has twenty four carbon atoms placed on the corners of seven hexagons (in a flat sheet like arrangement) inside the Si_{60} cage. The 3bowl structure (b) has twenty four carbon atoms arranged among three pentagons and five hexagons inside the Si_{60}cage. For 1bowl structure (c), twenty four carbon atoms are arranged among one pentagon and six hexagons inside the Si_{60} cage. The Cage (d), Rcage (e) and Ring (f) structures have C_{24} clusters inside Si_{60} cage in fullerene like cage, square cage (having pentagonal, hexagonal and square faces) and ring like arrangement respectively. As a test of Si-C bond strength, we also put the carbon atoms closer to the surface, with the same surface orientations in Table 5.5, at an initial optimized SiC dimer bond length of 1.77 Å (at GGA-DFT) but the optimized structures were energetically unfavorable.

The Sheet structure has the highest BE per atom of 4.599 eV and also highest VEA of 4.142 eV in this set. This structure has the strongest Si-C and C-C interaction evident from its average Si-C and C-C bond length. The dipole moment value of 2.15 Debye indicates a mixed ionic-covalent bonding nature contributing to its stability. NBO analysis of this structure yielded 30 C-C σ bonds, 13 C-C π bonds and 12 Si-C σ bonds. NBO analysis of the 3bowl structure yielded 31 C-C σ bonds, 11 C-C π bonds and 12 Si-C σ bonds. The total number of C-C bonds in this structure is lower compared to previous structure. The average occupancies of C-C π bonds and Si-C σ bonds are lower compared to the previous structure. These might be the reasons for 3bowl structure to have lower binding energy compared to Sheet structure. NBO analysis of 1bowl structure yielded 30 C-C σ bonds, 12 C-C π bonds and 12 Si-C σ bonds. One of

the C-C σ bonds in 3bowl is replaced by C-C π bond in 1bowl structure whose occupancy is lower compared to σ bond. This might be the reason for 1bowl structure to have lower stability. For the Cage structure, NBO analysis yielded the maximum number of C-C bonds in this set (36 σ bonds and 8 π bonds) but the number of Si-C bonds (11 σ bonds) were lower and also weaker. The C-C interactions are also weaker for this structure (average C-C bond length of 1.53 Å) clearly indicating that Si-C bonding and C-C bonding together are important for stability. The Rcage structure also has weaker Si-C interactions, as evident from the average Si-C bond length similar to Cage structure. The number of C-C bonds is also lower in this structure (36 σ bonds and 6 π bonds) compared to Cage structure. These might be the factors for Rcage to have lower stability. NBO analysis of the Ring structure yielded the maximum number of Si-C bonds (28 σ bonds) and minimum number of C-C bonds (22 σ bonds and 12 π bonds) in this set. Less C-C interactions in this structure contribute to its lower stability. The 3bowl structure has the highest VIP and 1bowl structure has the highest HOMO-LUMO gap in this set. The vibrational frequencies for the most stable Sheet structure are reported in Table 5.12.

A common feature of the above $Si_{60}C_{24}$ structures is that the carbon atoms put inside the Si_{60} cage interact with the silicon atoms on the surface of the cage thereby pushing a few silicon atoms outside the surface of fullerene like cage, and as a result those silicon atoms are loosely bounded to the cage. This might be one of the reasons for the lower binding energy of these set compared to $Si_{36}C_{24}$ nanostructures. For example, the structure 1bowl (Fig 5.5 c) BE per atom in this set is 0.033 eV lower than

the most stable structure in this set. As discussed before the NBO analysis of this structure yielded 30 C-C σ bonds, 12 C-C π bonds and 12 Si-C σ bonds. NBO analysis of the most stable Sheet structure in this set (Fig 5.5 a) yielded 30 C-C σ bonds, 13 C-C π bonds and 12 Si-C σ bonds. This structure has one extra C-C π bond and also stronger Si-C interactions compared to the 1bowl structure. This might indicate that Si-C interactions and C-C interactions together are important for stability. Comparing the 1bowl structure with the Sur2 structure (Fig 5.3 b), the arrangement of carbon atoms in both the structures is the same, one at surface and the other inside the cage. NBO analysis of this Sur2 structure yielded 30 C-C σ bonds, 12 C-C π bonds and 12 Si-C σ bonds similar to the 1bowl ($Si_{60}C_{24}$) structure. The average occupancies of C-C π bonds and Si-C σ bonds were higher, contributing to its increased binding energy. This might again indicate that both Si-C and C-C interactions are important for stability and their interactions are stronger at the surface than inside the cage. In fact, the increase in Si-C bonding at the expense of C-C bonding contributes to lower stability. For example, in the Ring structure which has the maximum number of Si-C bonds (28 σ bonds), the number of and C-C bonds are lower (22 σ bonds and 12 π bonds) leading to lower stability. Also in some structures, some of the silicon atoms gain charge similar to carbon atoms, which offsets the stability of the nanostructures because of repulsive effect between the silicon and carbon atoms.

Similar conclusions can be made to the set of $Si_{60}C_{20}$ and $Si_{40}C_{20}$ nanostructures. For the set of $Si_{60}C_{20}$ fullerene like nanostructures, the carbon atoms in C_{20} clusters interact with the surface silicon atoms of the cage thereby pushing silicon atoms out of

the cage surface, thus loosely bonded to the cage. From Table 5.3, the structure Sheet1 (Fig 5.2 c) BE per atom differs from the most stable structure by 0.048 eV. NBO analysis of this structure yielded 24 C-C σ bonds, 10 C-C π bonds and 12 Si-C σ bonds. NBO analysis for the most stable Bowl structure in this set yielded 25 C-C σ bonds, 11 C-C π bonds and 11 Si-C σ bonds, clearly indicating that increased Si-C and C-C interaction contributed to its higher binding energy. This might indicate that Si-C and C-C interactions together are important for stability. Comparing this Bowl structure with the most stable Sur1 structure ($Si_{40}C_{20}$) from Table 5.1, the arrangement of twenty carbon atoms are the same, one on the surface and the other inside the cage. NBO analysis of this Sur1 structure yielded 25 C-C σ bonds, 10 C-C π bonds and 10 Si-C σ bonds. This structure has one C-C π bond and 1 Si-C σ bond less than the Bowl structure ($Si_{60}C_{20}$). The average occupancies of C-C π bond (1.70) and Si-C σ bond (1.94) in this Sur1 structure a are greater than the most stable Bowl Structure (1.67 and 1.89 respectively), clearly indicating stronger Si-C interactions and C-C interactions at the surface contribute to its higher binding energy. Some silicon atoms bonded with carbon atoms in the Bowl structure gain charge similar to carbon atoms, indicating that repulsive interaction could have brought down the stability compared to the Sur1 structure. This might again indicate that Si-C interactions and C-C interactions together are important for stability.

In general, all the optimized structures considered here are stable nanostructures with higher binding energies per atom compared to the bare Si_{60} cage which has a binding energy per atom of 3.61eV at GGA-DFT level of theory. In our

previous discussions,[28] we have seen that binding energies per atom for the $Si_{58}C_2$, $Si_{60}C_2$, $Si_{56}C_4$, $Si_{60}C_4$, $Si_{54}C_6$, $Si_{60}C_6$ fullerene like nanostructures were higher compared to the bare Si_{60} cage and they increase with the number of carbon atoms from two to six. Also, the structures with carbon atoms substituting silicon atoms on the surface of the Si_{60} fullerene cage give higher binding energies compared to the structures with carbon atoms put inside the Si_{60} cage. Here too from Tables 5.1, 5.3, 5.5 and 5.7, the binding energies of $Si_{40}C_{20}$, $Si_{60}C_{20}$, $Si_{36}C_{24}$ and $Si_{60}C_{24}$ nanostructures were higher compared to the results for two, four and six carbon atoms and agree with the trend of increasing binding energies with increase in carbon atoms. The stability of the nanostructures here is found to be dependent on the orientations of carbon atoms inside or on the surface of fullerene like cage. All the optimized nanostructures tend to be distorted and not a smoother fullerene like silicon nanostructures.

As mentioned before that for the most part carbon-carbon interactions and the Si-C interactions contribute to the cage stability. The inclusion of twenty carbon atoms on the surface of the Si_{60} cage increased the BE per atom by 31.5% and the inclusion of twenty carbon atoms inside the Si_{60} cage increased BE per atom by 24% compared to the bare Si_{60} cage. This clearly indicates that Si-C and C-C bonding are stronger at the surface than inside the cage. For the case of twenty four carbon atoms on the surface of the cage, BE per atom increased by 38% and for twenty four carbon atoms inside the Si_{60} cage, BE per atom increased by 27% compared to bare Si_{60} cage. This again indicates that Si-C and C-C bonding are stronger at the surface than inside the cage.

This could be evident from the fact that inclusion of carbon atoms inside the Si_{60} cage pushes silicon atoms outside the surface, thus loosely bonded with the cage.

Table 5.1: Binding energy per atom (BE), HOMO-LUMO gap, VEA, VIP (all in eV), Dipole moment (Debye), Average Si-C bond length (Å) and C-C bond length (Å) for optimized $Si_{40}C_{20}$ fullerene like nanostructures.

Structures	State	BE per atom (eV)	HOMO-LUMO gap (eV)	VEA (eV)	VIP (eV)	Dipole Moment (Debye)	Avg Si-C BL (Å)	Avg C-C BL (Å)
Sur1	^{1}A	4.748	0.528	3.722	6.494	1.36	1.91	1.45
Sur2	^{1}A	4.747	0.453	3.747	6.424	2.90	1.85	1.48
Sur3	^{1}A	4.744	0.354	3.779	6.341	2.99	1.88	1.46
Tb1	^{3}A	4.690	0.150	3.936	6.289	1.93	1.91	1.45
Tb2	^{1}A	4.662	0.347	3.675	6.219	0.33	1.85	1.46
Dia	^{1}A	4.639	0.498	3.673	6.533	0.02	1.89	1.44

Table 5.2: NBO σ and π bonds between C-C and Si-C for the $Si_{40}C_{20}$ nanostructures

Structures	C-C σ bonds	C-C π bonds	Si-C σ bonds	Si-C π bonds
Sur1	25	10	10	------
Sur2	24	8	10	3
Sur3	25	8	10	------
Tb1	22	8	16	------
Tb2	22	8	16	------
Dia	20	10	20	------

Table 5.3: Binding energy per atom (BE), HOMO-LUMO gap, VEA, VIP (all in eV), Dipole moment (Debye), Average Si-C bond length (Å) and C-C bond length (Å) for optimized $Si_{60}C_{20}$ fullerene like nanostructures.

Structures	State	BE per atom (eV)	HOMO-LUMO gap (eV)	VEA (eV)	VIP (eV)	Dipole Moment (Debye)	Avg Si-C BL (Å)	Avg C-C BL (Å)
Bowl	^{5}A	4.482	0.163	4.105	6.282	2.73	1.94	1.46
Sheet2	^{1}A	4.454	0.159	3.995	6.162	3.86	1.93	1.43
Sheet1	^{1}A	4.434	0.153	4.044	6.233	4.42	1.93	1.43
Cage	^{1}A	4.349	0.109	4.153	6.281	0.02	2.06	1.50
Ring	^{1}A	4.306	0.321	3.832	6.174	2.67	1.99	1.40

Table 5.4: NBO σ and π bonds between C-C and Si-C for the $Si_{60}C_{20}$ nanostructures

Structures	C-C σ bonds	C-C π bonds	Si-C σ bonds	Si-C π bonds
Bowl	25	11	10	------
Sheet2	24	10	12	------
Sheet1	24	10	12	------
Cage	30	6	4	------
Ring	20	12	18	------

Table 5.5: Binding energy per atom (BE), HOMO-LUMO gap, VEA, VIP (all in eV), Dipole moment (Debye), Average Si-C bond length (Å) and C-C bond length (Å) for optimized $Si_{36}C_{24}$ fullerene like nanostructures.

Structures	State	BE per atom (eV)	HOMO-LUMO gap (eV)	VEA (eV)	VIP (eV)	Dipole Moment (Debye)	Avg Si-C BL (Å)	Avg C-C BL (Å)
Sur4	^{1}A	4.977	0.557	3.621	6.450	1.41	1.84	1.46
Sur1	^{1}A	4.975	0.531	3.617	6.456	0.72	1.84	1.47
Sur5	^{1}A	4.975	0.486	3.733	6.661	1.66	1.87	1.46
Sur2	^{1}A	4.971	0.332	3.662	6.282	1.16	1.90	1.45
Sur3	^{1}A	4.967	0.406	3.635	6.339	1.09	1.85	1.47
Tb4	^{1}A	4.960	0.277	3.479	6.154	0.01	1.89	1.45
Tb2	^{1}A	4.932	0.371	3.647	6.262	0.72	1.85	1.46
Tb3	^{1}A	4.920	0.574	3.565	6.401	0.01	1.89	1.45
Tb1	^{1}A	4.867	0.430	3.534	6.201	0.01	1.85	1.47
Tb5	^{1}A	4.851	0.525	3.526	6.242	0.00	1.87	1.47

Table 5.6: NBO σ and π bonds between C-C and Si-C for the $Si_{36}C_{24}$ nanostructures

Structures	C-C σ bonds	C-C π bonds	Si-C σ bonds	Si-C π bonds
Sur4	31	10	10	4
Sur1	30	11	12	2
Sur5	31	11	10	2
Sur2	30	12	12	------
Sur3	31	11	10	------
Tb4	28	11	16	------
Tb2	29	11	16	------
Tb3	26	10	20	4
Tb1	26	8	20	4
Tb5	27	9	20	5

Table 5.7: Binding energy per atom (BE), HOMO-LUMO gap, VEA, VIP (all in eV), Dipole moment (Debye), Average Si-C bond length (Å) and C-C bond length (Å) for optimized $Si_{60}C_{24}$ fullerene like nanostructures.

Structures	State	BE per atom (eV)	HOMO-LUMO gap (eV)	VEA (eV)	VIP (eV)	Dipole Moment (Debye)	Avg Si-C BL (Å)	Avg C-C BL (Å)
Sheet	^{3}A	4.599	0.100	4.142	6.222	2.15	1.91	1.42
3bowl	^{1}A	4.579	0.209	4.130	6.292	2.21	1.95	1.44
1bowl	^{1}A	4.566	0.252	4.013	6.287	3.11	1.93	1.43
Cage	^{3}A	4.529	0.202	4.132	6.272	0.75	2.02	1.53
Rcage	^{5}A	4.487	0.016	4.094	6.179	0.07	2.06	1.53
Ring	^{3}A	4.358	0.112	4.106	6.143	0.59	1.91	1.44

Table 5.8: NBO σ and π bonds between C-C and Si-C for the $Si_{60}C_{24}$ nanostructures

Structures	C-C σ bonds	C-C π bonds	Si-C σ bonds	Si-C π bonds
Sheet	30	13	12	------
3bowl	31	10	12	------
1bowl	30	12	12	------
Cage	36	8	11	------
Rcage	36	6	12	------
Ring	22	12	28	------

Table 5.9: Harmonic vibrational frequencies (in cm^{-1}) for the most stable Sur1 ($Si_{40}C_{20}$) structure

69.1868	72.5062	74.6430	75.9697	77.3926	78.7858
85.4664	87.6806	89.5212	90.2037	92.1768	95.9080
97.4955	99.3853	100.4297	102.9859	109.9211	110.6330
112.7168	119.1461	120.9073	124.1143	124.6768	126.5773
129.6551	131.4392	133.2237	136.5148	137.5910	140.3258
145.3238	146.6337	150.3133	151.2486	152.0599	156.9749
158.3018	159.9206	161.1874	163.6731	165.8101	166.6356
170.6843	171.7886	173.3329	173.9498	177.4486	184.3473
186.8439	187.8012	188.9813	191.6655	198.7381	217.2553
218.9426	224.0926	226.8844	228.4426	233.6086	247.0623
261.7598	270.7924	274.2130	278.9846	279.5238	285.2772
286.4757	290.2573	295.4691	304.5021	310.7885	313.1771
320.9484	327.7168	336.5581	347.5252	350.0250	358.5673
367.4746	370.5038	381.2733	384.6418	389.7332	392.7343
396.8919	400.1850	405.5784	410.7108	414.3892	420.0841
422.2047	428.2150	433.6767	437.8665	445.0843	451.3884
456.5818	459.7117	460.4163	463.8732	465.8409	467.1764
470.4557	472.8382	477.1843	479.5450	493.1091	500.4756
502.3382	504.6478	505.5586	508.7373	511.9875	514.7033
516.2534	523.4642	525.6648	526.1769	528.2713	532.4924
534.5215	535.4496	539.0209	541.3186	542.6832	545.8841
552.0735	553.5130	562.2945	581.4910	583.5128	608.0247
621.6052	638.0022	654.2438	661.4314	668.9527	688.2972
693.1031	696.6979	718.2367	731.0947	734.9075	773.0036
807.0167	831.9208	846.9238	859.5819	863.6355	916.4698
925.0564	979.4381	1080.4062	1085.4977	1101.8644	1135.6884
1138.3733	1202.7086	1210.3410	1257.8950	1262.6586	1267.8444
1278.8005	1282.9494	1331.7588	1335.4858	1360.4915	1393.3586
1398.7423	1543.8811	1547.3874	1573.6115	1578.5767	1583.9395

Table 5.10: Harmonic vibrational frequencies (in cm^{-1}) for the most stable Bowl ($Si_{60}C_{20}$) structure

47.8652	58.0540	61.3978	63.8593	65.2518	68.0595
71.7444	74.7570	77.6103	80.4787	82.9165	85.5739
86.0652	86.8978	91.6497	92.0180	92.8213	94.5777
95.8686	98.5680	99.8014	101.3995	103.2236	104.8129
105.7021	107.2374	111.8704	112.3425	113.5606	115.7614
118.1775	120.3705	120.7243	121.6476	123.4662	124.6510
125.3767	127.9262	129.7463	131.8845	132.6928	133.4686
137.2060	138.2498	139.1921	140.1598	140.3658	141.4948
143.6509	144.9629	147.1222	150.2090	150.8913	151.2644
152.7900	154.5162	156.5399	157.8603	159.5862	162.3158
162.6436	164.8406	166.9561	168.9485	173.0446	175.2182
177.7581	178.6399	180.8783	182.2542	185.6506	186.9025
187.5396	189.6658	190.1950	192.0965	195.3023	196.1718
200.9642	204.9578	208.8051	213.2403	217.5365	224.7985
229.1943	234.9472	237.5462	243.0140	248.2539	253.4463
256.4654	259.5632	266.4653	269.8386	273.5209	277.6824
281.3416	284.2027	288.4042	294.0147	295.6664	302.4830
306.5006	309.0158	311.5097	317.7529	322.0972	326.2919
328.9378	333.7557	336.5865	337.3648	342.7433	348.3886
349.6052	352.2135	356.5923	358.3357	365.2603	365.6797
370.2217	372.6807	377.1683	378.5427	381.1813	386.1053
388.8205	389.5617	391.6153	393.7493	396.4950	401.5599
407.4701	409.4661	410.9022	417.9696	418.8953	424.2096
427.8469	430.7199	432.8499	433.7900	435.5643	438.2202
440.5330	443.2536	444.6762	447.4314	450.4935	452.5598
454.2409	455.9078	458.7498	460.4571	461.7352	462.2861
464.8361	468.7014	471.7618	473.2253	475.4521	477.4206
478.6086	479.6500	484.1121	486.2939	487.7457	489.7723
490.9919	494.6892	497.2659	500.6813	501.5602	503.2524
505.8962	512.0070	512.7626	515.7218	519.0499	521.6649
526.0331	528.0862	530.2936	538.1661	539.1128	541.8941
545.4918	546.9284	549.6276	554.1669	566.0576	584.8644
604.9488	606.9733	628.1332	636.3201	639.0015	675.8406
685.0327	685.6295	691.9802	692.7712	740.5218	757.4642
765.6625	782.0775	801.0386	851.4470	865.1275	928.3833
939.6409	976.5178	1104.6727	1109.3502	1125.7417	1149.7527
1187.6420	1240.6496	1246.8283	1261.6209	1264.2359	1281.9541
1334.4159	1339.1623	1360.0936	1376.2134	1385.4268	1411.5599
1428.8046	1520.3321	1535.8860	1573.5888	1595.2046	1625.7016

Table 5.11: Harmonic vibrational frequencies (in cm^{-1}) for the most stable Sur4 ($Si_{36}C_{24}$) structure

51.3778	53.2057	66.6908	69.1253	78.3993	81.4681
84.8605	87.5311	93.5519	94.1375	97.3473	99.2959
105.1222	109.2544	112.8913	113.4681	118.9682	122.1120
129.5507	131.4454	133.3602	137.1037	139.4284	140.8465
144.3100	145.7234	148.9174	150.5705	151.3504	151.7271
157.9953	161.1147	162.9284	163.7436	166.0532	166.5575
169.4358	169.6637	170.9449	174.4283	178.2012	179.0108
180.3338	182.5602	186.0855	189.9762	193.4231	198.6127
204.8832	220.7224	227.8153	231.1576	231.8511	236.8699
243.9175	254.3201	260.7212	264.3434	267.5290	279.6149
282.1120	289.5588	292.2262	301.9418	309.0755	315.3951
318.7579	327.5512	332.4122	336.2140	343.5351	354.1274
356.4748	362.8003	370.2979	376.8192	385.0887	392.8822
399.3219	404.6888	407.6068	414.6946	416.9068	420.1816
427.4430	431.1895	432.9534	437.7746	440.6909	444.7043
447.4727	449.4947	453.7827	457.1556	459.2217	461.9631
470.3081	472.7367	474.9218	480.9693	482.0246	485.3705
490.3951	493.2577	495.2837	498.9443	504.5915	507.4969
510.6243	513.3783	515.5024	520.2286	521.4946	525.1352
529.3500	530.7932	537.9481	541.0939	558.4238	567.0531
569.2933	572.9653	591.5329	608.3111	622.9720	647.1988
660.2563	661.4996	678.5956	695.6014	699.1374	701.3785
715.4025	722.6675	724.5561	761.5346	789.9227	805.5790
809.3094	842.0756	842.8986	855.4780	876.1376	948.4932
972.5378	999.0483	1045.7502	1056.8096	1074.3244	1093.4105
1125.4824	1133.8542	1174.9000	1175.1509	1199.9885	1213.6664
1219.7407	1241.4130	1253.1855	1291.5775	1300.3245	1321.4180
1325.1401	1331.5157	1340.4540	1355.2141	1365.8131	1413.3130
1443.7077	1459.6057	1484.3033	1558.6373	1609.5245	1612.6979

Table 5.12: Harmonic vibrational frequencies (in cm^{-1}) for the most stable Sheet ($Si_{60}C_{24}$) structure

14.8035	51.4087	58.3546	62.2060	63.2391	64.4743
69.9757	73.0198	75.3870	78.3544	80.8084	82.1062
82.9955	84.7685	86.8275	86.8994	88.3498	90.2894
91.5488	93.9268	94.8418	95.5706	97.5897	98.6667
99.1061	100.6248	101.0582	102.2105	104.4339	107.3274
109.3135	112.2933	113.6556	114.2567	117.1424	119.2666
119.9282	121.4724	123.0205	124.4197	126.2563	127.3889
128.9638	129.5897	130.4049	132.2755	133.5735	134.6157
138.7514	139.1206	140.2021	141.8533	143.0537	146.9407
148.8038	150.9906	152.4245	155.1268	155.9190	157.6161
157.9931	160.3987	163.0479	163.6016	164.8765	167.7385
171.1689	171.5667	173.5997	174.8658	176.6575	177.7178
182.1000	183.7748	184.7771	185.6803	188.4642	189.2103
190.2164	194.6755	205.9185	208.2545	208.5324	213.7014
217.2691	220.9548	221.5839	225.1628	234.3004	244.1992
245.1834	246.0319	251.0493	256.6947	257.4224	258.8784
260.9562	263.7597	268.2638	269.2994	275.5928	276.2888
278.6555	280.1646	288.6795	293.2864	296.4412	297.0050
303.1589	304.0091	308.7700	320.9053	322.3862	323.7078
324.4226	326.0182	334.3896	335.9640	337.4374	339.0437
340.2873	342.6136	347.6096	353.0021	355.1695	362.4463
363.4144	366.7825	368.0930	370.8879	373.1488	374.5060
380.0161	382.5123	385.8397	387.1921	389.5289	390.7277
393.8852	399.2629	400.5606	401.1784	402.0774	403.9835
405.1936	409.8985	410.3803	413.2404	418.2490	422.5931
425.5563	434.4432	435.5962	436.8413	438.0609	439.8520
442.6484	454.3761	455.4248	456.3043	456.9170	461.4967
462.4600	464.1924	464.8638	465.7641	466.5813	479.2449
487.4737	490.3230	491.1662	492.5911	492.9355	494.8287
496.6062	497.8029	501.8161	502.3092	503.5920	508.1607
510.0453	511.3069	512.9675	518.4819	520.0633	522.7383
523.3155	525.4378	528.9741	530.8723	532.9232	533.7153
536.2266	537.4119	543.5243	545.2679	588.1544	588.4957
619.8559	622.1450	623.6613	638.8672	675.8923	684.5099
687.1595	709.2587	711.4248	728.8386	757.2808	764.9896
780.8139	830.6957	831.1118	884.0144	885.8586	947.5697
950.4125	1000.3850	1006.9443	1094.7883	1095.8941	1158.4235
1222.3157	1248.8163	1268.2485	1270.9173	1273.1898	1276.5001
1392.5506	1395.0880	1412.7619	1426.9491	1439.0273	1441.0113
1444.0002	1445.6122	1464.0607	1464.8415	1465.2713	1491.4507
1504.8835	1536.4554	1542.1274	1544.3355	1586.1088	1586.6558

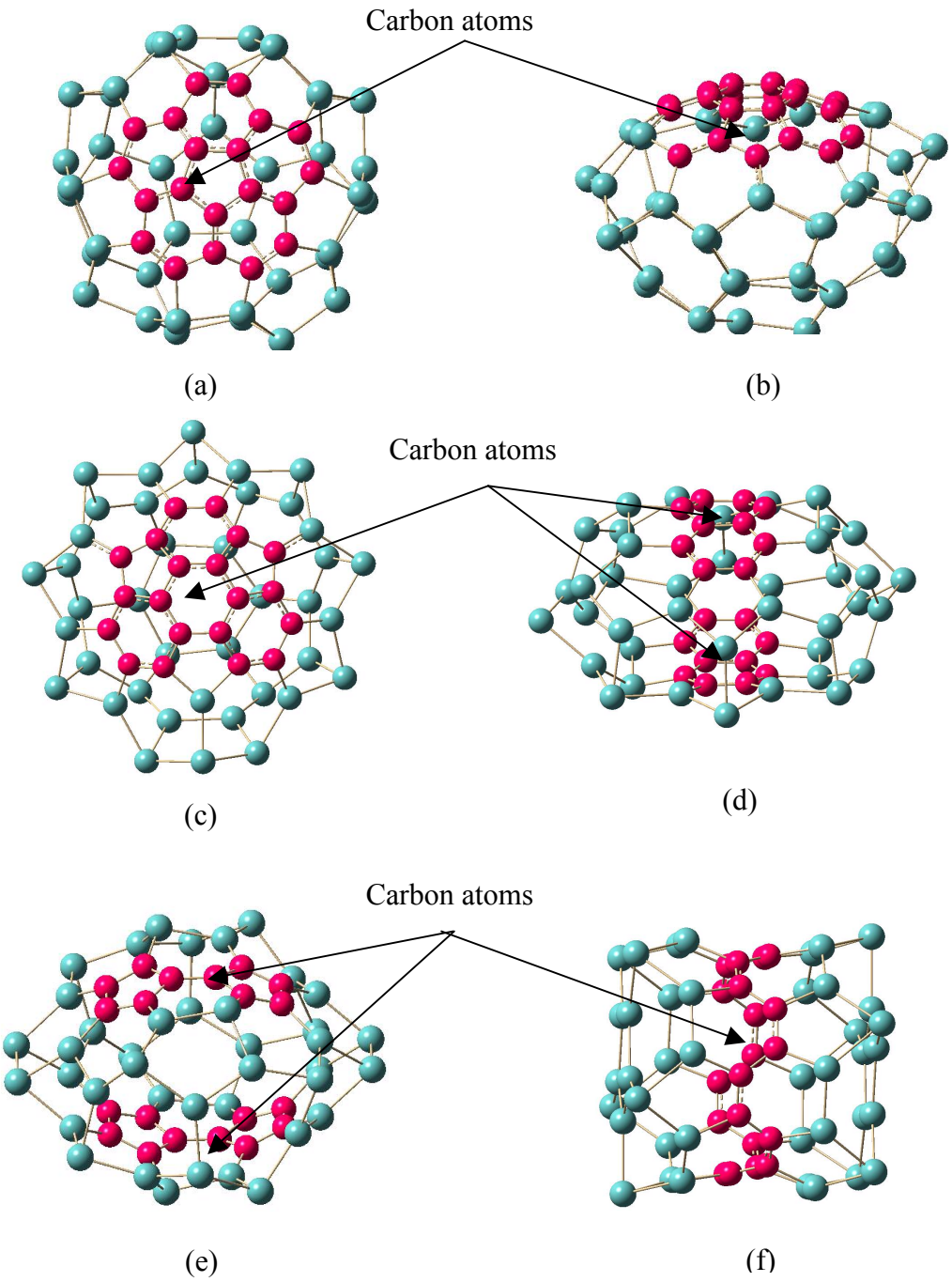

Figure 5.1: Optimized structures of $Si_{40}C_{20}$ silicon-carbon fullerene like nanostructures (a) Sur1 (b) Sur2 (c) Sur3 (d) Tb1 (e) Tb2 (f) Dia (Carbon atoms denoted by dark pink color)

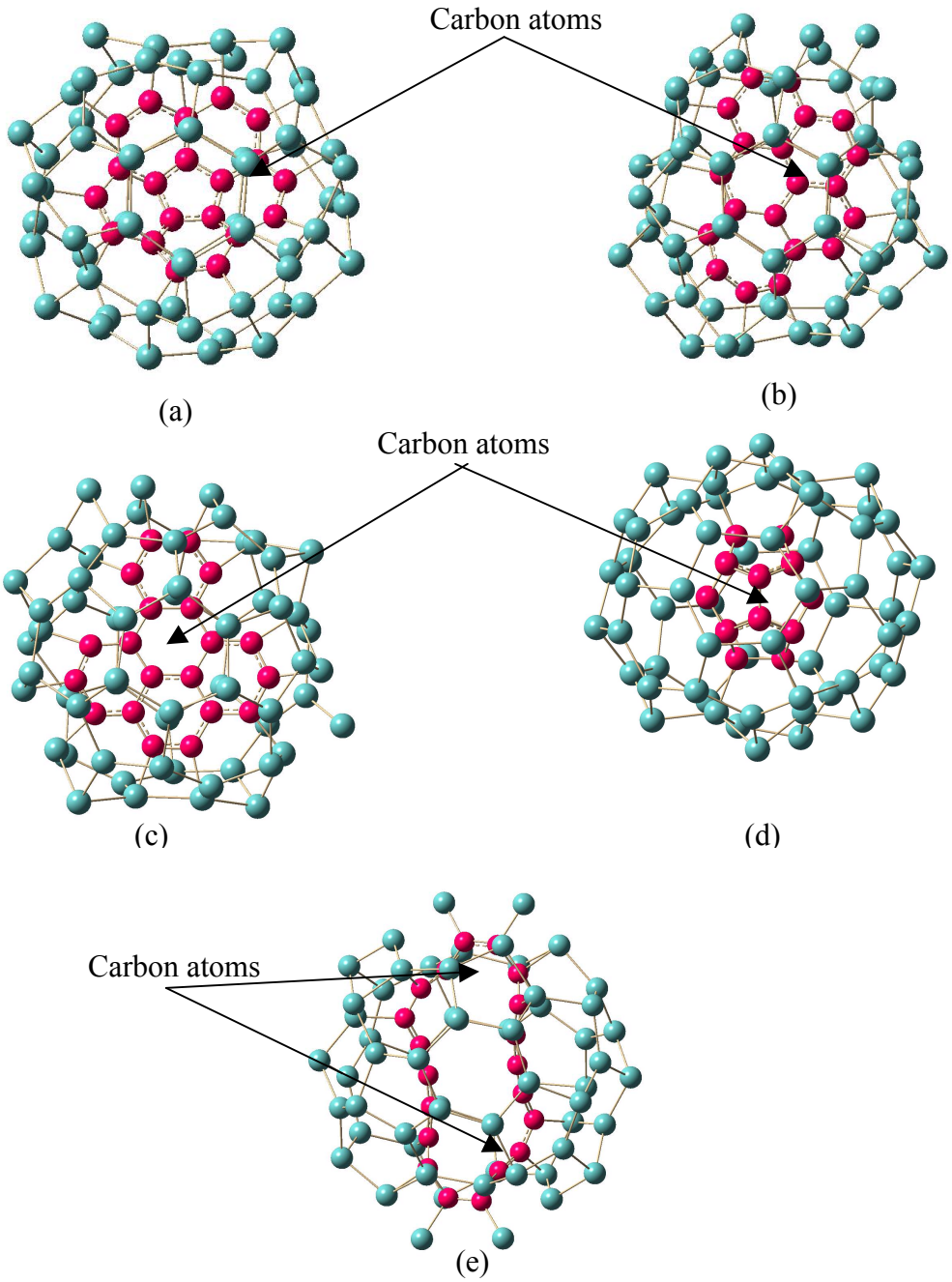

Figure 5.2: Optimized structures of $Si_{60}C_{20}$ silicon-carbon fullerene like nanostructures (a) Bowl (b) Sheet2 (c) Sheet1 (d) Cage (e) Ring (Carbon atoms denoted by dark pink color)

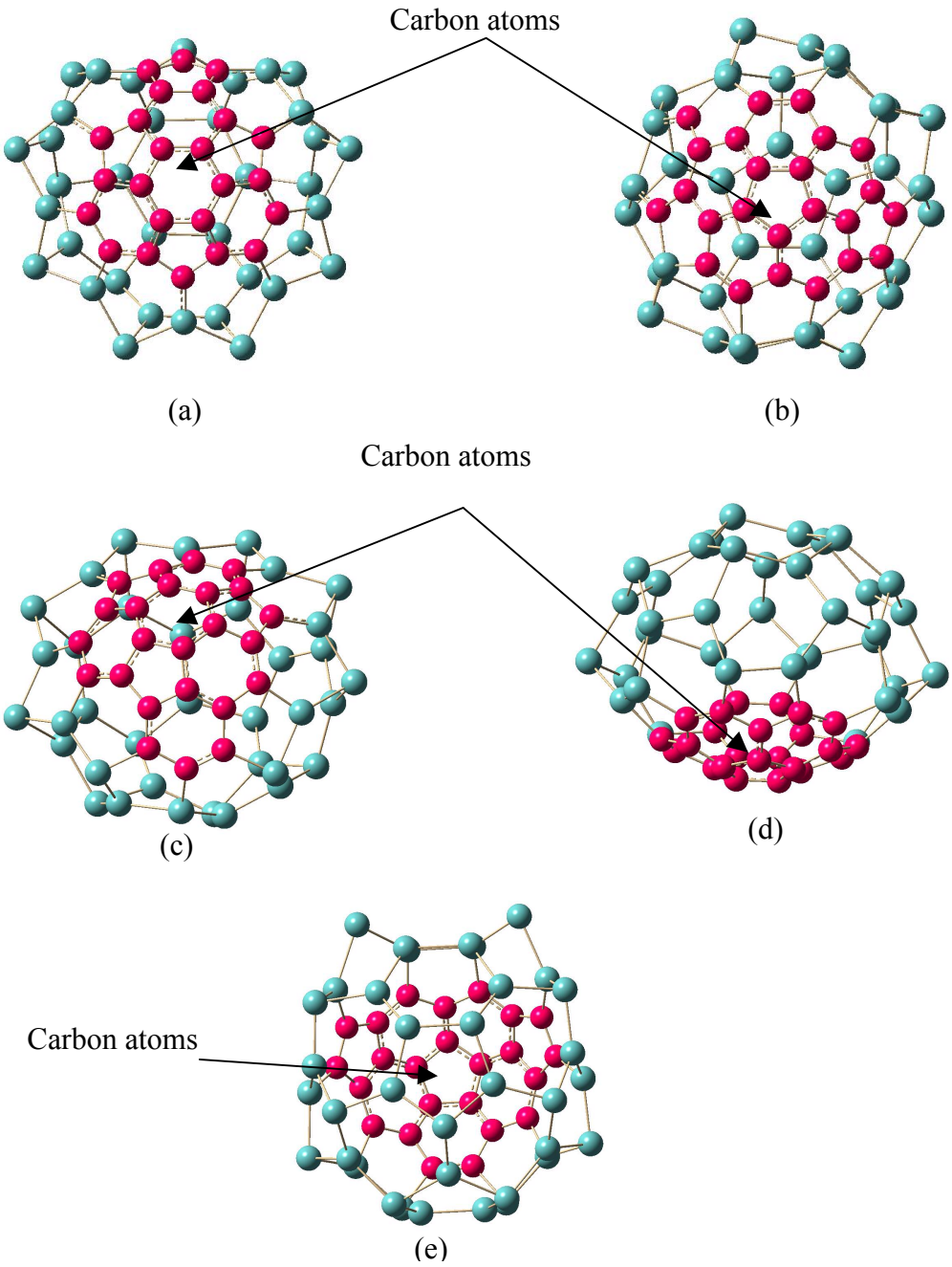

Figure 5.3: Optimized structures of $Si_{36}C_{24}$ silicon-carbon fullerene like nanostructures (a) Sur4 (b) Sur1 (c) Sur5 (d) Sur2 (e) Sur3
(Carbon atoms denoted by dark pink color)

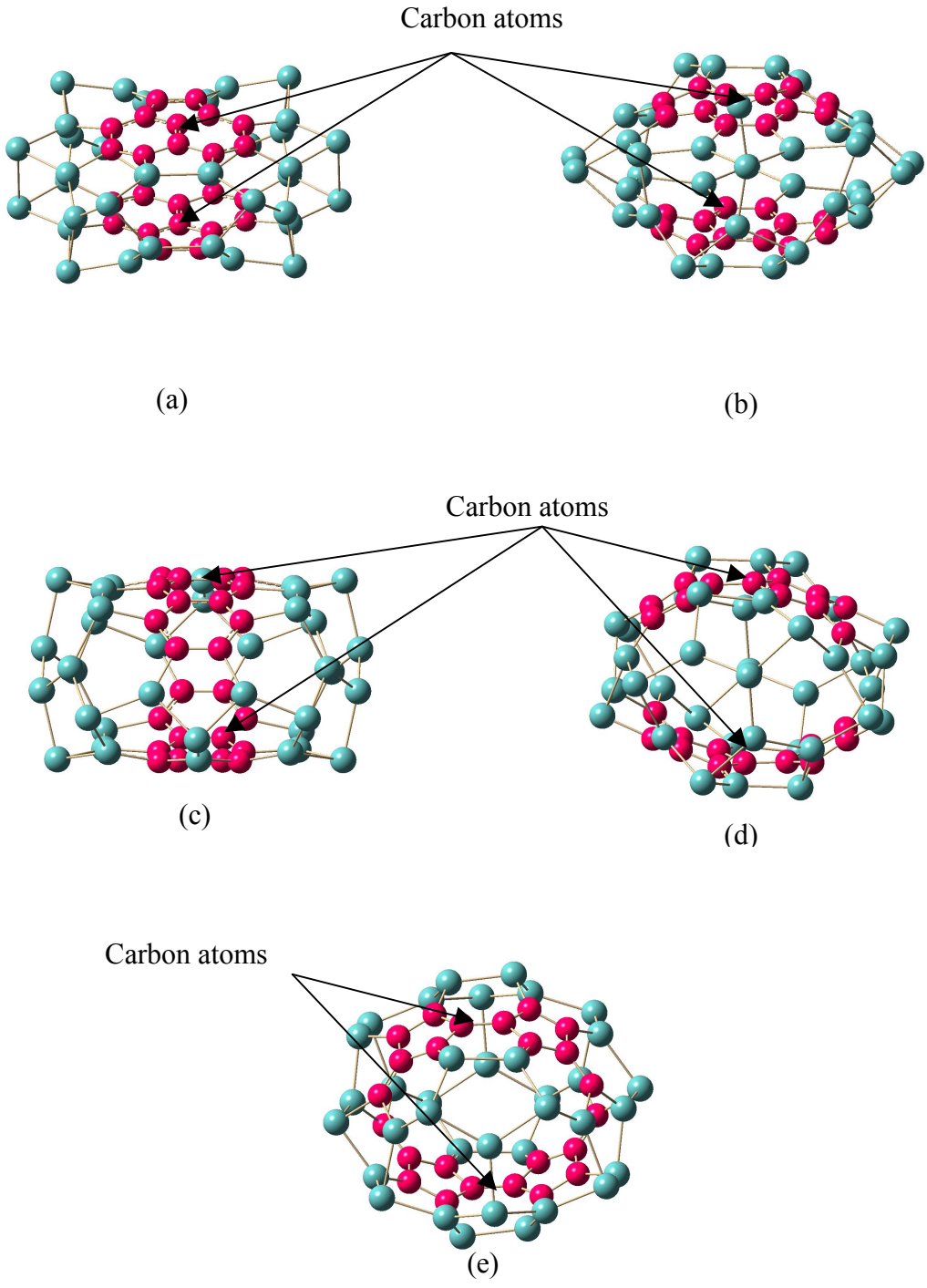

Figure 5.4: Optimized structures of $Si_{36}C_{24}$ silicon-carbon fullerene like nanostructures (a) Tb4 (b) Tb2 (c) Tb3 (d) Tb1 (e) Tb5
(Carbon atoms denoted by dark pink color)

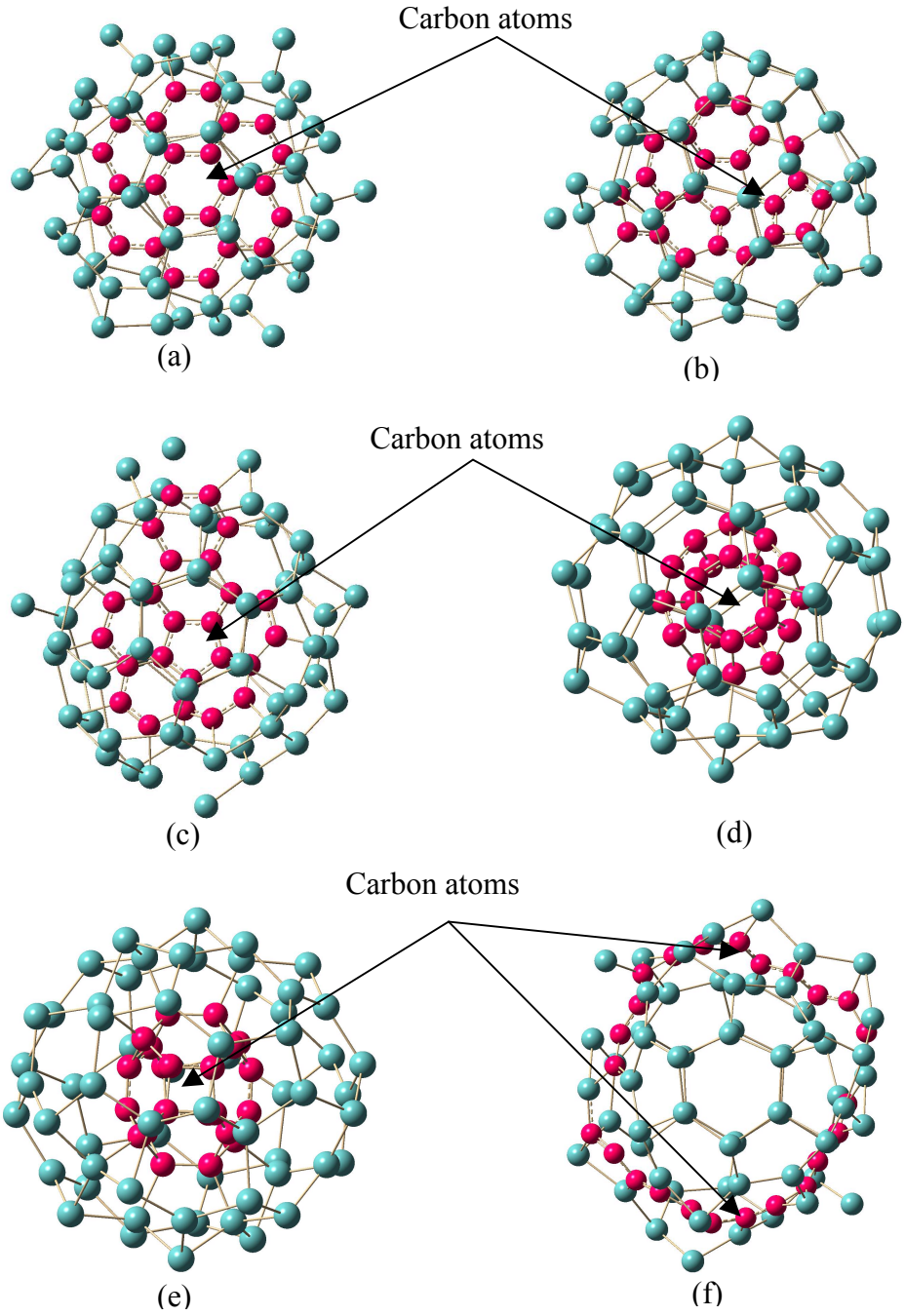

Figure 5.5: Optimized structures of $Si_{60}C_{24}$ silicon-carbon fullerene like nanostructures (a) Sheet (b) 3bowl (c) 1bowl (d) Cage (e) Rcage (f) Ring (Carbon atoms denoted by dark pink color)

5.2 Charge distributions for the most stable $Si_{40}C_{20}$, $Si_{60}C_{20}$, $Si_{36}C_{24}$ and $Si_{60}C_{24}$ Nanostructures

We also performed detailed Mulliken charge population analysis [101-103] for the clusters reported here. In general, Mulliken charge analysis for all the structures indicates that carbon atoms gain charge and the silicon atoms lose charge, as expected from their electro-negativities. Some exceptions were noted in which carbon atoms lose charge and silicon atoms gain charge indicating asymmetric charge distribution and total dipole moment values for the structures. Mulliken charge distribution diagrams for the four most stable structures in each set along with the electronic charges for all atoms are reported in Figs 5.6 – 5.9 and Tables 5.13 to 5.17. All the charges are noted in electronic charge unit. In general, these most stable structures have mostly covalent and partly ionic bonding between the silicon and carbon atoms and also for bonding between carbon atoms. Increase in the exceptions of silicon atoms gaining charge translates in to increased repulsive interaction between them and carbon atoms bringing down the stability. For example, in the $Si_{40}C_{20}$ Sur1 structure (Fig 5.6) we notice exceptions in the case of five carbon atoms have positive electronic charges and this increases ionic contribution to the covalent bonding between the carbon atoms. All the silicon atoms bonded with carbon atoms have positive electronic charges and the asymmetric charge distribution between the silicon and carbon atoms increases the asymmetric contribution between the C-C bonding. For the most stable $Si_{60}C_{20}$ Bowl structure (Fig 5.7), we notice several exceptions for the silicon atoms (gaining charges) along with exceptions for five carbon atoms having positive charges, indicating slight

ionic contribution to strong covalent bonding between carbon atoms. Some silicon atoms bonded with carbon atoms gain charge similar to carbon atoms, increasing the repulsive columbic interaction between the silicon and carbon atoms. Electronic charges for all atom labels for this structure are given in Table 5.14. For example the silicon atoms (labels 28, 46, 58) having electronic charges of -0.16, -0.06 and -0.06 respectively are bonded with carbon atoms (labels 76, 77 and 79) having electronic charges of -0.28, -0.43 and -0.14, which indicates the repulsive interaction between the silicon and carbon atoms offsetting the increased C-C interaction, bringing down the stability for this structure. NBO analysis confirmed the ionic contribution to the C-C interaction among the C-C π bonds with C-C σ bonds strongly covalent in nature. Similar discussions can be made for the most stable $Si_{36}C_{24}$ and $Si_{60}C_{24}$ fullerene like nanostructures. The VIPs and the VEAs for all the optimized nanostructures reported in this work are considerably high indicating stability and do not follow any specific pattern with increase in carbon atoms. In general Mulliken charge analysis for the novel silicon-carbon fullerene like nanostructures ($Si_{40}C_{20}$, $Si_{60}C_{20}$, $Si_{36}C_{24}$ and $Si_{60}C_{24}$) indicates a mixed ionic-covalent bonding contributing to the stability.

Table 5.13: Mulliken electronic charges for the atoms of the most stable Sur1 ($Si_{40}C_{20}$) structure

1	Si	0.13	31	C	0.48
2	C	-0.42	32	C	-0.33
3	C	0.48	33	C	-0.57
4	C	-0.57	34	Si	0.32
5	Si	0.33	35	Si	-0.21
6	Si	-0.21	36	Si	0.18
7	Si	0.22	37	Si	-0.17
8	Si	0.13	38	Si	0.14
9	C	-0.32	39	Si	-0.10
10	C	0.47	40	Si	-0.03
11	C	-0.04	41	Si	0.15
12	C	-0.05	42	Si	-0.20
13	C	-0.05	43	Si	0.19
14	C	0.49	44	Si	-0.11
15	C	-0.42	45	Si	0.31
16	Si	0.12	46	Si	0.12
17	Si	0.15	47	C	-0.31
18	Si	0.11	48	C	-0.57
19	Si	-0.16	49	Si	0.32
20	Si	0.19	50	Si	0.12
21	Si	-0.04	51	Si	0.23
22	Si	-0.14	52	Si	-0.09
23	Si	0.19	53	Si	-0.11
24	Si	-0.11	54	Si	0.15
25	Si	0.30	55	Si	-0.15
26	C	-0.45	56	Si	0.10
27	C	-0.46	57	Si	-0.17
28	C	0.47	58	Si	0.22
29	C	-0.05	59	Si	-0.17
30	C	-0.04	60	Si	0.03

Table 5.14: Mulliken electronic charges for the atoms of the most stable Bowl ($Si_{60}C_{20}$) structure

1	Si	0.19	41	Si	0.25
2	Si	-0.18	42	Si	-0.09
3	Si	0.24	43	Si	-0.11
4	Si	-0.02	44	Si	0.11
5	Si	0.00	45	Si	-0.06
6	Si	0.30	46	Si	0.16
7	Si	-0.02	47	Si	0.32
8	Si	-0.06	48	Si	-0.15
9	Si	0.05	49	Si	0.19
10	Si	0.20	50	Si	-0.13
11	Si	-0.12	51	Si	0.14
12	Si	-0.02	52	Si	-0.19
13	Si	0.13	53	Si	0.14
14	Si	-0.12	54	Si	-0.03
15	Si	0.15	55	Si	0.22
16	Si	-0.16	56	Si	0.08
17	Si	0.13	57	Si	0.23
18	Si	-0.17	58	Si	0.28
19	Si	0.23	59	Si	0.07
20	Si	-0.24	60	Si	0.27
21	Si	0.24	61	C	-0.10
22	Si	-0.10	62	C	-0.13
23	Si	0.12	63	C	-0.01
24	Si	-0.13	64	C	-0.15
25	Si	0.12	65	C	-0.07
26	Si	-0.18	66	C	0.56
27	Si	0.20	67	C	-0.75
28	Si	-0.16	68	C	-0.24
29	Si	0.25	69	C	0.68
30	Si	-0.17	70	C	-0.33
31	Si	0.15	71	C	-0.44
32	Si	-0.06	72	C	0.36
33	Si	0.01	73	C	-0.27
34	Si	0.11	74	C	-0.43
35	Si	-0.11	75	C	0.54
36	Si	-0.04	76	C	-0.14
37	Si	-0.02	77	C	-0.77
38	Si	-0.16	78	C	0.69
39	Si	0.24	79	C	-0.97
40	Si	-0.17	80	C	-0.40

Table 5.15: Mulliken electronic charges for the atoms of the most stable Sur4 ($Si_{36}C_{24}$) structure

1	C	0.00	31	Si	0.19
2	C	0.22	32	Si	-0.22
3	C	-0.45	33	Si	0.25
4	C	0.19	34	Si	-0.08
5	C	-0.08	35	Si	0.35
6	C	-0.08	36	Si	-0.24
7	C	0.19	37	C	-0.18
8	C	0.12	38	C	0.17
9	C	0.12	39	C	-0.18
10	C	-0.27	40	C	-0.18
11	Si	0.16	41	Si	-0.05
12	Si	0.12	42	Si	0.24
13	Si	0.24	43	Si	-0.22
14	Si	-0.04	44	Si	0.22
15	C	-0.19	45	Si	-0.18
16	C	-0.18	46	Si	0.11
17	C	0.18	47	Si	0.03
18	C	-0.06	48	Si	-0.08
19	C	-0.07	49	Si	-0.09
20	C	0.00	50	Si	0.17
21	C	0.22	51	Si	-0.15
22	C	-0.45	52	Si	-0.09
23	Si	0.12	53	Si	0.36
24	Si	0.17	54	Si	-0.11
25	C	-0.27	55	Si	0.27
26	C	-0.38	56	Si	-0.18
27	Si	0.34	57	Si	0.18
28	Si	-0.16	58	Si	-0.16
29	Si	0.22	59	Si	0.11
30	Si	-0.22	60	Si	0.02

Table 5.16: Mulliken electronic charges for the atoms of the most stable Sheet ($Si_{60}C_{24}$) structure

1	Si	-0.14	43	Si	-0.15
2	Si	0.07	44	Si	0.15
3	Si	0.09	45	Si	-0.14
4	Si	-0.14	46	Si	0.15
5	Si	0.15	47	Si	-0.14
6	Si	-0.14	48	Si	0.15
7	Si	0.08	49	Si	-0.14
8	Si	-0.16	50	Si	0.07
9	Si	0.14	51	Si	-0.15
10	Si	0.11	52	Si	0.17
11	Si	0.25	53	Si	0.11
12	Si	0.17	54	Si	0.24
13	Si	0.11	55	Si	0.16
14	Si	0.25	56	Si	0.10
15	Si	-0.16	57	Si	0.05
16	Si	0.16	58	Si	-0.14
17	Si	-0.17	59	Si	0.16
18	Si	0.16	60	Si	-0.16
19	Si	-0.13	61	C	-0.52
20	Si	0.15	62	C	0.63
21	Si	-0.14	63	C	0.05
22	Si	0.09	64	C	0.05
23	Si	0.17	65	C	0.62
24	Si	0.12	66	C	-0.72
25	Si	0.25	67	C	0.05
26	Si	0.17	68	C	0.06
27	Si	0.09	69	C	0.06
28	Si	0.07	70	C	0.05
29	Si	-0.15	71	C	0.64
30	Si	0.15	72	C	-0.71
31	Si	-0.14	73	C	-0.54
32	Si	0.09	74	C	0.62
33	Si	0.17	75	C	-0.72
34	Si	0.11	76	C	-0.51
35	Si	0.23	77	C	-0.73
36	Si	0.15	78	C	-0.53
37	Si	0.13	79	C	0.66
38	Si	0.03	80	C	-0.68
39	Si	-0.14	81	C	-0.54
40	Si	0.16	82	C	0.65
41	Si	0.10	83	C	-0.53
42	Si	0.24	84	C	-0.70

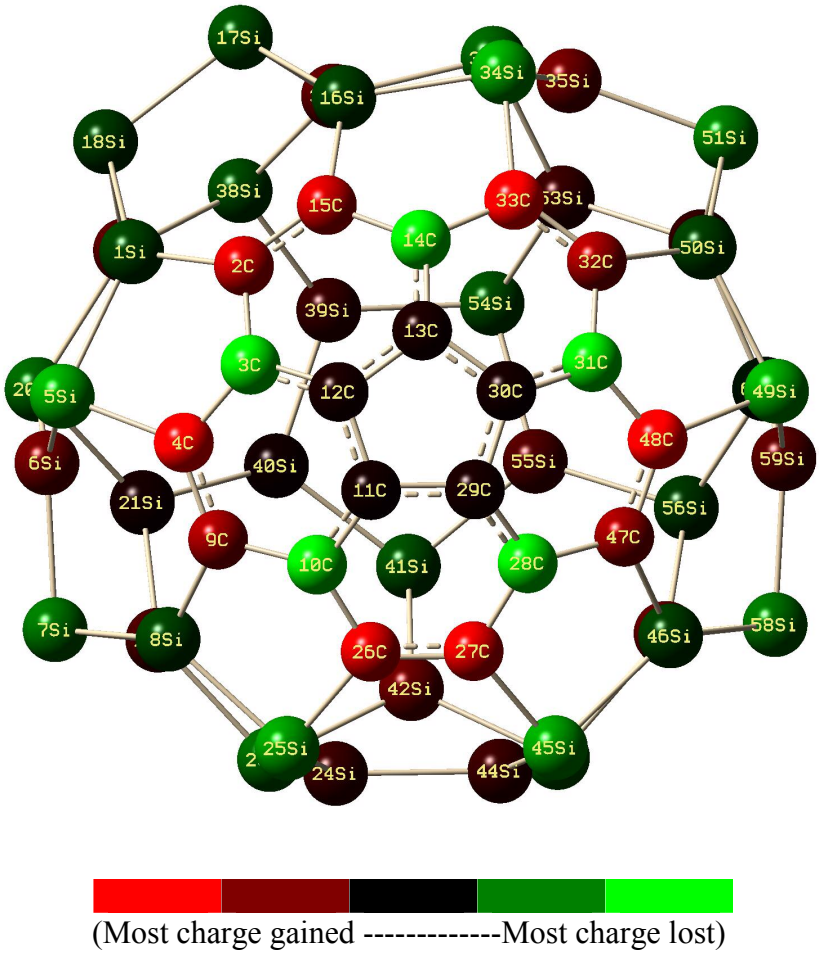

Figure 5.6: Mulliken charge distribution for the most stable Sur1 ($Si_{40}C_{20}$) structure.

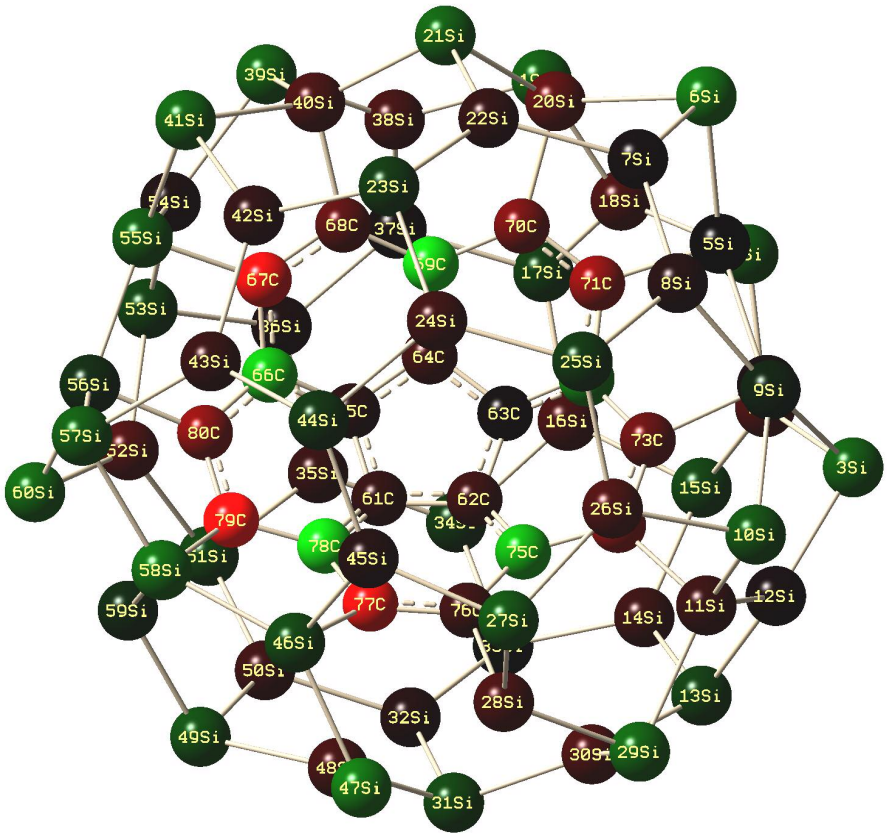

(Most charge gained ----------Most charge lost)

Figure 5.7: Mulliken charge distribution for the most stable Bowl ($Si_{60}C_{20}$) structure.

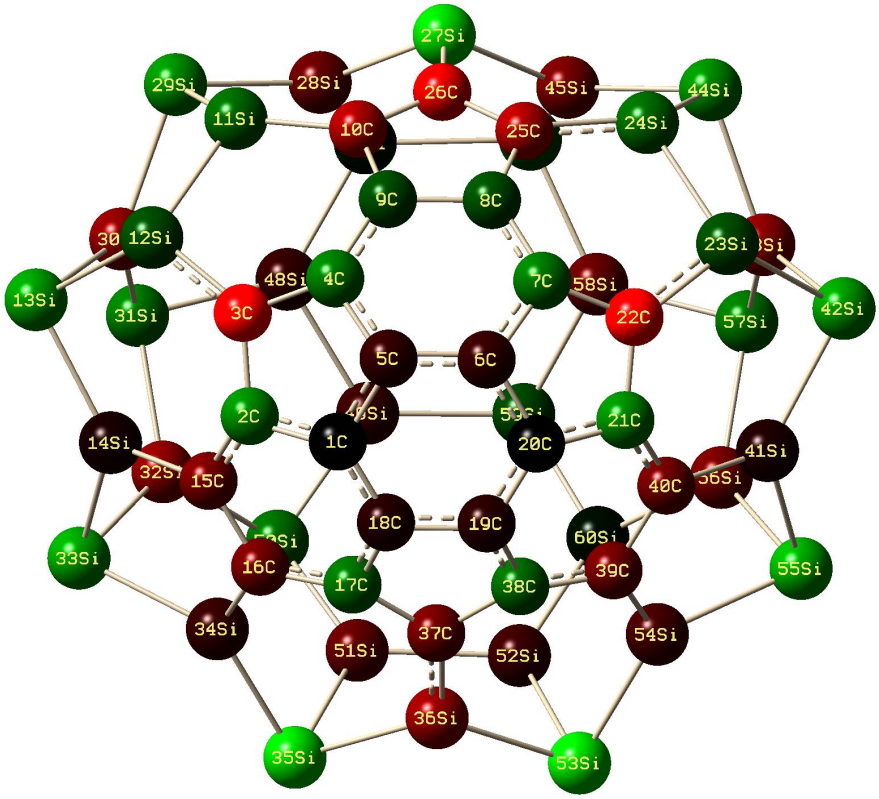

(Most charge gained ----------Most charge lost)

Figure 5.8: Mulliken charge distribution for the most stable Sur4 ($Si_{36}C_{24}$) structure.

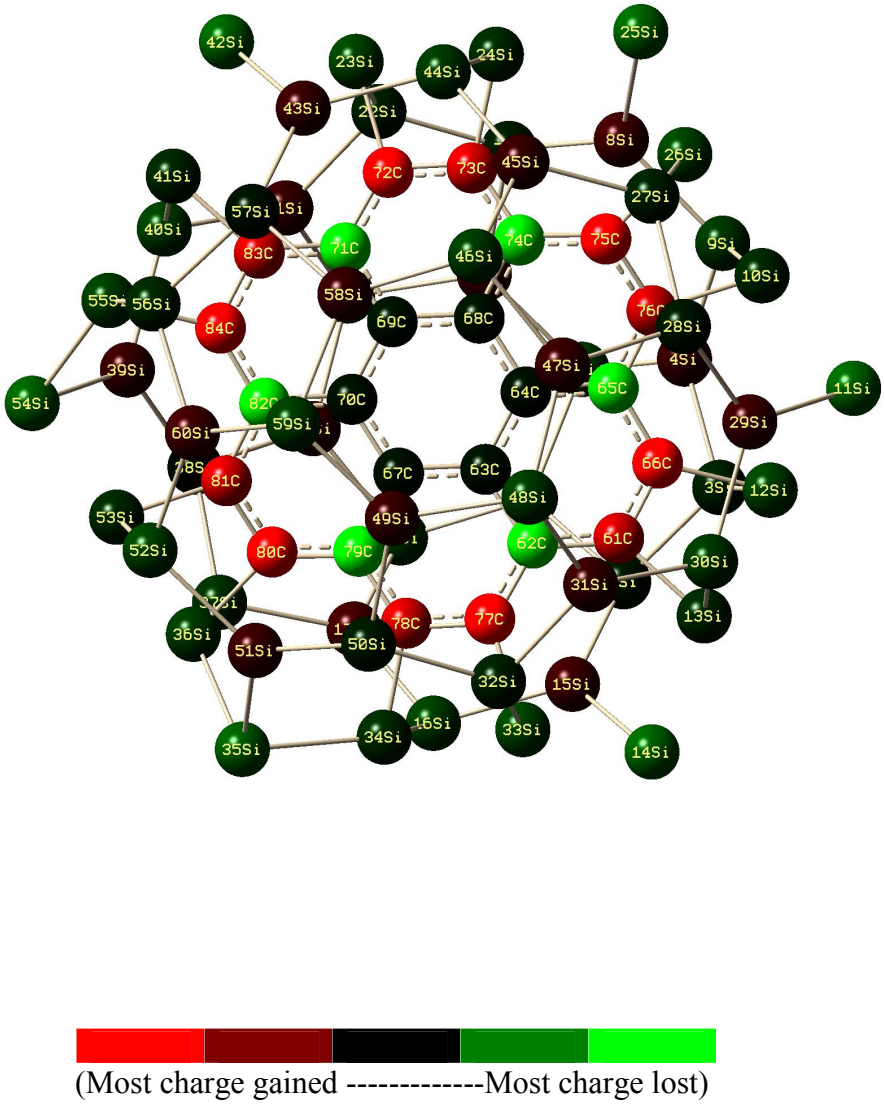

Figure 5.9: Mulliken charge distribution for the most stable Sheet ($Si_{60}C_{24}$) structure.

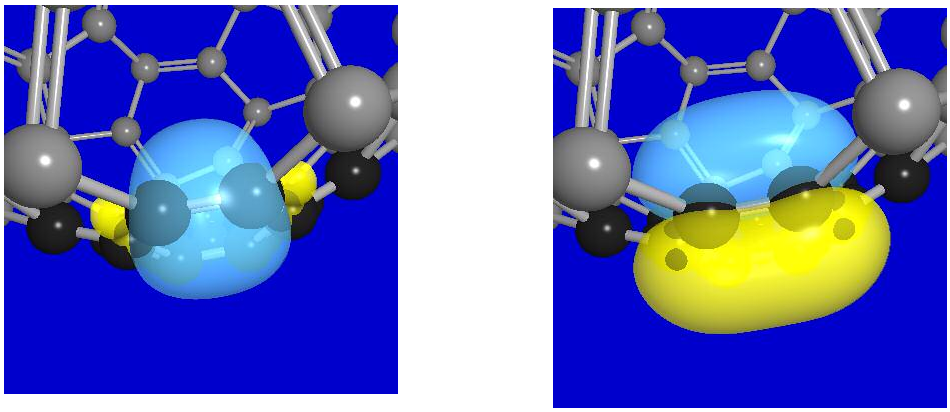

(a) (b)

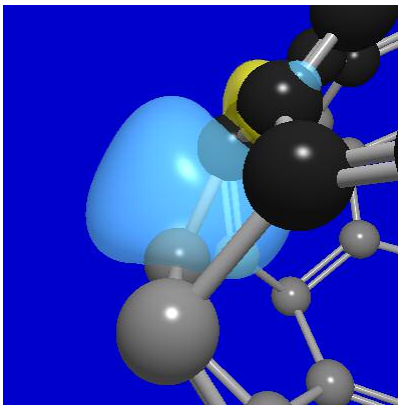

(c)

Figure 5.10: Natural Bond Orbital (NBO) plots generated using NBO program & NBO View for the most stable Sur1 structure ($Si_{40}C_{20}$) (a) σ bond between C-C (b) π bond between C-C (c) σ bond between Si-C.

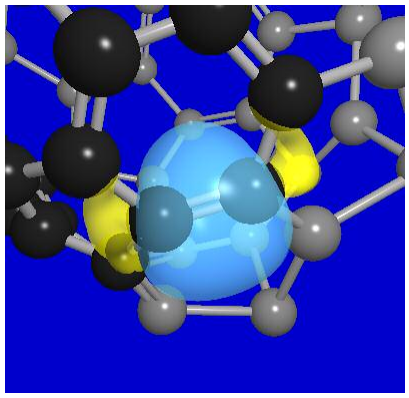

(a)

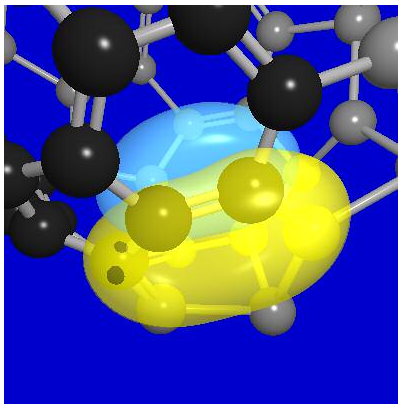

(b)

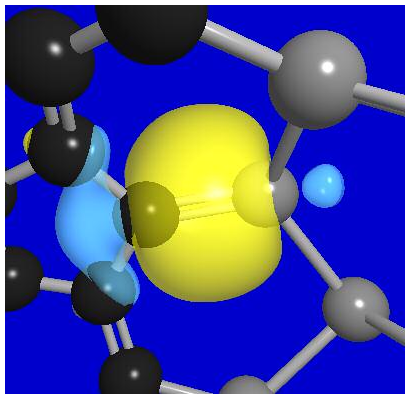

(c)

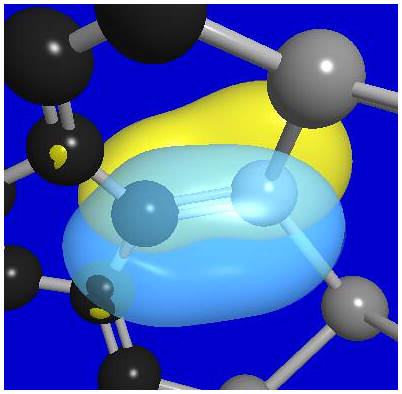

(d)

Figure 5.11: Natural Bond Orbital (NBO) plots generated using NBO program & NBO View for the most stable Sur4 structure ($Si_{36}C_{34}$). (a) σ bond between C-C (b) π bond between C-C (c) σ bond between Si-C (d) π bond between Si-C

CHAPTER 6

CONCLUSIONS

6.1 Stability of $Si_{60}C_{2n}$ (n=1, 2, 3, 10, 12) Fullerene like Nanostructures

In conclusion, we have studied a class of stable $Si_{58}C_2$, $Si_{60}C_2$, $Si_{56}C_4$, $Si_{60}C_4$, $Si_{54}C_6$, $Si_{60}C_6$, $Si_{40}C_{20}$, $Si_{60}C_{20}$, $Si_{36}C_{24}$ and $Si_{60}C_{24}$ fullerene like nanostructures. These structures have increased stability compared to the bare Si_{60} cage and their stability depends on the number and the orientation of the carbon atoms inside or on the surface of the cage. As seen from results and discussions, binding energies per atom of the stable novel silicon carbon fullerene like nanostructures increase with the increase in the number of carbon atoms and they are higher compared to the bare Si_{60} cage (3.61 eV at GGA-DFT).

For the carbon atoms on the surface of the cage, all the ground state structures are of singlet state (no magnetic structures have been found). In the case of two carbon atoms on the surface of the cage, strong covalent bonding contributed to the stability and C-C interactions did not have any significant impact on the stability. For four carbon atoms on the surface of the cage, a mixture of ionic-covalent bonding contributed to stability and here too C-C interactions did not have any significant impact on the stability of the cage, rather Si-C interactions are more important. For six, twenty and twenty four carbon atoms on the surface of the cage, a mixture of ionic –

covalent bonding contributed to the stability and both Si-C and C-C interactions were important for the stability of the nanostructures. Increase in binding energies per atom with respect to bare Si_{60} cage for the most stable structures varied from 3% ($Si_{58}C_2$), 5.8% ($Si_{56}C_4$), 8.7% ($Si_{54}C_6$), 31.5% ($Si_{40}C_{20}$) to 38% ($Si_{36}C_{24}$). Graph for BE per atom with the number of carbon atoms is shown in Fig 6.1. A common feature of carbon atoms on the surface of the cage is that they strongly bond with neighboring atoms thereby compressing the cage. Significant reconstructions were shown by $Si_{36}C_{24}$ nanostructures from fullerene like geometry to flat tube like geometry indicating the possible existence of Si-C nanotubes. Further studies are needed to explore this possibility.

For the two, four and six carbon atoms inside the Si_{60} cage, the ground state structures are in singlet state (no magnetic structures have been found). For C_{20} and C_{24} clusters inside the Si_{60} cage, the ground state structures have multiplicities of 5 and 3 indicating the possibility of magnetic silicon-carbon nanostructures. Further theoretical and experimental studies are needed to ascertain the probable magnetism associated with these structures. In the case of two carbon atoms inside the Si_{60} cage, a mixture of ionic-covalent bonding and Si-C interactions contributed to the stability of the cage. The C-C interactions did not have significant impact on the stability. In the case of four carbon atoms inside the Si_{60} cage, a mixture of ionic-covalent bonding and C-C interactions did have significant impact on the stability. For six, twenty and twenty four carbon atoms inside the cage, mixture of ionic-covalent bonding and Si-C, C-C interactions together contributed to the stability. Increase in binding energies per atom

with respect to the bare Si_{60} cage varied from 2.5 % ($Si_{60}C_2$), 4.9% ($Si_{60}C_4$), 7.9% ($Si_{60}C_6$), 24% ($Si_{60}C_{20}$) to 27% ($Si_{60}C_{24}$). Graph for BE per atom with the number of carbon atoms is shown in Fig 6.2

This suggests that binding energies for carbon atoms on the surface of the cages are higher than inside the cage, indicating that Si-C and C-C interactions are stronger at the surface of the cage than inside the cage. This could be evident from the fact average occupancies of the Si-C and C-C bonds are higher at the surface than inside the cage (NBO analysis). For small carbon clusters at the center of the cage, structures were energetically unfavorable and for large closed cage carbon clusters at the center of the cage, structures were of lower stability indicating that as the carbon atoms are increased inside the cage, local Si-C interactions and C-C interactions are the dominant factors in deciding the stability of the nanostructures. All the optimized silicon-carbon nanostructures reported in this study are not smoother, indicating that proper arrangement of carbon atoms are needed to obtain smoother fullerene like carbon based silicon nanostructures.

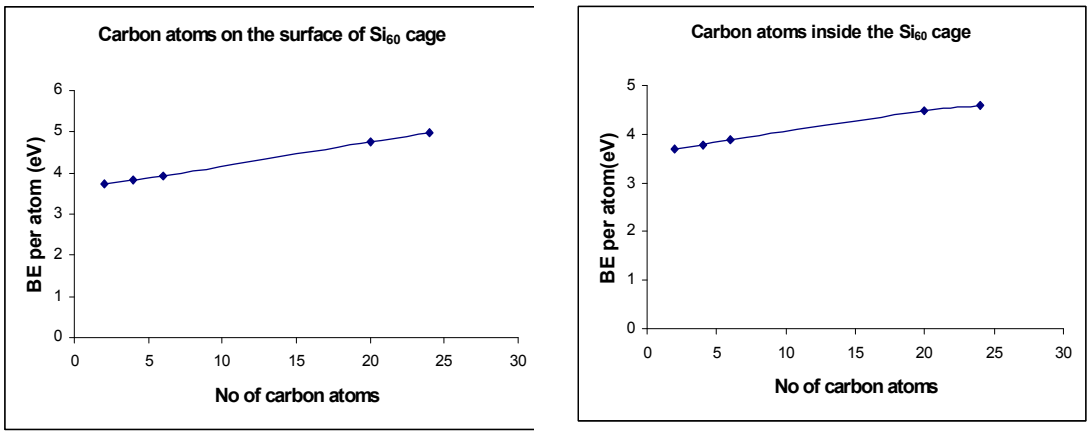

(a) (b)

Fig 6.1: (a) Graph between BE per atom of the most stable structures Vs the number of carbon atoms on the surface of the cage. (b) Graph between BE per atom of the most stable structures Vs the number of carbon atoms inside the Si_{60} cage respectively.

6.2 Future Work

We have stated before that to the best of our knowledge, no results are available for the Si-C fullerene structures reported here and further theoretical and experimental studies are needed to understand the hybrid nature of the bonding and the stability of the nanostructure fullerene cages reported in this study. Possible extension of this work might be to have a look at odd number of carbon atoms both at surface and inside the cage. It might be more interesting to complete a systematic study of the increase in the even number of carbon atoms beyond six and also to have equal number of silicon and carbon atoms in the silicon –fullerene cage nanostructure.

Potential applications in quantum memory devices suggest that probable magnetism associated with the $Si_{60}C_{20}$ and $Si_{60}C_{24}$ nanostructures needed a more

extensive study. Significant reconstructions shown by the $Si_{36}C_{24}$ nanostructures after optimization to look like flat tube like geometry needed extensive study and it would be interesting to add dopant atoms such as transition metal atoms inside these structures and to explore the possibility of smoother silicon-carbon nanostructures. One more possible work might be to find a proper orientation of carbon atoms to make a smoother silicon nanostructure.

APPENDIX A

COORDINATES FOR MOST STABLE SILICON-CARBON FULLERENE LIKE NANOSTRUCTURES

Table A.1: Coordinates for the most stable Maindiag ($Si_{58}C_2$) structure.

Atom	X(Å)	Y(Å)	Z(Å)
Si	-0.167046	-0.693300	-0.092999
Si	0.125243	0.004851	2.090240
C	1.914351	0.178099	2.577849
Si	3.075483	0.006646	1.132131
Si	2.026321	-0.685205	-0.803775
Si	2.591810	0.760412	-2.439084
Si	4.711362	1.636000	-2.807719
Si	5.623246	1.876897	-0.732062
Si	5.342849	0.426879	1.065369
Si	5.677187	1.986554	2.734889
Si	4.594607	1.651568	4.690059
Si	2.427352	0.942074	4.157392
Si	0.987794	1.650568	5.863974
Si	-1.038244	1.984605	4.918388
Si	-1.747803	0.424504	3.370623
Si	-3.031351	1.874242	2.080560
Si	-3.512211	1.634190	-0.135295
Si	-1.574860	0.767903	-1.080279
Si	-1.088572	1.828257	-3.039111
Si	1.044199	1.845041	-3.711648
Si	2.054991	3.702140	-4.651566
Si	4.089925	3.738087	-3.558203
Si	5.331461	5.625494	-3.299707
Si	6.424012	5.599964	-1.247508
Si	6.808441	3.727523	-0.086024
Si	7.123237	3.702846	2.217372
Si	6.271828	5.591288	3.153001
Si	5.254184	5.624181	5.223095
Si	4.079493	3.731245	5.561459
Si	1.911559	3.734683	6.254253
Si	0.765703	5.626951	6.701819
Si	-1.269009	5.590952	5.607671
Si	-2.510660	3.703653	5.349038
Si	-3.602993	3.729219	3.296765
Si	-3.988224	5.601655	2.135573
Si	-4.302346	5.626110	-0.167944
Si	-3.451002	3.737765	-1.103718
Si	-2.434006	3.704885	-3.174296
Si	-1.258672	5.597778	-3.511909

Table A.1 *Continued*

Si	0.909116	5.594471	-4.205163
Si	1.833043	7.678612	-3.814879
Si	3.858998	7.344498	-2.869011
Si	4.568637	8.904826	-1.321378
Si	5.852004	7.454846	-0.031266
Si	6.332852	7.694902	2.184646
Si	4.395043	8.560441	3.129434
Si	3.910511	7.502339	5.090105
Si	1.776639	7.482550	5.759187
Si	0.228633	8.569292	4.489096
Si	-1.890699	7.692947	4.857158
Si	-2.802483	7.452011	2.781447
Si	-2.522138	8.902118	0.984055
Si	-2.856471	7.342484	-0.685524
Si	-1.773746	7.677483	-2.640659
Si	0.393567	8.386983	-2.108138
C	0.906544	9.150713	-0.528398
Si	2.695600	9.323971	-0.040658
Si	2.988407	10.023382	2.142397
Si	0.794898	10.013191	2.852849
Si	-0.254769	9.322323	0.917114

Table A.2: Coordinates for the most stable Penta-hexa ($Si_{60}C_2$) structure.

Atom	X(Å)	Y(Å)	Z(Å)
Si	-2.541649	-4.828919	0.114989
Si	-3.495099	-4.206424	2.126130
Si	-1.549316	-3.872288	3.357461
Si	0.198850	-5.249873	2.693673
Si	-0.398995	-5.499974	0.462070
Si	1.046004	-5.424079	-1.242069
Si	3.020786	-4.354206	-0.813635
Si	3.839464	-3.996695	1.263410
Si	2.069981	-3.924808	2.744536
Si	2.528703	-2.497824	4.517217
Si	0.623695	-1.408774	5.126701
Si	-1.458997	-2.432691	5.128350
Si	-2.737401	-0.580532	4.602086
Si	-4.714236	-0.588766	3.481524
Si	-4.562246	-2.217732	1.837737
Si	-5.663852	-1.608447	-0.098411
Si	-4.489531	-2.358940	-1.889100
Si	-3.381892	-4.385582	-1.942939
Si	-1.693171	-3.884751	-3.432215
Si	0.415502	-4.657251	-3.316263
Si	2.022537	-3.065715	-3.759986
Si	4.064950	-3.402884	-2.651942
Si	4.544319	-1.221769	-1.836974
Si	6.254085	-0.687020	-0.079223
Si	4.489054	-1.706696	1.301326
Si	3.769490	-0.945469	3.366502
Si	4.160122	1.221741	3.779633
Si	2.052181	1.921159	4.436204
Si	0.578819	0.812876	5.786099
Si	-1.568067	1.327367	5.053279
Si	-2.183101	3.201388	3.990147
Si	-4.065367	3.355520	2.637132
Si	-4.839862	1.284192	2.135514
Si	-5.579371	0.703615	0.064163
Si	-5.008176	2.036589	-1.635870
Si	-4.081362	1.017462	-3.444028
Si	-4.248402	-1.197022	-3.865162
Si	-2.277981	-2.088607	-4.705263
Si	-0.586663	-0.815625	-5.420306

Table A.2 *Continued*

Si	1.654425	-1.415609	-5.275294
Si	2.619641	0.476683	-4.351459
Si	4.688972	0.570519	-3.381022
Si	4.494690	2.043587	-1.528199
Si	6.408275	2.060030	0.104648
Si	4.371601	2.051741	1.552491
Si	2.859785	3.856335	1.637996
Si	1.676697	4.030538	3.590109
Si	-0.502277	4.403325	3.037636
Si	-1.307499	5.641017	1.243988
Si	-3.155572	4.318357	0.741386
Si	-4.039483	4.134085	-1.345958
Si	-2.269133	4.000412	-2.834381
Si	-2.700726	2.503385	-4.551457
Si	-0.792442	1.429337	-5.156164
Si	1.320167	2.302837	-4.932362
Si	1.377368	3.881525	-3.345740
Si	3.037866	3.821176	-1.783353
Si	2.482540	5.263769	-0.098504
Si	0.187271	5.417381	-0.451671
Si	-0.367730	5.269460	-2.699568
C	3.987025	0.908939	0.018317
C	3.950410	-0.517959	-0.124760

Table A.3: Coordinates for the most stable Hex ($Si_{56}C_4$) structure.

Atom	X(Å)	Y(Å)	Z(Å)
Si	0.795101	4.637365	-2.933267
Si	2.832302	3.712654	-2.893036
Si	4.039142	4.328600	-0.999610
Si	2.128895	4.907794	0.235277
Si	0.396078	5.876011	-1.006118
Si	-1.602246	5.127389	-0.202821
Si	-1.994621	4.808649	2.026649
Si	-0.127360	4.204171	3.114931
Si	2.053719	4.747882	2.517429
Si	3.070577	2.734461	3.095463
Si	4.958602	1.931564	2.118771
Si	4.808247	2.350400	-0.148168
Si	5.726400	0.641283	-1.450419
Si	4.248150	0.249818	-3.152350
Si	2.818438	1.790264	-4.030543
C	1.186324	0.894700	-4.373675
C	-0.128353	1.457559	-4.369891
Si	-0.599119	3.246553	-3.981844
Si	-2.727869	3.249829	-3.180465
Si	-3.473095	4.590439	-1.486565
Si	-4.431834	3.036804	-0.025898
Si	-3.870373	3.459944	2.157243
Si	-3.646682	1.581756	3.373554
Si	-2.013403	1.219037	4.958216
Si	-0.145988	2.413290	4.518717
Si	2.018188	1.690933	4.876428
Si	2.050910	-0.563894	4.611454
Si	3.733416	-1.638502	3.498873
Si	4.962858	-0.389191	2.109141
Si	5.277493	-1.143600	-0.018376
Si	4.842934	-3.293903	-0.626495
Si	3.559911	-3.276275	-2.543869
Si	3.671867	-1.708653	-4.199143
Si	1.439124	-0.981898	-4.370737
C	-0.040817	-2.003724	-4.079471
C	-1.397654	-1.419213	-4.080011
Si	-1.669954	0.358258	-4.370764

Table A.3 *Continued*

Si	-4.553709	-0.416867	2.772733
Si	-3.512898	-2.161912	3.922987
Si	-1.631145	-1.041713	4.679713
Si	0.357507	-2.037625	5.186067
Si	0.752172	-3.658137	3.568851
Si	2.958456	-3.731337	2.927737
Si	3.250232	-4.240626	0.754876
Si	1.571355	-5.161026	-0.491522
Si	2.029524	-4.988477	-2.800619
Si	0.157556	-3.735166	-3.395558
Si	-1.969224	-4.609766	-3.114822
Si	-2.792445	-2.465580	-3.400635
Si	-4.977976	-1.943095	-2.802439
Si	-4.794088	-2.380533	-0.502217
Si	-3.954218	-4.276168	0.461290
Si	-2.788013	-3.674256	2.375845
Si	-0.850391	-4.900409	2.602198
Si	-0.400197	-5.676557	0.460068
Si	-2.112964	-4.859326	-0.832076

Table A.4: Coordinates for the most stable Triangle ($Si_{60}C_4$) structure.

Atom	X(Å)	Y(Å)	Z(Å)
Si	-4.335017	-2.380599	-2.065737
Si	-6.513804	-1.595229	-1.212164
Si	-5.064402	-3.115526	0.944455
Si	-3.218725	-4.461383	0.470434
Si	-3.192440	-4.454534	-1.797499
Si	-1.062386	-4.646771	-2.509555
Si	0.653808	-5.764164	-1.412142
Si	0.297327	-5.434269	0.822591
Si	-1.747023	-5.474273	1.929210
Si	-1.191221	-3.844016	3.523980
Si	-2.689488	-2.363764	4.474772
Si	-3.874740	-1.954444	2.518207
Si	-4.082609	1.274771	2.660214
Si	-5.211891	2.477653	1.095705
Si	-6.582168	1.383975	-0.916951
Si	-4.394855	2.102723	-1.841296
Si	-3.440085	1.104806	-3.651483
Si	-3.264589	-1.112104	-3.635209
Si	-1.509430	-1.729410	-5.016603
Si	-0.221674	-3.365424	-4.179871
Si	2.077505	-3.528062	-4.241597
Si	2.403405	-4.401674	-2.109839
Si	4.328891	-4.080485	-0.937457
Si	3.819981	-3.971851	1.331975
Si	1.981359	-4.843420	2.247700
Si	1.020061	-3.976744	4.174074
Si	1.791408	-1.897410	4.639528
Si	0.517199	-0.241523	5.642655
Si	-1.588566	-0.328963	4.782835
Si	-2.868694	1.604413	4.602256
Si	-1.559878	3.357381	3.917343
Si	-2.044613	4.631750	2.062152
Si	-3.964677	4.472742	0.855277
Si	-3.260519	4.052465	-1.258132
Si	-1.629842	5.194180	-2.351355
Si	-0.629161	3.695969	-3.800288
Si	-1.691783	2.029773	-4.874096
Si	-0.296199	0.221676	-5.151482
Si	1.949352	0.314969	-5.480315
Si	2.939759	-1.426095	-4.323928
Si	4.944101	-0.830548	-3.312308

Table A.4 *Continued*

Si	5.008473	-1.895378	-1.297392
Si	5.856715	-0.915595	0.621961
Si	4.616763	-2.030721	2.213780
Si	3.945162	-1.202302	4.209852
Si	3.699285	1.099037	4.142200
Si	1.597221	1.633093	4.840085
Si	0.647155	3.671016	4.489664
Si	1.434382	4.608291	2.516892
Si	-0.181781	5.870240	1.411365
Si	0.107363	5.422308	-0.826861
Si	2.172682	5.242728	-1.871546
Si	1.630194	3.846153	-3.653277
Si	2.875715	2.143803	-4.391566
Si	4.455672	1.405147	-2.930628
Si	5.234515	2.677094	-1.207498
Si	5.351169	1.293766	0.640888
Si	4.458454	2.346347	2.452913
Si	3.582175	4.399325	1.819616
Si	3.581418	4.129148	-0.481975
C	-4.788543	-1.523506	-0.292302
C	-4.377121	-0.259557	0.362169
C	-3.990901	-0.299091	1.748970
C	-4.731721	1.055341	-0.219408

Table A.5: Coordinates for the most stable Hexa ($Si_{54}C_6$) structure.

Atom	X(Å)	Y(Å)	Z(Å)
Si	-2.198322	4.807796	2.022736
Si	-2.718377	4.625472	-0.214478
Si	-1.192146	5.733839	-1.617729
Si	0.684196	5.356463	-0.263986
Si	0.103694	5.062071	1.916742
Si	1.515780	3.880927	3.196159
Si	3.657699	3.309896	2.554288
Si	3.983101	3.607274	0.334768
Si	2.833859	5.124636	-1.000579
Si	2.781724	3.681486	-2.808628
Si	0.998259	3.124871	-4.030752
Si	-0.853269	4.041226	-3.148085
Si	-2.185662	2.480079	-4.076194
Si	-3.996014	2.292653	-2.766013
Si	-4.623077	3.612418	-0.971848
Si	-5.130734	1.766760	0.365534
Si	-4.551485	1.584535	2.529473
Si	-2.777667	2.905542	3.111078
Si	-1.557710	1.912771	4.805891
Si	0.663441	2.149898	4.412411
Si	2.308220	0.594533	4.911101
Si	3.778662	1.090491	3.173987
Si	5.174707	-0.412639	2.227746
Si	5.764552	0.076156	0.026293
Si	5.059071	1.995787	-0.887232
Si	4.579101	2.313993	-3.167647
Si	3.294768	0.444996	-3.551504
C	1.433497	0.184521	-3.972445
C	0.484446	1.262142	-4.084100
C	-0.964756	0.966495	-4.078989
C	-1.409217	-0.396188	-3.950479
Si	-3.225540	-0.884254	-3.515156
Si	-5.141036	0.342229	-3.136559
Si	-5.388537	-0.155854	-0.853201
Si	-5.468325	-2.241228	0.051575
Si	-4.288860	-2.206049	2.046533
Si	-4.224691	-0.495519	3.518716
Si	-2.128560	-0.300003	4.443635
Si	-0.764647	-2.043795	4.925653
Si	1.426918	-1.462747	4.463393
Si	2.669769	-3.244438	3.638869

Table A.5 *Continued*

Si	4.072225	-2.432611	2.024734
Si	4.694931	-3.601008	0.101960
Si	4.973842	-1.694973	-1.204186
Si	4.383614	-1.567552	-3.444378
Si	2.293105	-2.524926	-3.412677
C	0.971287	-1.204563	-3.875968
C	-0.437194	-1.491927	-3.862394
Si	-1.128080	-3.225793	-3.389980
Si	-3.426260	-3.160863	-3.388479
Si	-3.920524	-3.505142	-1.151492
Si	-2.928704	-5.190257	0.105297
Si	-2.864599	-3.986017	2.116137
Si	-1.079187	-3.790459	3.440538
Si	0.941165	-4.347733	2.550228
Si	1.110004	-5.465083	0.584785
Si	2.745986	-4.509446	-0.731018
Si	2.153518	-4.745329	-2.966566
Si	-0.142475	-5.226210	-2.967635
Si	-0.774877	-5.207650	-0.723813

Table A.6: Coordinates for the most stable Dhex-pepar ($Si_{60}C_6$) structure.

Atom	X(Å)	Y(Å)	Z(Å)
Si	0.302636	3.991508	4.010187
Si	0.453118	2.014977	5.162988
Si	-1.596766	0.986760	5.059541
Si	-3.222638	2.470744	4.331516
Si	-1.838390	3.940205	3.170422
Si	-2.496344	5.210645	1.404094
Si	-3.899239	3.902072	0.103508
Si	-5.318870	2.327834	0.886874
Si	-4.475462	1.339031	2.799277
Si	-5.093271	-0.884673	2.956234
Si	-3.331815	-2.068467	3.766748
Si	-1.904437	-1.237300	5.391983
Si	0.006372	-2.379786	4.783605
Si	2.101222	-1.547322	4.680649
Si	2.171842	0.680097	4.603563
Si	3.661165	1.111713	2.844846
Si	4.113264	3.390441	2.457350
Si	1.945785	4.279391	2.435455
Si	1.471483	5.675303	0.624733
Si	-0.692626	5.401695	-0.048656
Si	-1.340775	5.262514	-2.260804
Si	-3.272992	3.994481	-2.083062
Si	-3.892865	2.334932	-3.458078
Si	-5.218382	0.557571	-2.771754
Si	-5.450617	0.513771	-0.523231
Si	-5.429519	-1.393579	0.710714
Si	-4.636372	-3.230642	-0.279897
Si	-3.068954	-4.421290	0.872325
Si	-2.777915	-4.222496	3.113958
Si	-0.500054	-4.237531	3.590562
Si	1.109898	-4.779455	2.080965
Si	3.334598	-4.187767	2.075829
Si	3.348024	-1.947967	2.718441
Si	5.439915	-0.626707	3.038418
Si	5.693168	-0.582892	0.619565
Si	5.493427	1.300640	-0.882920
Si	3.919401	2.828871	0.144700
Si	2.705072	4.494155	-0.911532
Si	2.507614	4.025008	-3.084107
Si	0.214423	4.069920	-3.419399

Table A.6 *Continued*

Si	-0.286608	2.614515	-5.132583
Si	-2.224735	1.468436	-4.747023
Si	-2.627004	-0.751538	-5.284545
Si	-3.989947	-1.270993	-3.469330
Si	-4.204644	-3.351765	-2.558059
Si	-2.121923	-4.356534	-2.503101
Si	-1.756519	-5.639679	-0.605625
Si	0.439733	-5.429259	-0.018507
Si	2.304923	-5.221451	-1.403671
Si	3.313225	-3.440177	-0.173886
Si	5.435763	-2.406263	-0.815441
Si	4.750207	-1.213984	-2.704155
Si	5.334707	1.056097	-3.319978
Si	2.927180	1.645861	-2.947775
Si	1.341181	1.083738	-4.593486
Si	1.489183	-1.062856	-5.171839
Si	-0.671695	-1.858771	-4.875384
Si	-0.552823	-4.050571	-4.146278
Si	1.408532	-3.862246	-2.941817
Si	2.476977	-1.769396	-3.114488
C	2.822909	1.200783	0.001613
C	2.500253	0.598527	-1.284525
C	2.807249	0.411522	1.200495
C	2.327118	-0.825960	-1.346277
C	2.632552	-1.002803	1.135940
C	2.496969	-1.641057	-0.147412

Table A.7: Coordinates for the most stable Sur1 (Si40C20) structure.

Atom	X(Å)	Y(Å)	Z(Å)
Si	4.111847	2.021419	-1.881193
C	2.564199	1.924315	-2.953897
C	2.386861	0.554023	-3.466424
C	3.226237	-0.585614	-3.041769
Si	4.942254	-0.051888	-2.309471
Si	5.051351	-0.968593	-0.213731
Si	4.776283	-3.273443	-0.225987
Si	3.235257	-3.316518	-1.940667
C	2.657236	-1.897786	-3.025651
C	1.272702	-2.153051	-3.499100
C	0.606701	-1.074272	-4.094931
C	1.149628	0.256825	-4.053646
C	0.054096	1.188145	-4.043702
C	0.148707	2.452880	-3.450194
C	1.474912	2.847736	-2.943221
Si	1.324265	4.368426	-1.838958
Si	2.786359	5.118844	-0.254778
Si	4.551104	3.542115	-0.256702
Si	4.139779	2.074026	1.487545
Si	5.221441	0.064443	1.866056
Si	3.637580	-1.392887	2.832253
Si	3.312988	-3.299273	1.608782
Si	1.644051	-4.842836	1.988461
Si	0.753880	-4.995613	-0.147594
Si	1.486469	-4.715802	-2.280128
C	0.438101	-3.305070	-3.086439
C	-0.984611	-3.196490	-3.077745
C	-1.641292	-1.930441	-3.484948
C	-0.829754	-0.964768	-4.093187
C	-1.170762	0.434142	-4.066868
C	-2.338291	0.921557	-3.467765
C	-2.314774	2.327998	-2.997733
C	-1.111845	3.098949	-3.019082

Table A.7 *Continued*

Si	-0.852490	4.868198	-2.279550
Si	-1.805779	4.836400	-0.204203
Si	-0.769784	5.097705	1.872177
Si	1.409774	4.415873	1.486846
Si	2.586153	3.026712	2.912145
Si	1.227649	1.466024	3.826792
Si	1.798173	-0.740537	3.932128
Si	-0.130200	-2.002668	4.251440
Si	-0.264495	-3.713829	2.768596
Si	-2.339783	-4.535284	2.021739
Si	-1.519119	-4.801326	-0.134288
Si	-2.225123	-4.447709	-2.273561
Si	-3.717696	-2.781939	-1.889200
C	-2.962076	-1.464447	-2.994592
C	-3.327670	-0.080697	-3.020534
Si	-4.938853	0.709474	-2.284752
Si	-3.806107	2.637660	-1.896022
Si	-4.030995	4.200647	-0.215113
Si	-3.816307	2.751465	1.624920
Si	-1.876748	3.238664	2.747214
Si	-1.032908	1.723557	4.221764
Si	-1.776597	-0.429887	3.785432
Si	-3.901226	-0.934765	3.158268
Si	-3.716577	-2.712291	1.691029
Si	-5.183709	-2.505680	-0.137194
Si	-5.144980	-0.196310	-0.188514
Si	-4.846454	0.774313	1.860062

Table A.8: Coordinates for the most stable Bowl ($Si_{60}C_{20}$) structure.

Atom	X(Å)	Y(Å)	Z(Å)
Si	0.187551	-5.371695	2.012880
Si	1.973118	-4.199254	2.912914
Si	3.956247	-4.456213	1.651151
Si	2.754535	-3.997783	-0.388069
Si	0.519762	-4.836559	-0.305216
Si	-0.941194	-5.901646	-1.899522
Si	-0.297525	-4.286733	-3.530876
Si	1.780676	-3.473605	-4.014580
Si	3.534198	-3.694471	-2.561035
Si	5.232237	-2.103609	-2.676781
Si	4.945836	-1.142422	-0.467675
Si	4.832771	-2.312187	1.613243
Si	4.844131	-0.710153	3.262248
Si	2.938604	-0.975628	4.481494
Si	1.765746	-2.938002	4.812326
Si	-0.382935	-2.069696	4.948889
Si	-2.279442	-3.154251	4.354084
Si	-1.857225	-4.496749	2.537048
Si	-3.640192	-4.558587	1.022877
Si	-2.573349	-4.225730	-1.093421
Si	-3.885972	-3.364301	-2.849959
Si	-2.035922	-2.886076	-4.144924
Si	-1.781186	-0.927366	-5.267481
Si	0.382377	-0.158633	-5.362669
Si	2.188995	-1.470566	-5.089965
Si	3.909080	-0.557219	-3.834187
Si	4.255609	1.704001	-3.667333
Si	4.486981	2.238086	-1.322061
Si	5.981958	0.981028	0.011463
Si	4.907982	1.281992	2.064690
Si	3.950022	3.235081	2.835477
Si	2.077603	2.737178	4.088337
Si	1.722905	0.829773	5.192456
Si	-0.409626	0.106458	5.664668
Si	-2.038591	1.343530	4.715045
Si	-3.953748	0.446946	3.881439
Si	-3.977672	-1.782509	3.576976
Si	-4.713564	-2.552581	1.552483
Si	-6.033798	-1.322128	0.084898
Si	-4.598255	-1.341640	-1.894514
Si	-5.135266	0.517662	-3.394356
Si	-3.006711	0.782916	-4.315579
Si	-1.634495	2.684259	-4.211849

Table A.8 *Continued*

Si	0.417134	2.132439	-5.119546
Si	2.232223	2.747731	-3.925530
Si	1.993642	4.164350	-2.071206
Si	4.090215	4.665529	-0.985916
Si	2.955940	4.458168	1.115149
Si	1.015677	5.636413	1.888300
Si	0.318978	4.041695	3.417053
Si	-1.822498	3.505871	3.987933
Si	-3.351241	3.629529	2.252239
Si	-5.016015	2.001004	2.509359
Si	-5.497684	0.962761	0.524568
Si	-4.682959	1.903115	-1.485617
Si	-3.395882	3.917649	-1.365884
Si	-2.209360	4.769893	-3.338009
Si	-0.236135	4.964914	-1.885603
Si	-0.751719	5.451638	0.322367
Si	-3.213808	5.327635	0.643496
C	0.193488	1.449912	0.488977
C	1.102461	0.356723	0.516163
C	0.315040	-0.833111	0.550066
C	-1.071076	-0.500387	0.432385
C	-1.139928	0.915176	0.451824
C	-2.176612	1.600063	-0.179246
C	-3.244756	0.813145	-0.736073
C	-3.131178	-0.613272	-0.854405
C	-1.988711	-1.320792	-0.285324
C	-1.526796	-2.704344	-0.501180
C	-0.177390	-3.050346	-0.242562
C	0.808615	-2.043323	0.087762
C	2.232257	-2.120586	-0.164829
C	3.028617	-0.941537	-0.217666
C	2.400344	0.386711	-0.049935
C	2.776886	1.674831	-0.630970
C	1.811349	2.741455	-0.735753
C	0.485550	2.626790	-0.199134
C	-0.613822	3.503264	-0.573318
C	-1.948120	2.956706	-0.582554

Table A.9: Coordinates for the most stable Sur4 ($Si_{36}C_{24}$) structure.

Atom	X(Å)	Y(Å)	Z(Å)
C	-1.409211	0.535156	-3.949243
C	-2.676682	0.254621	-3.315248
C	-2.794418	-1.226143	-3.241784
C	-1.477812	-1.780999	-3.614145
C	-0.696585	-0.697869	-4.166135
C	0.701652	-0.700796	-4.162837
C	1.476888	-1.787043	-3.610616
C	0.738928	-2.875756	-3.039682
C	-0.745619	-2.872298	-3.040529
C	-1.191918	-3.755001	-1.956366
Si	-2.943641	-3.826790	-1.447929
Si	-4.111959	-2.215496	-2.517781
Si	-5.767841	-1.152241	-1.239491
Si	-4.680733	0.888388	-1.317745
C	-3.262691	1.287371	-2.507064
C	-2.515754	2.547634	-2.246237
C	-1.189455	2.726676	-2.791511
C	-0.711112	1.719434	-3.710533
C	0.724295	1.716270	-3.707461
C	1.418616	0.529604	-3.941908
C	2.681832	0.244285	-3.301973
C	2.793911	-1.236134	-3.231835
Si	4.103320	-2.228251	-2.498781
Si	2.927169	-3.842481	-1.441949
C	1.179490	-3.760962	-1.956071
C	-0.007497	-4.225936	-1.242233
Si	-0.007393	-4.847335	0.530168
Si	-1.783962	-4.009625	1.711712
Si	-3.835394	-4.064826	0.703636
Si	-4.590494	-1.826011	0.716748
Si	-4.361045	-0.511328	2.607892
Si	-3.962249	1.651466	1.808382
Si	-5.127316	2.716462	0.066099
Si	-3.131491	3.612306	-0.824774
Si	-2.011430	5.531847	-0.117540
Si	0.020895	4.822966	-1.115412
C	0.008431	3.465692	-2.304223
C	1.203011	2.720945	-2.786145

Table A.9 *Continued*

C	2.524644	2.536428	-2.232035
C	3.268511	1.275079	-2.490576
Si	4.692572	0.883759	-1.306609
Si	5.759129	-1.171566	-1.220673
Si	4.583654	-1.858439	0.727743
Si	3.796741	-4.084731	0.717513
Si	1.749111	-3.980089	1.728311
Si	1.202104	-2.996578	3.751808
Si	-1.150623	-2.927813	3.626074
Si	-2.242703	-0.960213	3.498635
Si	-1.073976	0.986434	3.752731
Si	-2.330642	2.765331	3.027068
Si	-1.162173	4.176273	1.662741
Si	1.153719	4.223415	1.679434
Si	2.048677	5.561296	-0.121750
Si	3.145431	3.610792	-0.817039
Si	5.175720	2.732794	0.049427
Si	4.002208	1.627487	1.775607
Si	4.331427	-0.533923	2.604916
Si	2.175850	-0.955073	3.423069
Si	1.149764	1.008326	4.056896
Si	2.239806	2.633355	2.852174

Table A.10: Coordinates for the most stable Sheet ($Si_{60}C_{24}$) structure.

Atom	X(Å)	Y(Å)	Z(Å)
Si	1.496118	-1.571041	-4.708962
Si	3.084258	-2.873663	-3.670829
Si	4.603996	-1.288779	-2.878284
Si	3.939023	0.781422	-3.652910
Si	2.251605	0.561059	-5.212562
Si	0.603963	2.043229	-4.720175
Si	0.943012	4.093018	-3.726404
Si	2.790505	4.296714	-2.367815
Si	4.506135	2.676758	-2.547831
Si	5.200114	2.157067	-0.251281
Si	6.776895	0.377833	0.624698
Si	5.460687	-1.317772	-0.669362
Si	4.474601	-3.408864	0.279759
Si	3.694170	-5.645791	-0.575524
Si	2.332373	-4.580505	-2.334134
Si	0.082271	-5.299832	-2.559594
Si	-1.286108	-3.811488	-3.617120
Si	-0.607311	-2.288244	-5.210131
Si	-2.091118	-0.570476	-4.755260
Si	-1.621833	1.607305	-5.179526
Si	-2.660968	2.987392	-3.662170
Si	-1.190890	4.607968	-2.928335
Si	-1.564472	5.388786	-0.723184
Si	0.734186	5.584523	0.231075
Si	3.065551	6.048091	-0.634592
Si	3.876961	4.070350	0.675944
Si	3.397714	3.356447	2.888536
Si	4.002741	1.254008	3.695654
Si	5.128150	-0.246475	2.369028
Si	4.576115	-2.541425	2.566784
Si	2.650278	-2.996329	3.681328
Si	1.196544	-4.623696	2.940570
Si	1.591078	-5.371859	0.729312
Si	-0.680553	-5.573039	-0.258894
Si	-2.975976	-5.866392	0.605483
Si	-3.865223	-4.016932	-0.735364
Si	-3.488927	-3.465810	-3.017422
Si	-3.983399	-1.281435	-3.667883
Si	-5.128425	0.249464	-2.400497
Si	-4.616406	2.561742	-2.585401
Si	-4.471099	3.408569	-0.296529
Si	-3.673638	5.617140	0.569191
Si	-2.353975	4.574415	2.345902

Table A.10 *Continued*

Si	-0.089297	5.250766	2.513047
Si	1.265792	3.828409	3.644227
Si	0.585332	2.254810	5.182384
Si	2.069289	0.542763	4.723489
Si	1.609968	-1.626764	5.214913
Si	-0.614814	-2.053107	4.730347
Si	-0.938814	-4.102365	3.737811
Si	-2.800589	-4.266992	2.406178
Si	-4.578231	-2.704740	2.591557
Si	-5.176007	-2.171076	0.281966
Si	-6.636581	-0.367331	-0.606702
Si	-5.430588	1.342011	0.700208
Si	-4.676930	1.295968	2.947936
Si	-3.102648	2.853861	3.671521
Si	-1.526693	1.556687	4.729257
Si	-2.278958	-0.582134	5.217008
Si	-3.946012	-0.781000	3.634187
C	3.028186	-2.197721	0.042472
C	1.628308	-2.332584	0.178236
C	0.812893	-1.164048	0.033746
C	1.422658	0.119938	-0.007786
C	2.844149	0.238897	-0.137804
C	3.612260	-0.952951	-0.285520
C	-0.603735	-1.277713	-0.006043
C	0.615402	1.290742	0.006844
C	-0.801755	1.176843	-0.028034
C	-1.411224	-0.107339	0.017133
C	-1.616464	2.346861	-0.173378
C	-0.965308	3.604580	-0.329320
C	0.403743	3.726866	-0.008483
C	1.223641	2.583461	0.128686
C	2.637323	2.652739	0.292463
C	3.427308	1.519301	-0.009776
C	0.979075	-3.593106	0.330457
C	-0.387704	-3.710999	0.002752
C	-1.210418	-2.570814	-0.133758
C	-2.624293	-2.636055	-0.271038
C	-3.410205	-1.508615	0.029436
C	-2.832823	-0.226417	0.151223
C	-3.016303	2.207317	-0.041633
C	-3.598253	0.966645	0.278348

REFERENCES

[1]**.** E. R. Bernstein (Ed.), *Atomic and Molecular Clusters* (Elsevier, New York, 1990).

[2]. P. Jena, S. N. Khanna, and B. K. Rao (Eds.), *Physics and Chemistry of Finite Systems – From Clusters to Crystals, Proceedings of the NATO Advanced Research Workshop* (Kluwer Academic Publishing, 1991).

[3]. H. Haberland (Ed.), *Clusters of Atoms and Molecules* (Springer-Verlag, Berlin, 1994).

[4]. U. Naher, S. Bjornholm, S. Frauendorf, F. Garcias, and C. Guet, Phys. Rep. 285, 245 (1997).

[5]. S. Sugano and H. Koizumi, *Microcluster Physics* (Springer-Verlag, New York, 1998).

[6]. J. Jellinek, R. S. Berry, and J. Jortner (Eds.), *Theory of Atomic and Molecular Clusters : With a Glimpse at Experiments* (Springer-Verlag, New York, 1999).

[7]. S. Bjornholm and J. Borggreen, Philos. Mag. B 79, 1321 (1999).

[8]. P. Jena, S. N. Khanna, and B. K. Rao, *Theory of Atomic and Molecular Clusters* (Springer -Verlag, Berlin, 1999).

[9]. Roy. L. Johnston, and R. L. Johnston, *Atomic and Molecular Clusters* (Routledge Publishing, New York, 2002).

[10]. F. Baletto and R. Ferrando, Rev. Mod. Phys. **77**, 371 (2005).

[11]. N. E. Frick, M.S. Thesis, The University of Texas at Arlington, May 2002 and references therein;

[12]. N. E. Frick, A. S. Hira, and A. K. Ray, to be published.

[13]. R.-H. Xie, G. W. Bryant, J. Zhao, V. H. Smith, Jr., A. D. Carlo, and A. Pecchia, Phys. Rev. Lett. 90, 206602 (2003).

[14]. R. –H. Xie, G. W. Bryant, G. Sun, T. Kar, Z. Chen, V. H. Smith, Jr., Y. Araki, N. Tagmatarchis, H. Shinohara, and O. Ito, Phys. Rev. B 69, 201403 (2004).

[15]. A. Szabo and N. S. Ostlund, *Modern Quantum Chemistry* (Macmillan, New York, 1982).

[16]. W. J. Hehre, P. v. R. Schleyer, and J. A. Pople, *Ab Initio Molecular Orbital Theory* (Wiley, New York, 1982).

[17]. R. G. Parr and W. Yang, *Density Functional Theory of Atoms and Molecules* (Oxford University Press, New York, 1989).

[18]. L. R. Marim, M. R. Lemes, and A. Dal Pino Jr, J. Mol. Struct. (Theochem) 663, 159 (2003).

[19]. L. Mitas, J. C. Grossman, I. Stich and J. Tobik, Phys. Rev. Lett 84, 1479 (2000).

[20]. Z-Y. Lu, C-Z. Wang and K-M. Ho, Phys. Rev. B 61, 2329 (2000).

[21]. X. L. Zhu, X. C. Zeng, Y. A. Lei and B. Pan, J. Chem. Phys. 120, 8985 (2004).

[22]. K.-M. Ho, A. A. Shvartsburg, B. Pan, Z.-Y. Lu, C.-Z. Wang, J. G. Wacker, J. L. Fye, and M. F. Jarrold, Nature 392, 582 (1998).

[23]. G. V. Helden, M. T. Hsu, N. Gotts, and M. T. Bowers, J. Phys. Chem. 97, 8182 (1993).

[24]. M. F. Jarrold, Nature 407, 26 (2000).

[25]. J. C. Grossman, L. Mitas, and K. Raghavachari, Phys. Rev. Lett. 75, 3870 (1995).

[26]. B.-X. Li, P.-L. Cao, and D.-L. Que, Phys. Rev. B 61, 1685 (2000).

[27]. B.-X. Li, P.-L. Cao, B. Song, and Z.-Z. Ye, J. Mol. Struct. (Theochem) 620, 189 (2003).

[28]. M. C. Piqueras, R. Crespo, E. Orti, and F. Tomas, Chem. Phys. Lett. 213, 509 (1993).

[29]. R. Crespo, M. C. Piqueras, and F. Tomas, Synthetic metals **77,** 13 (1996).

[30]. K. Jug and M. Krack, Chem. Phys. 173, 439 (1993).

[31]. F. S. Khan and J. Q. Broughton, Phys. Rev. B 43, 11754 (1991).

[32]. Z. Chen, H. Jiao, G. Seifert, A. H. C. Horn, D. Yu, T. Clark, W. Thiel, and P. V. R. Schleyer, J. Comp. Chem. 24, 948 (2003).

[33]. M. Menon, and K. R. Subbaswamy, Chem. Phys. Lett. 219, 219 (1994).
[34]. M. Menon, J. Chem. Phys. 114, 7731 (2001).
[35]. S. Yoo, J. Zhao, J. Wang, and X. C. Zeng, J. Am. Chem. Soc. 126**,** 13845 (2004).
[36]. J. Wang, X. Zhou, G. Wang, and J. Zhao, Phys. Rev. B 71, 113412 (2005).
[37]. J. Zhao, J. Wang, J. Jellinek, S. Yoo, and X. C. Zeng, Eur. Phys. J. D. 34, 35 (2005).
[38]. S. Yoo and X. C. Zeng, Angew. Chem. Int. Ed. 44, 1491 (2005).
[39]. H. Hiura, T. Miyazaki, and T. Kanayama, Phys. Rev. Lett. 86, 1733 (2001).
[40]. T. Miyazaki, H. Hiura, and T. Kanayama, Phys. Rev. B 66, 121403 (R) (2002).
[41]. S. N. Khanna, B. K. Rao, and P. Jena, Phys. Rev. Lett. 89, 016803 (2002).
[42]. W. Zheng, J. M. Nilles, D. Radisic and K. H. Bowen, J. Chem. Phys. 122, 071101 (2005).
[43]. V. Kumar and Y. Kawazoe, Phys. Rev. Lett. 87, 045503 (2001).
[44]. V. Kumar and Y. Kawazoe Phys. Rev. B 65, 073404 (2002).
[45]. H. Kawamura, V. Kumar, and Y. Kawazoe, Phys. Rev. B 70, 245433 (2004).
[46]. A. K. Singh, V. Kumar, and Y. Kawazoe, Phys. Rev. B 71, 115429 (2005)
[47]. K. Jackson, and B. Nellermoe, Chem. Phys. Lett. 254, 249 (1996).
[48]. C. Xiao, F. Hagelberg, and W. A. Lester, Phys. Rev. B 66, 075425 (2002).
[49]. Q. Sun, Q. Wang, P. Jena, B. K. Rao, and Y. Kawazoe, Phys. Rev. Lett 90, 135503 (2003).
[50]. Q. Sun, Q. Wang, P. Jena, J. Z. Yu, and Y. Kawazoe, Sci. Tech. Adv. Mats 4, 361 (2003).
[51]. Q. Sun, Q. Wang, Y. Kawazoe, and P. Jena, Eur. Phys. J. D 29, 231 (2004).
[52]. J. Cernicharo, C. A. Gottlieb, M. Guelin, P. Thaddeus, and J. M. Vrtilek, Astrophys. J. 341, L25 (1989).
[53]. M. Oshishi, N. Kaifu, K. Kawaguchi, A. Murakami, S. Saito, S. Yamamoto, S.-I. Ishikawa, Y. Fujita, Y. Shiratori, and W. M. Irvine, Astrophys. J. 34, L83 (1989).
[54]. J. D. Parsons, R. F. Bunshah, O. M. Stafsudd, Solid State Tech. 28, 133 (1985).

[55]. V. D. Gordon, E. S. Nathan, A. J. Apponi, M. C. McCarthy, P. Thaddeus, and P. Botschwina, J. Chem. Phys. 113, 5311 (2000).

[56]. S. Hunsicker and R. O. Jones, J. Chem. Phys. 105, 5048 (1996).

[57]. S. Osawa, M. Harada, and E. Osawa, Fullerene Sci. Tech. 3, 225 (1995)

[58]. M. Pellarin, C. Ray, J. Lerme, J. L. Vialle, M. Broyer, X. Blase, P. Keghelian, P. Melinon, and A. Perez, J. Chem. Phys. 110, 6927 (1999).

[59]. C. Ray, M. Pellarin, J. L. Lerme, J. L. Vialle, M. Broyer, X. Blase, P. Keghelian, P. Melinon, and A. Perez, Phys. Rev. Lett. 80, 5365 (1998).

[60]. W. Branz, I. M. L. Billas, N. Malinowski, F. Tast, M. Heinebrodt, and T. P. Martin, J. Chem. Phys. 109, 3425 (1998).

[61]. P. Pradhan and A. K. Ray, J. Mol. Struc. (Theochem) 716, 109 (2004)

[62]. P. Pradhan and A. K. Ray, Eur. Phys. J. D, in press.

[63]. M. N. Huda and A. K. Ray, Phys. Rev. A 69, 011201 (R) (2004).

[64]. M. N. Huda and A. K. Ray, Eur. Phys. J. D 31, 63 (2004).

[65]. J. Sha, J. Niu, X. Ma, J. Xu, X. Zhang, Q. Yang, D. Yang, Adv. Mater. 14, 1219 (2002).

[66]. S. Jeong, J. Kim, H. Yang, B. Yoon, S. Choi, H. Kang, C. Yang, Y. Lee, Adv. Mat. 15, 1172 (2004).

[67]. P. Pradhan, and A. K. Ray, J. of Comp. and Theo. Nanoscience, in press.

[68]. K. Capelle, A Bird's- Eye View of Density Functional Theory , www.arxive:cond-mat/0211443 (2004).

[69]. A. Nagy, Phys. Rep. 298, 1 (1998).

[70]. P. Hohenberg and W. Kohn, Phys. Rev. 136, B864 (1964).

[71] T. Kato, Commun. Pure Appl. Math. **10**, 151 (1957).

[72]. M. Levy, Proc. Natl. Academy Sci. USA, **76**, 6002 (1972).

[73]. M. Levy, Phys. Rev. A **26**, 1200 (1982).

[74]. M. Leib, Int. J. Quant. Chem. **24**, 243 (1982).

[75]. W. Kohn and L. J. Sham, Phys. Rev. **140**, A1133 (1965).

[76]. J. P. Perdew, Phys. Rev. B 33, 8822 (1986).

[77]. J. P. Perdew, J. A. Chevary, S. H. Vosko, K. A. Jackson, M. R. Pederson, D. J. Singh, and C. Fiolhais, Phys. Rev. B 46, 6671 (1992).

[78]. J. P. Perdew, J. A. Chevary, S. H. Vosko, K. A. Jackson, M. R. Pederson, D. J. Singh, and C. Fiolhais, Phys. Rev. B 48, 4978 (1993).

[79]. J. P. Perdew, K. Burke, and Y. Wang, Phys. Rev. B 54, 16533 (1996).

[80]. J. P. Perdew, K. Burke, and M. Ernzerhof, Phys. Rev. Lett. 77, 3865 (1996).

[81]. C. Lee, W. Yang and R. G. Parr, Phys. Rev. B 37, 785 (1988).

[82]. A. D. Becke, J. Chem. Phys. 98, 5648 (1993).

[83]. P. J. Hay and W. R. Wadt, J. Chem. Phys. 82, 284 (1985).

[84]. T. H. Dunning Jr. and P. J. Hay, in *Modern Theoretical Chemistry*, Ed. H. F. Schaefer III, Vol. 3 (Plenum, New York, 1976) 1-28.

[85]. *Gaussian 03* (Revision C.02), M. J. Frisch *et al*., Gaussian Inc., Pittsburgh, PA, 2003.

[86]. *CRC Handbook of Chemistry and Physics*, 76th edition,1995-1996.

[87]. P. F. Bernath, S. A. Rogers, L. C. O'Brien and C. R. Brazier, Phys. Rev. Lett 60,197 (1998).

[88]. M. Grutter, P. Freivogel and J. P. Maier, J. Phys. Chem. A 101, 275 (1997).

[89]. A. I. Boldyrev, J. Simons, V. G. Zakrzewski, W. von Niessen, J. Phys. Chem. 98, 1427 (1994).

[90]. F. Ruette, M. Sanchez, R. Anez, A. Bermudez, A. Sierraalta, J. Mol. Struct. THEOCHEM 729, 19 (2005).

[91]. A. K. Ray, J. Phys. B 20**,** 5233 (1987).

[92]. L. S. Ott and A. K. Ray, Proc. NATO Adv. Wksp. and Int. Symp. Phys. Chem. Small Clusters, p. 95 (P. Jena, B. K. Rao, and S. N. Khanna, Eds., Plenum Pub., New York, 1987).

[93]. K. Raghavachari and J. S. Binkley, J. Chem. Phys. 87, 2191 (1987)

[94]. R. O. Jones, J. Chem. Phys. 110, 5189 (1999).

[95]. A. V. Orden and R. J. Saykally, Chem. Rev. 98, 2313 (1998)

[96]. C. Zhang, X. Xu, H. Wu, and Q. Zhang, Chem. Phys. Lett. 364, 213 (2002)

[97]. W. Chai, N. Shao, X. Shao, and Z. Pan, J. Mol. Struct. (Theochem) 678, 113 (2004)

[98]. B. R. Eggen, R. L. Johnston, and J. N. Murell, J. Chem. Soc. Faraday Trans. 90(20), 3029 (1994).

[99] A. Srinivasan, M. N. Huda and A. K. Ray, Phys. Rev. A, in press.

[100]. *NBO 5.0.* E. D. Glendening, J, K. Badenhoop, A. E. Reed, J. E. Carpenter, J. A. Bohmann, C. M. Morales, and F. Weinhold, Theoretical Chemistry Institute, University of Wisconsin, Madison (2001).

[101]. R. S. Mulliken, J. Chem. Phys. **23**, 1833 (1955).

[102]. R. S. Mulliken, J. Chem. Phys. **23**, 1841 (1955).

[103]. R. S. Mulliken, J. Chem. Phys. **23**, 234 (1955).

[104]. K. Raghavachari, J. Chem. Phys. 85, 6623 (1986).

[105]. A. Srinivasan and A. K. Ray, J. of Nanoscience and Nanotech., in press.

[106]. R. O. Jones, L. Turker, J. Mol. Struct. (Theochem) 625, 169 (2003).

[107]. P. R. C. Kent, M. D. Towler, R. J. Needs and G. Rajagopal, Phys. Rev. B 62, 15394 (2000).

[108]. J. M. L. Martin, J. El-Yazal, and J.-P. Francois, Chem. Phys. Lett 255, 7 (1996).

[109]. R. O. Jones and G. Seifert, Phys. Rev. Lett 79, 443 (1997).

[110]. J. I. Chavez, M. M. Carrillo, and K. A. Beran, J. Comput. Chem 25, 322 (2004).

BIOGRAPHICAL INFORMATION

The author completed his undergraduate degree in Electronics and Communication engineering in the University of Madras, India. His undergraduate project was in the design of Spread spectrum transmission and receiver design using simple digital gates. Simulation was done by C programming. He was among the top five students in his undergraduate studies among a class of 80 students. After completing undergraduate studies, he worked as part time tutor in Mathematics.

He completed his Master's in Electrical engineering at University of Texas at Arlington in Spring 2002. He specialized in the area VLSI design and engineering. He has done projects using Cadence IC design tools for the design of Sample and Hold circuit and also for 16 bit Carry Lookahead Adder. In the course of Master's in physics, he was involved with the simulations and study on the stabilities of stable silicon-carbon fullerene like nanostructures which has great industrial importance. He has authored and co-authored quite a few papers in scientific journals and also presented papers at international conferences. In future, he intends to work in research labs in the field of semiconductors, especially in the field of IC design (Analog/Digital) and IC fabrication.